U.S. Department of Transportation

Federal Railroad Administration

DAMAGE ASSESSMENT OF RAILROAD TANK CARS INVOLVED IN ACCIDENTS: Phase II — Modeling and Validation

Office of Research and Development
Washington, D.C. 20590

REPORT DOCUMENTATION PAGE

Public reporting burden for this collection of information is estimated to average 1 hour per response, including the time for reviewing instructions, searching existing data sources, gathering and maintaining the data needed, and completing and reviewing the collection of information. Send comments regarding this burden estimate or any other aspect of this collection of information, including suggestions for reducing this burden to Washington Headquarters Services, Directorate for Information Operations and Reports, 1215 Jefferson Davis Highway, Suite 1204, Arlington, VA 22202-4302, and to the Office of Management and Budget, Paperwork Reduction Project (0702-0288), Washington, D.C. 20503

1. AGENCY USE ONLY (Leave blank)	2. REPORT DATE December 2002	3. REPORT TYPE AND DATES COVERED Final — March 1996 to June 1999

4. TITLE AND SUBTITLE	5. FUNDING NUMBERS
DAMAGE ASSESSMENT OF RAILROAD TANK CARS INVOLVED IN ACCIDENTS: Phase II — Modeling and Validation	DTFR53-93-C-00001
6. AUTHOR(S) Richard W. Kloop, Steven W. Kirkpatrick, and Donald A. Shockey	TASK ORDER 115

7. PERFORMING ORGANIZATION NAME(S) AND ADDRESS(ES)	8. PERFORMING ORGANIZATION REPORT NUMBERS
Transportation Technology Center, Inc. P.O. Box 11130 Pueblo, CO 81001	PYU-1229

9. SPONSORING/MONITORING AGENGY NAME(S) AND ADDRESS(ES)	10. SPONSORING/MONITORING AGENCY REPORT NUMBER
U.S. Department of Transportation Federal Railroad Administration Office of Research and Development 1120 Vermont Avenue, NW Washington, DC 20590	DOT/FRA/ORD-02/04

11. SUPPLEMENTARY NOTES

12a. DISTRIBUTION/ABAILABILITY STATEMENT	12b. DISTRIBUTION CODE -
This document is available through National Technical Information Service, Springfield, VA 22161	

13. ABSTRACT

The Accident Damage Assessment Guidelines used to make decisions on the safety of damage pressure tank cars were formulated in the 1970s by the Association of American Railroads (AAR) under the auspices of the Federal Railroad Administration. Although these Guidelines have served their purpose, their validity has not been quantitatively established. This report describes an effort by AAR/TTCI and SRI International to examine and refine the Guidelines.

Damage mechanics was applied to evaluate the effect of gouges and wheel burns. Notched round bar tensile tests were combined with finite element analysis to predict cleavage failure in the absence of a macroscopic crack. Fracture mechanics was applied to evaluate the stability of a thumbnail crack at a dent root and a through-wall crack. J-resistance tests were used to support the analysis. Laboratory dent/undent tests in which plate was bent then pulled straight in tension were applied to evaluate the effects of denting.

The research showed that the present Guidelines are valid, with reasonable factors-of-safety, except for otherwise-undamaged dents that do not involve welds. Consideration of dent root radius should be removed from the Guidelines because radius has little bearing on the likelihood of failure. Tank pressures above about 100 psi are sufficient to straighten longitudinal dents and leave them with large root radii. Accordingly, the largest root radii have seen the highest pressures and the most deformation, yet previously were considered the safest. Fortunately, the dent/undent tests showed that otherwise-undamaged dents that do not involve welds fail at loads equal to those for virgin plate.

The crack stability analyses and toughness measurements showed that through-wall cracks are stable up to at least several inches in length. Thumbnail dent root cracks are likely to be unstable and can grow readily to be as long as the dent. Thus, the risk of dent failure depends on the likelihood of a dent containing a crack. The research shows that the likelihood is very low unless the dent involves other damage or welds.

14. SUBJECT TERMS		15. NUMBER OF PAGES
Railroad tank cars, accident damage assessment, local fracture, damage mechanics, finite element modeling, cleavage, notched round bars, gouges, reversed bending, dents		
		16. PRICE CODE

17. SECURITY CLASSIFICATION	18. SECURITY CLASSIFICATION OF THIS PAGE	19. SECURITY CLASSIFICATION OF ABSTRACT	20. LIMITATION OF ABSTRACT
UNCLASSIFIED	UNCLASSIFIED	UNCLASSIFIED	SAR

METRIC CONVERSION FACTORS

Approximate Conversions to Metric Measures

Symbol	When You Know	Multiply by	To Find	Symbol

LENGTH

Symbol	When You Know	Multiply by	To Find	Symbol
in	inches	*2.50	centimeters	cm
ft	feet	30.00	centimeters	cm
yd	yards	0.90	meters	m
mi	miles	1.60	kilometers	km

AREA

Symbol	When You Know	Multiply by	To Find	Symbol
in^2	square inches	6.50	square centimeters	cm^2
ft^2	square feet	0.09	square meters	m^2
yd^2	square yards	0.80	square meters	m^2
mi^2	square miles	2.60	square kilometers	km^2
	acres	0.40	hectares	ha

MASS (weight)

Symbol	When You Know	Multiply by	To Find	Symbol
oz	ounces	26.00	grams	g
lb	pounds	0.45	kilograms	kg
	short tons (2000 lb)	0.90	tonnes	t

VOLUME

Symbol	When You Know	Multiply by	To Find	Symbol
tsp	teaspoons	5.00	milliliters	ml
Tbsp	tablespoons	15.00	milliliters	ml
fl oz	fluid ounces	30.00	milliliters	ml
c	cups	0.24	liters	l
pt	pints	0.47	liters	l
qt	quarts	0.95	liters	l
gal	gallons	3.80	liters	l
ft^3	cubic feet	0.03	cubic meters	m^3
yd^3	cubic yards	0 76	cubic meters	m^3

TEMPERATURE (exact)

Symbol	When You Know	Multiply by	To Find	Symbol
°F	Fahrenheit temperature	5/9 (after subtracting 32)	Celsius temperature	°C

* 1 in. = 2.54 cm (exactly)

Approximate Conversions from Metric Measures

Symbol	When You Know	Multiply by	To Find	Symbol

LENGTH

Symbol	When You Know	Multiply by	To Find	Symbol
mm	millimeters	0.04	inches	in
cm	centimeters	0.40	inches	in
m	meters	3.30	feet	ft
m	meters	1.10	yards	yd
km	kilometers	0.60	miles	mi

AREA

Symbol	When You Know	Multiply by	To Find	Symbol
cm^2	square centim.	0.16	square inches	in^2
m^2	square meters	1.20	square yards	yd^2
km^2	square kilom.	0.40	square miles	mi^2
ha	hectares (10,000 m^2)	2.50	acres	

MASS (weight)

Symbol	When You Know	Multiply by	To Find	Symbol
g	grams	0.035	ounces	oz
kg	kilograms	2 2	pounds	lb
t	tonnes (1000 kg)	1.1	short tons	

VOLUME

Symbol	When You Know	Multiply by	To Find	Symbol
ml	milliliters	0.03	fluid ounces	fl oz
l	liters	2.10	pints	pt
l	liters	1.06	quarts	qt
l	liters	0.26	gallons	gal
m^3	cubic meters	36.00	cubic feet	ft^3
m^3	cubic meters	1.30	cubic yards	yd^3

TEMPERATURE (exact)

Symbol	When You Know	Multiply by	To Find	Symbol
°C	Celsius temperature	9/5 (then add 32)	Fahrenheit temperature	°F
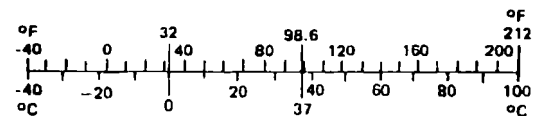
ACKNOWLEDGMENTS

(BLANK PAGE)

EXECUTIVE SUMMARY

Since 1985, the Association of American Railroads/Transportation Technology Center, Inc. (AAR/TTCI) and other organizations have used a set of Accident Damage Assessment Guidelines developed in the late 1970s to assist emergency response personnel to evaluate the severity of damage to tank cars involved in accidents, and to make judgments in the field regarding rerailing, unloading, or moving the tank cars. Unfortunately, the Guidelines were developed by a few individuals who are no longer available to substantiate them. Thus, the Guidelines lack validation. To investigate the validity of the Guidelines, SRI International performed a research program combining laboratory tests and computer simulations based on modern fracture mechanics concepts including the so-called local fracture or damage mechanics approach. SRI focused on DOT 112A340W tanks and used laboratory tests on small smooth and notched round bar specimens of A515 Grade 70 plate and welds and TC-128B as-rolled plate to calibrate a finite element failure model. The specific model chosen was the Beremin cleavage failure model. As a check on the results, laboratory tests were also performed to directly measure the behavior of plates containing damage in the form of simulated gouges and dents. Conventional fracture mechanics analyses and tests were also performed to understand the stability of through-wall cracks and thumbnail cracks at the roots of dents.

The research program provided the following results pertaining to DOT 112A340W tanks:

- The Guidelines involving cracks are valid, for the most part, because the Guidelines require tank unloading for almost any crack. For the case where a crack is in an attachment weld, the Guidelines are valid because, unless the crack is accompanied by other damage or is extraordinarily long, such cracks will result in leaks instead of extending catastrophically.

- The Guidelines for base-metal scores and gouges are valid, with safety factors ranging from 1.3 to 2.1. The Guidelines for scores or gouges removing only weld bead reinforcement are valid because of the extra strength of the weld filler metal and because, even if the weld contains an undetected crack, the crack is unlikely to extend catastrophically in the absence of other damage, e.g., a dent.

- The Guidelines for wheel burn are valid with a safety factor of roughly 1.4 to 1.7.

- The Guidelines for otherwise undamaged dents need to be modified to remove dependence on dent radius of curvature, because radius of curvature has little

bearing on propensity for failure. At pressures above approximately 100 psi, dents are forced back out to yield large radii of curvature and can almost disappear at relief valve discharge pressures.

- Dents that have no other damage such as cracks, scores, or gouges and that do not involve welds appear unlikely to crack no matter what the radius of curvature. On the other hand, dents with cracks are dangerous, because cracks at dent roots can easily extend, driven by the pressure-induced bending moment. Thus, it appears that the dent Guidelines should be reformulated to be based on an assessment of the likelihood that a dent contains a hidden crack. Two extremes to this assessment are (1) to assume that all dents contain cracks or (2) to assume that dents that have no obvious cracks, scores, or gouges and that do not involve welds never contain cracks. The best approach is probably somewhere in between.

- As demonstrated in this work, stresses in an undamaged tank are primarily due to internal pressure and not gravity loads induced by the lading. Thus, rerailing operations on undamaged tank cars will generate stresses that are negligible in magnitude compared with the pressure stresses.

The local fracture approach to validating the Guidelines has resulted in a computational tool that allows extension of the Guidelines to other tank cars, damage scenarios, and salvage operations. We recommend that this tool be applied to address the effects of different lifting scenarios on tank cars with damage. We also recommend that the local fracture approach be extended to the case of a reversed cycle of plastic deformation as occurs at the root of a dent that undergoes in/out bending.

The reliable 15-year history of the Guidelines is, in itself, partial validation. The history implies a reasonable level of conservatism since, fortunately, only very few catastrophic delayed ruptures have occurred, and those ruptures occurred in cases where the tank damage would not have passed the Guidelines' rules.

Table of Contents

List of Figures

List of Tables

(blank page)

1.0 INTRODUCTION

1.1 BACKGROUND

Under Federal Railroad Administration Contract No. DTFR53-93-C-00001, Task Order 115, the Association of American Railroads, Transportation Technology Center, Inc. (AAR/TTCI) conducted a research project to establish guidelines for proven and reliable assessment of damage to tank cars. The final objective of the project is to produce a companion handbook to the current handbook, *Field Removal Methods for Tank Cars*, that will help emergency response personnel at an accident scene evaluate the criticality of damage to tank cars. From this evaluation, the emergency response personnel can decide on the most appropriate procedures for handling the damaged cars and their contents (e.g., unload, rerail, move).

Since 1985, TTCI and other organizations have used a set of guidelines (referred to as the Guidelines in the remainder of this report) developed in the late 1970s to teach emergency response personnel how to make judgments in the field as to the severity of damage to tank cars involved in accidents. These Guidelines could serve as a basis for the new Handbook, provided they ensure a sufficient level of safety during handling of damaged tank cars after an accident. Unfortunately, the Guidelines were developed by a few individuals who are no longer available to substantiate them. Therefore, a research program was begun to establish the validity of the Guidelines. In Phase I of the program, research focused on evaluating the technical foundation for the Guidelines and the degree to which they have been validated.

To assist TTCI in the performance of Phase I, SRI International performed a literature review [1] to identify which of the current Guidelines could be validated and which required additional modeling and validation in a Phase II effort. From the review of close to 100 references, we identified the analytical and experimental results that can serve to evaluate the criticality of the damage (cracks, scores, gouges, dents, and wheel burns). We found that the Guidelines reflect a good, overall, physical understanding of potentially dangerous damage to tank cars, except for the case of dents. Quantitative specifications are generally expressed in terms of convenient parameters that can be related to the degree of structural and material weakening caused by the damage. We also drew the following conclusions regarding the relevance and validity of the Guidelines:

- The Guidelines are often only qualitative and somewhat vague in their requirements.

1

- No record of analytical or experimental work was found to support and validate the specifications of the Guidelines.* We were, however, able to reconstruct some of the reasoning that must have led to the specifications. It appears that the Guidelines rely on twenty-year-old or older analysis methods and do not reflect recent advances in computational and fracture mechanics.

- The effect on damage of loads applied to move or lift the derailed tank car is not explicitly accounted for in the Guidelines, even though these loads could be important in causing damaged areas to rupture.

- The phenomenon of delayed fracture is not appropriately documented or understood. The Guidelines do not adequately address this important safety issue.

- The margins of safety associated with the specifications of the current Guidelines are not known.

- The Guidelines do not consider advanced nondestructive evaluation (NDE) methods identifying tank car damage and monitoring it during handling at the accident scene.

To alleviate these shortcomings and improve the reliability and usefulness of the Guidelines, we recommended the following research:

- Identify typical rerailing load scenarios and calculate by finite element analysis methods the stress and strain fields they induce in pressurized tank cars. Use these results as loading conditions to assess the criticality of various types of damage in tank cars.

- Assess the residual resistance of tank cars with large dents to buckling and plastic collapse when subjected to rerailing loads.

- Refine and validate the severity criteria for scores, gouges, and wheel burns using recent advances in analytical and experimental fracture mechanics.

- Assess the possibility for stable crack growth in fully plastic tank car steels and the implications for delayed fracture.

---

* Later, however, an excerpt [2] of some AAR training notes was found that gives some engineering rationale behind the Guidelines. Unfortunately, the rationale is incomplete and contains errors.

- Evaluate the applicability of current NDE equipment and recommend use of suitable NDE techniques in the guidelines.

- Monitor and participate in the activities of the committee on Post-Construction Standards of the Pressure Vessel and Piping Division of the American Society of Mechanical Engineers.

We recommended that the structural and fracture mechanics analysis parts of the proposed research be accomplished by combining nonlinear finite element simulations with advanced elasto-plastic fracture and local fracture theories to quantify the severity of various types of tank car damage. We also recommended that this analytical effort be performed in conjunction with an experimental effort, using small laboratory specimens to provide material properties data as well as validation for the analyses. The results of this research would be used to reformulate the Guidelines in more precise and quantitative terms, so that their use would contribute to increased safety at derailment sites.

From the recommendations of the Phase I program, we designed and performed a Phase II effort to address the highest priority issues. We designed a program to attempt to validate the Guidelines, estimate their margins of safety, and develop an analysis method for generating a damage evaluation handbook. This report describes the results of this Phase II program.

Although the Guidelines lack formal validation, numerous documents provide informal validation. In particular, Pellini's post-accident analyses [3-8] refer to and make numerous comments about the Guidelines. Also, training notes for damage assessment courses at AAR [2] provide rationale behind the Guidelines, but these notes are not readily available. In general, these documents are supportive of the Guidelines as they exist.

Pellini's analyses are based largely on the so-called Slide-Graph Fracture Analysis System (SGFAS) [6]. Pellini used SGFAS to develop guidelines for the fracture-safe [7] and fatigue-reliable [8] design of steel structures. Pellini used the SGFAS to explain the good safety record of tank cars and the few occurrences of arrested or catastrophic brittle fracture (in particular, the two known cases [3,9] of catastrophic delayed fracture in tank cars containing extensive rail burn damage). Fracture safety evaluations with the SGFAS are made by entering into a graph the service temperature relative to the nil ductility temperature (NDT) and the normalized service stress. The location of this point will fall either in a fracture arrest or a fracture propagation zone, and the tank car would be expected to behave accordingly. This procedure is simple and requires very little stress analysis because, in most reviewed references, the service stress is taken as either

3

the membrane hoop stress induced by the tank internal pressure or the yield stress. It also avoids the difficulties of dealing explicitly with fracture in the transition region and under elastic-plastic or fully plastic conditions.

SGFAS is therefore a useful engineering design tool, even though it is somewhat qualitative and is based on fracture experience and theories dating back to the early 1970s. Since then, several significant advances were made in the field of fracture mechanics that could be applied to the assessment of damaged tank cars. In particular, J-integral based elastic-plastic fracture mechanics and more recently developed damage mechanics or local fracture mechanics approaches can provide a more accurate estimate of the safety of a damaged tank car.

The reliable 15-year history of the Guidelines is, in itself, partial validation, but the level of conservatism has been unknown. Fortunately, only very few catastrophic delayed ruptures have occurred, and those ruptures occurred in cases where the tank damage would not have passed the Guidelines' rules. We are aware of no cases in which tanks have passed the Guidelines yet failed catastrophically.

1.2 EXISTING GUIDELINES

The portion of the existing Guidelines that requires validation is Section 5: Interpreting Tank Damage to Pressure Tank Cars. Damage is defined, then divided into four categories: (1) cracks, (2) scores and gouges, (3) wheel burns, and (4) dents (including rail burns). The Guidelines, verbatim for each category, follow.

1.2.1 Cracks

Since there is no way to detect a crack that has become critical, you have no way to predict an incipient failure. Decisions must be made quickly and the handling of severely damaged tank cars completed as quickly as possible.

- A crack in the tank metal indicates serious damage. Cracks in welds, used to attach brackets or reinforcement plates, are not critical unless the crack extends into the base metal.

- Welds securing attachments to reinforcement pads on the tank are designed to fail, allowing the attachment to break away without damage to the tank.

4

- Any crack found in the base metal of a tank, no matter how small, justifies unloading the tank as soon as possible. However, if in a yard, the car may be carefully moved to a designated remote location in the yard for transfer.

- When a crack is in conjunction with a dent, score, or gouge, the tank should be unloaded as soon as possible without moving it.

1.2.2 Scores and Gouges

Scores and gouges in conjunction with dents are discussed under the dents section.

- Scores or gouges crossing a weld and removing only the weld reinforcement are not critical.

- Longitudinal scores are the most dangerous. However, circumferential scores cannot be ignored for at any given section such scores also constitute a longitudinal notch.

- Longitudinal scores or gouges crossing a weld and affecting the heat affected zones are critical and the contents of the tank car should be transferred immediately.

- Tanks having scores or gouges should be unloaded in place when the internal pressure exceeds half of the allowable internal pressure listed in the tables below. Tables 1 and 2 show the allowable score depths and allowable pressures for 340W and 400W tanks, respectively.

1.2.3 Wheel Burns

Wheel burn damage does not include a high probability of failure.

If the maximum depth of the wheel burn exceeds 1/8", the tank should be unloaded as soon as possible. If the depth of the wheel burn is less than 1/8", the tank should be emptied at the closest loading facility, provided it is moved with care; not in ordinary train service.

Table 1. Limiting Score Depths for 340W Tanks

Depth of Score	Maximum Safe Internal Pressure, psig
1/16"	191 (89°F for commercial propane)
1/8"	170 (85°F for commercial propane)
3/16"	149 (76°F for commercial propane)
1/4"	127 (65°F for commercial propane)

5

Note: In no case should a tank containing a score in excess of 1/16" for 340W tanks be shipped by rail, although it could be uprighted and even moved short distances for transfer.

Table 2. Limiting Score Depths for 400W Tanks

Depth of Score	Maximum Safe Internal Pressure, PSIG
1/16″	228 (108°F for commercial propane)
1/8″	205 (99°F for commercial propane)
3/16″	188 (93°F for commercial propane)
1/4″	162 (82°F for commercial propane)

Note: In no case should a tank containing a score in excess of 1/8" for 400W tanks be shipped by rail, although it could be uprighted and even moved short distances for transfer.

While the values given in Tables 1 and 2 are conservative, they do not include the welded joint efficiency for tanks built prior to 1968. This amounts to an extra 10% safety factor.

1.2.4 Dents (Including Rail Burns)

- Sharp dents in the shell of the tank (cylindrical section) which are parallel to the long axis are the most serious as these dents drop the rating of the tank by 50%.

    1. For dents in the shell of tank cars built prior to 1967, the tank should be unloaded without moving it under the following conditions:

        -- A minimum radius of curvature of 4 inches or less;

        -- Have a crack anywhere;

        -- Cross a weld; or

        -- Include a score or gouge.

    Dents with a radius of curvature more than 4 inches are not a problem by themselves.

    2. For dents in the shell of tank cars built since 1967, the tank should be unloaded without moving it under the following conditions.

        -- A minimum radius of curvature of 2 inches or less;

        -- Have a crack anywhere;

        -- Cross a weld;

        -- Include a score or gouge; or

6

-- Show evidence of cold work.

- Dents with a radius of curvature more than 2 inches are not a problem by themselves.

- Massive dents in heads of the tank are generally not serious unless gouges or cracks are present with the dents.

- Small dents in heads not exceeding 12 inches in diameter in conjunction with cold work in the bottom of the dent are marginal if they show a radius of curvature less than 4" for tanks built prior to 1967 or less than 2" for tanks built since 1967. If at all possible, such tanks should be unloaded in place. In any case, the tank should be moved as little as possible and promptly unloaded.

The above tables complete the verbatim statement of the Guidelines.

2.0 OBJECTIVES

The objectives of Phase II were to validate or recommend appropriate changes to the current damage assessment Guidelines, estimate the margin of safety they provide, and develop an analysis method that can be used to generate a comprehensive handbook for tank car damage evaluation.

3.0 PROCEDURES

The approach of Phase II was to perform a combined experimental and computational program to

(1) Calibrate a local fracture cleavage failure model for typical tank car steels, then apply the model to various forms of damage and compare predicted failure loads with those determined from the Guidelines.

(2) Measure the fracture toughness properties of typical tank car steels and perform a crack stability analysis using elastic-plastic J-integral-based fracture mechanics.

In the following, we discuss our choice of steels, test temperature, the cleavage model, and experimental and computational procedures.

3.1 PRELIMINARIES

3.1.1 Steels

Pressure tank cars made of ASTM A212 Grade B steel still represent a significant portion (□15%) of the tank car fleet. A212 is an obsolete specification that was withdrawn by ASTM in 1966 and replaced by today's A515 and A516. Original A212B steel can be obtained only by scrapping an existing tank car. A212B steel generally has the highest transition temperature and the lowest lower shelf Charpy V-notch energy. It probably has the lowest lower shelf fracture toughness of the pressure tank car steels that we are considering. Thus, A212B tank cars represent the greatest accident risk.

Can we substitute A515 steel for A212 steel in the validation of damage assessment guidelines? We can if damage guidelines deemed safe for A515 are also deemed safe for A212. As can be seen in Table 3, the A212B specification is nearly identical to the A515 Grade 70 specification. The failure properties are expected to be nearly identical as a result. The 1965 *Metals Handbook*, p. 65 [10] shows graphical distributions of properties for 33 samples of A212B. The tensile strength is 70-85 ksi, yield strength is 40-50 ksi, elongation in 8 inches is 25%-29%, carbon content is 0.22%-0.28%, and manganese content is 0.70%-0.90%. The 1978 *Metals Handbook*, p. 195 [11] shows the same distributions, but calls the steel A515 Grade 70, further confirming that A212B and A515 Grade 70 mean nearly the same thing. The A516 steel specification, though very similar, calls for lower carbon content and is intended to result in a lower transition temperature than A515 steel.

Table 3. A212B and A515-70 Specifications

Steel	A212B	A515-70
C	<0.31	<0.31
Mn	<0.90	<1.20
P	<0.035	<0.035
S	<0.04	<0.04
Si	0.13-0.33	0.15-0.40
Tensile, ksi	70-85	70-90
Yield, ksi	>38	>38
Reduction of Area, %	–	17
Elongation, % in 2″	>21	21

Melting and rolling practices have improved over the years such that today's A515 Grade 70 may have fewer, smaller inclusions and may have smaller, more uniform microstructure than A212B. Thus, A515 Grade 70 and A212B steel may have different fracture properties both above and below the transition temperature. We expect the differences in microstructure between A212B and A515 Grade 70 to persist in weld heat-affected zones where failure has been found to initiate. However, we expect the differences between the two steels to be smaller than the scatter within different heats of either steel considered alone. Given the expected amount of scatter, which is further increased by welding, we decided that testing A515 Grade 70 was an acceptable, although slightly less conservative, approach. The approach is made more conservative by scaling results down to the worst expected strength and transition temperature behavior.

As shown in Figure 1, roughly 15% of the current DOT 112 tank car fleet was built before 1966, when the A212 specification was in use. Most of these cars will be in service at least another decade. Only about 20% of the fleet has been built since 1988, when the use of normalized TC-128B became mandatory. The remaining 65% of the fleet was assumed to be as-rolled TC-128, although available statistics are not broken down by steel type.
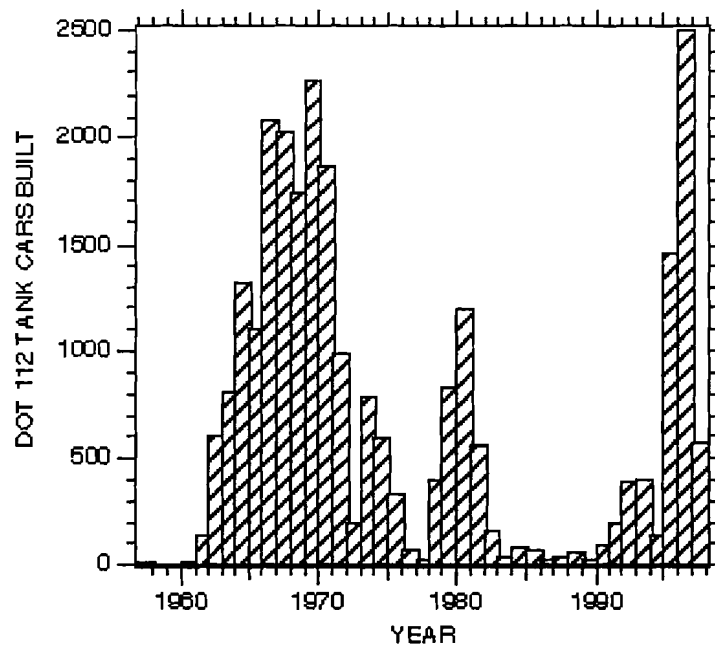
Yearly production of DOT 112 tanks cars
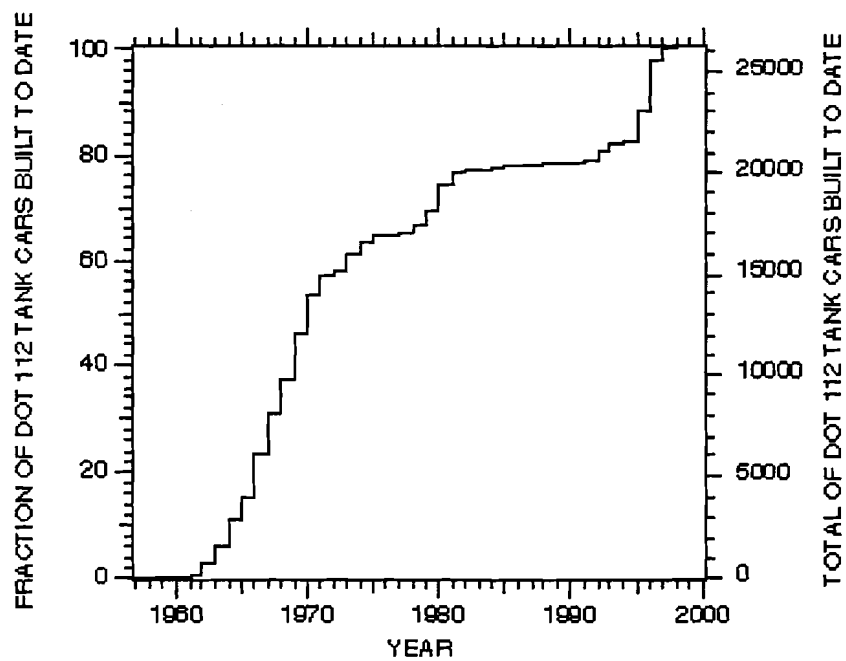
Cumulative total of DOT 112 tank cars built through mid-1997.

Figure 1. DOT 112 Tank Car Population Versus Year through Mid-1997

Can we test TC-128B steel as a substitute for A212B/A515 Grade 70 steel, since TC-128B steel represents the majority of the fleet? Table 4 compares handbook properties for A212B/A515 Grade 70 with those of TC-128B as-rolled. As Table 4 shows, TC-128B is not equivalent to A212B/A515 Grade 70. Their microstructures are different as well. Although it is possible that TC-128B as-rolled and A212B/A515 Grade 70 can be made to have the same fracture behavior on the lower shelf by, say, testing the TC-128B at 20°C lower temperature, the steels are enough different and their welding response is likely to be enough different that we should not try to substitute TC-128B as-rolled for A212B/A515 Grade 70 as-rolled. We decided to test both. Otherwise, we felt that the Guideline validation would not be sufficiently conservative.

Table 4. Comparison of Properties of Tank Car Steels

Steel	Yield (min. ksi)	Ultimate (ksi)	Elongation (% in 8 in)	C Content (max. wt %)	Mn Content (max. wt %)
A212B/ A515 Gr 70	38	70-85	27	0.31	0.9
TC-128B*	50	81-101	16	0.25	1.35

*This steel also contains maximum 0.25% Cr, 0.25% Ni, and 0.08% Mo.

The A515 Grade 70 as-rolled data will indicate the validity of the Guidelines as applied to older cars, and the TC-128B as-rolled data will do the same for the majority of present-day cars. Because cars constructed of TC-128B normalized are certainly more damage-tolerant than the cars constructed of TC-128B as-rolled, testing TC-128B as-rolled, rather than normalized, was considered a conservative approach.

Because we did not test TC-128B normalized steel in this program, the amount of conservatism obtained by testing TC-128B as-rolled instead of normalized is difficult to state in terms of stress or tank pressure. It is much easier to state in terms of temperature. Unfortunately, the Guidelines make scant mention of steel temperature or how to tell if a tank is made from normalized steel; therefore, the emergency responder cannot make use of the fact that a normalized TC-128B tank is much less prone to cleavage.

Pellini's slide-graph analyses [6] show that TC-128B normalized steel has about a 40°F (22°C) lower nil-ductility temperature than TC-128B as-rolled. Results obtained in an AAR program comparing TC-128B with controlled-rolled steels [4] indicate that TC-128B as-rolled steel has the same yield strength, 15% higher tensile strength, 14% lower elongation, and 12% lower reduction in area than TC-128B normalized steel. The as-rolled and normalized steels were manufactured

by different mills, which undoubtedly accounts for some of the differences in properties. The normalized steel had a 70°F (39°C) lower NDT. Charpy V-notch energies are similar for the two steels, except that the normalized transition curve is shifted roughly 200°F (111°C) to lower temperatures. The effect of normalization is to reduce the grain size, which in turn increases the yield strength and the fracture toughness. Apparently, the effect of normalization is also to raise the cleavage stress such that plastic flow is favored until the temperature becomes so low and the flow stress thereby becomes so high that plastic flow is no longer possible before cleavage occurs. Whatever the explanation for lower NDT in TC-128B normalized steel, we counted on the fact that Guidelines valid for TC-128B as-rolled would certainly be valid for TC-128B normalized steel.

3.1.2 Welds

Welded specimens for the notched round bar and bend tests were all prepared from A515-70 plate welded using the single-pass (that is, one pass on each side) tandem submerged-arc procedure used in the late 1960s for A515-70 DOT 111A100W tanks. The welding procedure is documented in Appendix A. The procedures used to weld A212 tank cars before 1967 are not well documented.

Thus, the procedure used in the current program may differ and probably produced better welds than the worst found in the fleet. To account for this effect, we derated the results obtained in the current program to the worst level expected in the field. For the most part, this means that we simply assumed that scored, gouged, or dented welds will contain macroscopic cracks, and we based the related analyses on fracture mechanics.

The Guidelines also appear to assume that welds contain preexisting cracks. That is why the Guidelines recommend that gouge, score, wheel burn, and/or dent damage in conjunction with welds should require unloading of the tank. Current inspection procedures cannot find all macroscopic cracks, and accident experience shows that macroscopic cracks in welds appear to have been associated with every delayed failure [3]. In some cases, the cracks appear to have existed for years before catastrophic failure occurred [3]. As we show in the crack stability analysis (Section 5.1), even a relatively large crack is relatively safe in an undented tank. Thus, the assumption that welds contain cracks is prudent yet not overly conservative.

3.1.3 Temperature

In choosing the temperature for the validation and calibration laboratory tests, we needed to satisfy three competing constraints. First, the tests for the local fracture approach must be

performed at a temperature low enough to ensure cleavage fracture, rather than ductile tearing. Cleavage cracks propagate with lower energy input, so results obtained are more conservative than for tearing. Second, we must perform all tests at temperatures that fairly represent the most brittle conditions likely to be found in the field, yet do not lead to overly conservative results. Third, the tests must be performed at a temperature that is practical to reach in the laboratory.

On page 5 of his report on rail burns [3], Pellini makes the case that as-rolled steels then in service (1983) (and still in service today) were susceptible to cleavage fracture. He then presents several actual incidents that support his case. In none of the incidents were temperatures unusually low. In fact, some were in the 60°F range. Thus, we conclude that, although ductile failure is a likely and preferred response, cleavage failure is a significant risk in any accident, and the Guidelines must allow that any failure could result in cleavage.

In the AAR literature on A212B/A515-70 as-rolled steel, we find that the lowest expected NDT is around 20°F (-7°C). The lowest NDT for TC-128B as-rolled steel is around -4°F (-20°C). Unfortunately, the NDT is measured under dynamic conditions and in the presence of a weld. Our tests were performed under quasi-static conditions mostly without welds, and steels are generally less prone to cleavage under such conditions. Thus, to ensure that cleavage occurred, we had to test at a temperature well below the lowest expected NDT. We found it necessary to test smooth, macroscopically unflawed TC-128B specimens at around -238°F (-150°C) to ensure that cleavage fracture occurred. Figure 2 shows that a TC-128B fracture surface produced at -112°F (-80°C) contains dimples indicative of ductile tearing, whereas a fracture surface produced at -238°F (-150°C) contains cleavage facets and is indicative of brittle failure. Thus, we chose -238°F (-150°C) as the temperature for most of our testing.

Since temperatures of -238°F (-150°C) are never expected in the field, are our results too conservative? The answer is no, except perhaps for dents, because once typical tank car steels are cooled into the cleavage regime, the variation of fracture resistance with temperature can be predicted from knowledge of the variation of cleavage stress and flow strength with temperature. For a given steel, cleavage stress is relatively constant with changes in temperature. Thus, once we are in the cleavage regime, results are expected to be similar for all cases in which cleavage occurs. However, the flow stress rises with decreasing temperature, so results must be adjusted to take this into account. For example, if a gouge specimen cleaves under a certain stress at -238°F (-150°C), we expect that, if cleavage were somehow initiated at a higher temperature, the stress would be nearly the same. We needed to verify, however, that the specimen did not first fail by plastic yielding at a lower stress due to the decreased flow stress at the higher temperature.

13
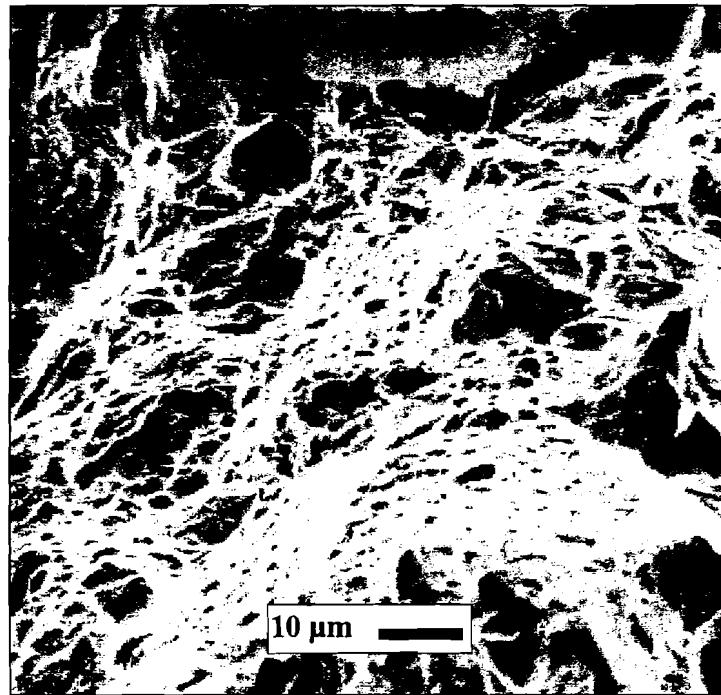
-112°F (-80°C)
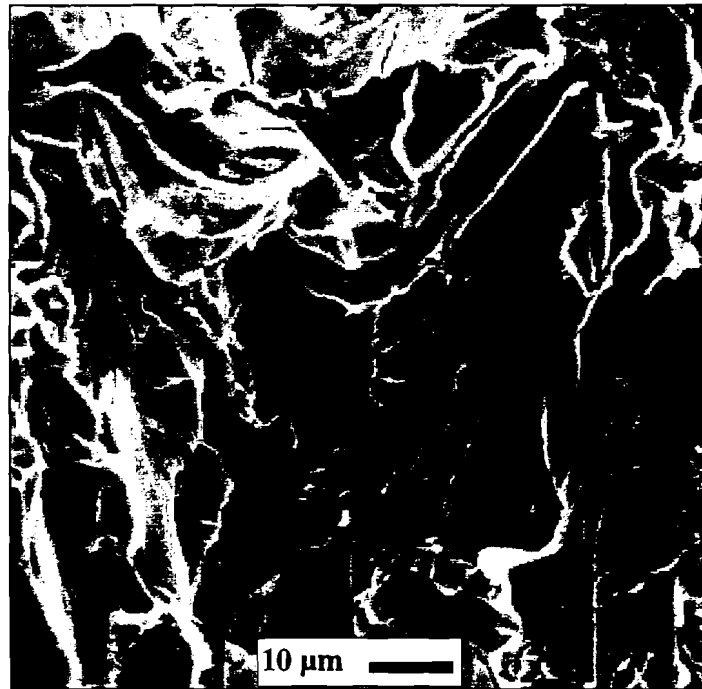
-238°F (-150°C)

Figure 2. Fracture Surface Appearance for TC-128B As-rolled Notch Round Bar Specimens

In the case of dents, if the tank steel is in the cleavage regime during dent formation, the tank will fail immediately. We showed this by performing cold bend tests at -238°F

14

(-150°C). TC-128B as-rolled, A515-70, and welded A515-70 plates all failed in cleavage at bend radii around 30 inches, far in excess of the 2-inch and 4-inch limits specified in the Guidelines. Apparently, if a dent is observed in a tank that has not ruptured, the dent was formed when the steel was in the ductile regime. Thus, to evaluate the validity of the dent guidelines, one must determine the later behavior of the tank, particularly whether a macroscopic crack could initiate and grow at the coldest temperatures expected in the field. We chose -40°F (-40°C) as the coldest temperature likely to be encountered in the field, considering the effects of both cold weather and refrigeration induced by the evaporation of liquid lading. For example, the equilibrium temperature of propane at atmospheric pressure is about -43° F (-42°C).

3.2   TECHNICAL APPROACH

We used several approaches to evaluate and validate the Guidelines. In the case of scores and gouges, we used two approaches to provide a cross-check on our results. One approach, which we call the local fracture approach, was to perform local fracture tests and modeling. The other, which we call an engineering approach, was to perform tension tests on grooved plates to simulate gouges. In the case of dents, we used an engineering approach that combined finite element modeling to determine impact-loading conditions with laboratory dent/undent tests to determine failure response.   In the case of crack stability, we used a single approach that combined laboratory fracture tests with mathematical analyses. Each approach is described in detail below.

3.2.1   Local Fracture Approach

Two important advances in fracture mechanics have occurred since Pellini's SGFAS. Both advances have resulted in more accurate and more general abilities to model and predict failure behavior. The first advance is so-called J-integral based elasto-plastic fracture mechanics (EPFM). Unlike SGFAS, EPFM can model cases when cracks are embedded in fully yielded regions, such as at the bottom of a rail burn dent. The second advance, brought into practice in the European nuclear industry, is the so-called local fracture or damage mechanics approach. Unlike SGFAS and EPFM, the local fracture approach need not assume a preexisting macroscopic crack.

The effect of dents on the structural integrity of tank cars can be conveniently assessed with structural analysis tools such as finite-element analysis. Linear elastic fracture mechanics or elasto-plastic fracture mechanics can evaluate the safety threat caused by the presence of cracks and whether leak will occur before break. In contrast, burns, scores, and gouges present a more complex problem to which novel tools must be applied. This class of problem can be examined

using the local fracture approach because it can predict fracture initiation in the absence of a preexisting macroscopic crack, it can treat cases of multiaxial loading such as exist in a tank car, and it can account for possible inhomogeneity in microstructure and properties. Local fracture methodology is at the core of SRI's approach.

The first steps in this approach were to identify a set of recommended loading configurations for lifting and moving damaged tank cars at accident sites and to determine the corresponding distribution of stresses and strains in the undamaged car by structural finite-element analysis. For the loads considered, these calculations allowed us to identify the regions most critically stressed as well as the most severe loading configurations.

The stress and strain fields in the most critically loaded regions can be used to evaluate the weakening effect of burns, scores, gouges, or small dents or the stability of cracks induced in these regions during an accident. The calculated fields can be used to define equivalent boundary conditions for analyzing small sections of the tank walls containing defects of various severities. Solid mechanics finite-element simulations of these regions can then be performed, with advanced local fracture models used to control the onset of fracture in dents or at burns, scores, or gouges. Fracture experiments with small specimens of tank car steels (notched and cracked round bars, compact tension specimens, plates with simulated scores and gouges) provide the necessary experimental information for calibrating the fracture models and validating the simulation results.

The cleavage model used in this program is the local cleavage criterion developed by Beremin [12]. The term local criterion describes a modeling approach in which damage is calculated locally within the material, based on the stress and strain histories and micromechanical model for the fracture processes.

Predicting cleavage fracture is different from predicting most ductile damage processes in that there is typically a fairly large scatter in the measured cleavage fracture stress for a sample of identical tests on a single batch of material. Thus a cleavage failure criterion will ideally predict a statistical probability of fracture for a given material, geometry, and stress level, rather than a deterministic failure stress.

The microstructural processes that produce a cleavage fracture are similar to many other classical fracture problems. The material is assumed to have a distribution of preexisting microcracks, typically initiated in the material from the inhomogeneities. For example, in mild steels, the microcracks are produced by fracture of sulfide inclusions or grain boundary carbides. The catastrophic propagation of these cracks results in a cleavage fracture, which occurs when the

16

stress normal to the microcrack planes reaches a critical value. This critical stress can be approximated as

$$\sigma_c = \left[\frac{2E\gamma}{p(1-v)l_o} \right]^{1/2} \tag{1}$$

where E is Young's modulus, γ is the fracture surface energy, v is Poisson's ratio, and l_o is the microcrack length.

The statistical nature of the cleavage criterion is introduced by the distribution of microcrack sizes within the material. Within a given microstructural characteristic volume (V_o), the probability of finding a crack of length between l_o and $l_o + dl_o$ is taken as

$$P(l_o)dl_o = \frac{\alpha}{l_o^{\beta}} dl_o \tag{2}$$

If we integrate the above microcrack distribution function over the range of crack lengths greater than or equal to the critical crack length at a given stress level, we obtain the probability of failure as

$$P(\sigma) = \left(\frac{\sigma}{\sigma_u} \right)^m \tag{3}$$

where $m = 2\beta - 2$ and σ_u is a material constant.

The remaining step in determining the cumulative failure probability of the structure is to combine the probabilities in each of the small representative volumes. Because the probability in any single representative volume is small, the cumulative rupture probability can be approximated as

$$P_R = 1 - \exp\left[\sum_j \frac{V_j}{V_0} \left(\frac{\sigma_j}{\sigma_u} \right)^m \right] \tag{4}$$

The above rupture probability function is used in this program to estimate cleavage failure. Additional information about this model can be found in reference 12.

3.2.2 Engineering Approach

The engineering approach was applied as an alternative to the local fracture model approach in the case of gouges and as the sole approach in the case of dents. The essence of the engineering approach is to combine the calculated stress and strain fields in the regions surrounding damage with empirically determined fracture conditions measured directly on specimens containing simulated damage. Although the engineering approach more closely simulates actual damage

geometries and actual service conditions, it lacks generality, requires many tests, and does not give much insight into what parameters affect fracture and how they affect it. The local fracture approach does not suffer these drawbacks. In the case of denting followed by pressurization, however, the local fracture approach could not be applied because the local fracture theory has not been developed for the case of reversed plastic deformation as occurs in denting. Development of the theory was outside the scope of the current project. Thus, we applied the engineering approach only in the case of denting followed by pressurization.

3.2.3 Conventional Fracture Approach

For cases in which a structure contains a macroscopic crack, linear elastic fracture mechanics (LEFM) and elastic-plastic fracture mechanics (EPFM) predict failure accurately and are far easier to apply than the local fracture approach. Furthermore, the methodology for using the local fracture approach to predict crack stability is not developed. For this reason, we chose to apply LEFM and EPFM as our approach to predicting the stability of two kinds of macroscopic tank car cracks, namely, thumbnail cracks at the root of a dent and through-wall cracks in the absence of a dent. In both cases, the cracks are considered to lie in a radial plane, so they are opened by the hoop stresses in the tank. The hoop stresses are, of course, the highest stresses in a cylindrical pressure vessel like a tank car.

The main parameter that characterizes the force tending to drive a crack is the energy release rate, which for our purposes is equivalent to the J integral. For a given crack size and tank pressure, we can calculate a value of applied J that is tending to drive the crack. By performing laboratory fracture toughness tests, we can find the material property called J_{IC} that represents the material's toughness resisting crack growth. EPFM predicts that a crack will extend when the applied J exceeds J_{IC}. For many materials including pressure tank car steels, J_{IC} is not constant but rises with the amount of crack extension from an initially sharp crack. This rise in J_{IC} is described by a so-called J-Resistance, or J-R, curve. Thus, EPFM may predict that a crack will extend initially but will stop as the resisting J rises. However, the applied J may also rise with crack extension, particularly in the case of constant load. For a given crack growth increment, if the applied J rises more than the J-R curve rises, the crack will not stop but will instead grow in an unstable fashion. A pressurized tank with a growing crack is a constant load situation and is therefore always susceptible to unstable crack growth once some critical crack length is exceeded. Our goal is to find that length as a function of pressure.

Our approach to determining the stability of the two cases of tank car cracks was to obtain the applied J as a function of tank pressure and crack length from the literature and to measure the J-R curves in the laboratory at room temperature and at -40°C.

3.3 FINITE ELEMENT MODELING

DYNA3D, the finite element code used in this work [13], is an explicit nonlinear dynamic finite element code for the analysis of materials and structures. The explicit finite element code architecture results in a stability requirement that the stable time step size must be shorter than the smallest transit time for an elastic stress wave to cross an element. Thus, calculations typically require many thousands or millions of time steps to solve the problem duration. However, the advantage of the explicit code architecture is that no coupled global system of equations needs to be solved; thus the computational requirements for each time step are much less than for an implicit code architecture.

A result of the explicit code architecture and small stable time step is that simple element types and algorithms are preferred to increase code efficiency. Consequently, the major element types in DYNA3D are 4-node shell and 8-node solid hexahedron (brick) elements with reduced (single-point) integration. Additionally, in an explicit code, a large percentage of the total computational time is usually devoted to the constitutive model algorithms. Thus, as much as possible, the constitutive models should be simplified, eliminating computationally intensive algorithms such as iteration loops.

To describe the modifications we made to DYNA3D, we first outline the solution procedure used in this code. DYNA3D is organized in a modular fashion, with each module performing a specific task. This procedure is common to most explicit finite element codes and is similar to those described by other authors (e.g., Owen and Hinton, [14]). The following simplified flow chart shows the tasks performed by DYNA3D. We will use this outline to describe where modifications to the code were made in the failure analyses.

> **Task 1: Input**—Data are input to describe the geometry, materials, boundary conditions, loading, and solution control parameters.
>
> **Task 2: Initialize**—Initial values are loaded into the structural and material data arrays.
>
> **Task 3: Calculate nodal forces**—Forces at the nodes are calculated as the difference between internal and external forces. External loading may include pressure, concentrated loads, and gravity. Internal forces are calculated from element stresses.

Task 4: Solve equations of motion for accelerations—At each node, the acceleration is calculated from the force divided by the nodal mass. For explicit codes such as DYNA3D, no global stiffness matrix coupling the degrees of freedom is needed.

Task 5: Update velocities and displacements—Nodal velocities and displacements are calculated and updated by using the nodal acceleration and the current time step.

Task 6: Calculate strain increment—From the nodal velocities, strain rates are calculated from which strain increments can be calculated.

Task 7: Calculate element stresses—Element stresses are calculated in the material constitutive models from the strain increments.

Task 8: Calculate internal forces—Nodal forces are calculated by integrating the element stresses.

Task 9: Output and check for problem termination—Output results if specified. If the calculation time is less than the specified termination time, return to Task 3.

The code changes made here to implement the Beremin cleavage model change primarily the way element stresses are calculated (in Task 7); however, other subroutines are also affected (such as material model input, summation of fracture probability, damage parameter output). The resulting model will calculate a probability of fracture at each time step (or stress level) for the structure being analyzed.

3.3.1 Full-Up Tank Cars

A finite element model of a 112A340W pressure tank car was generated to analyze the loads and stresses in the tank car as a result of service and salvage operating conditions. Because the model is generated for the nonlinear dynamic finite element code DYNA3D, the model could also be used to calculate damage due to an impact with another structure in derailment or collisions.

An external view of the tank car model is shown in Figure 3. The structure includes the tank with ellipsoidal heads, manway, stub sill, bolster, and bogie structures. Figure 4 gives detailed view of the model car end structures and the associated model mesh resolution. A pressure distribution on the inside of the tank and gravitational accelerations were used as boundary conditions to include the effects of the lading and pressure loads.

20

NAM-1229-005
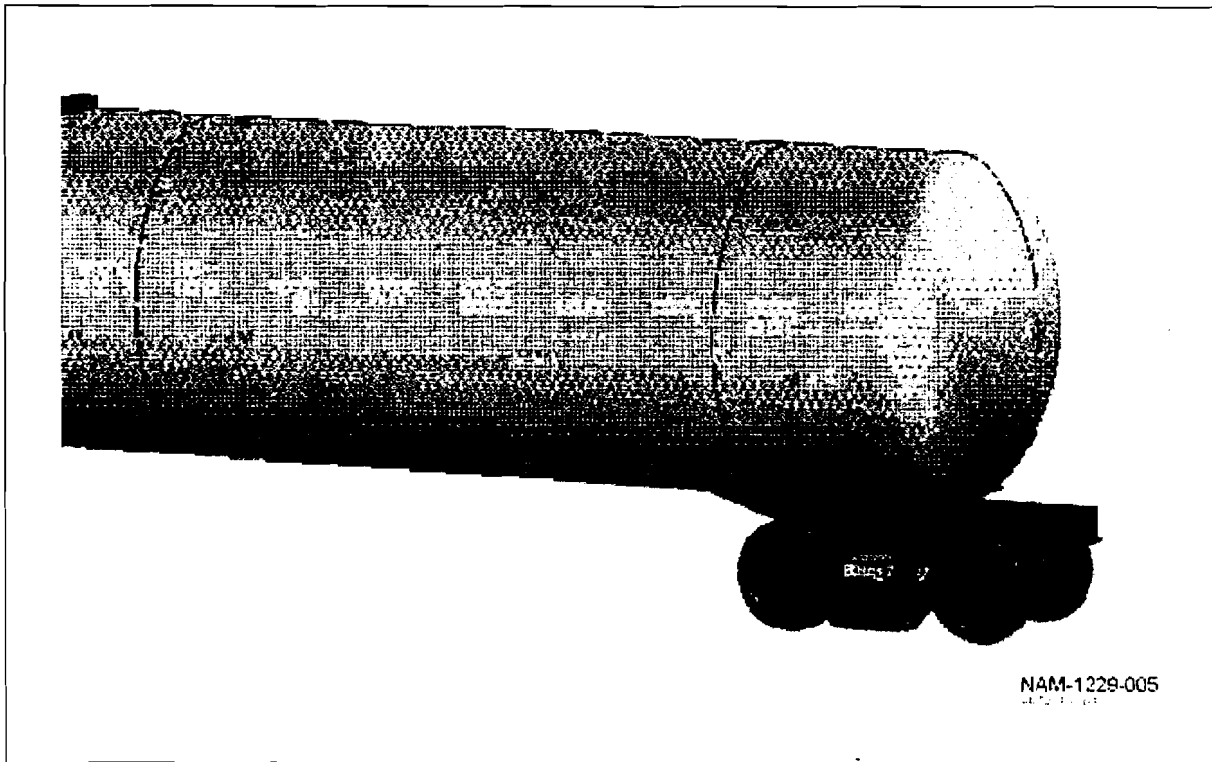
Figure 3. External View of the Tank Car Finite Element Model
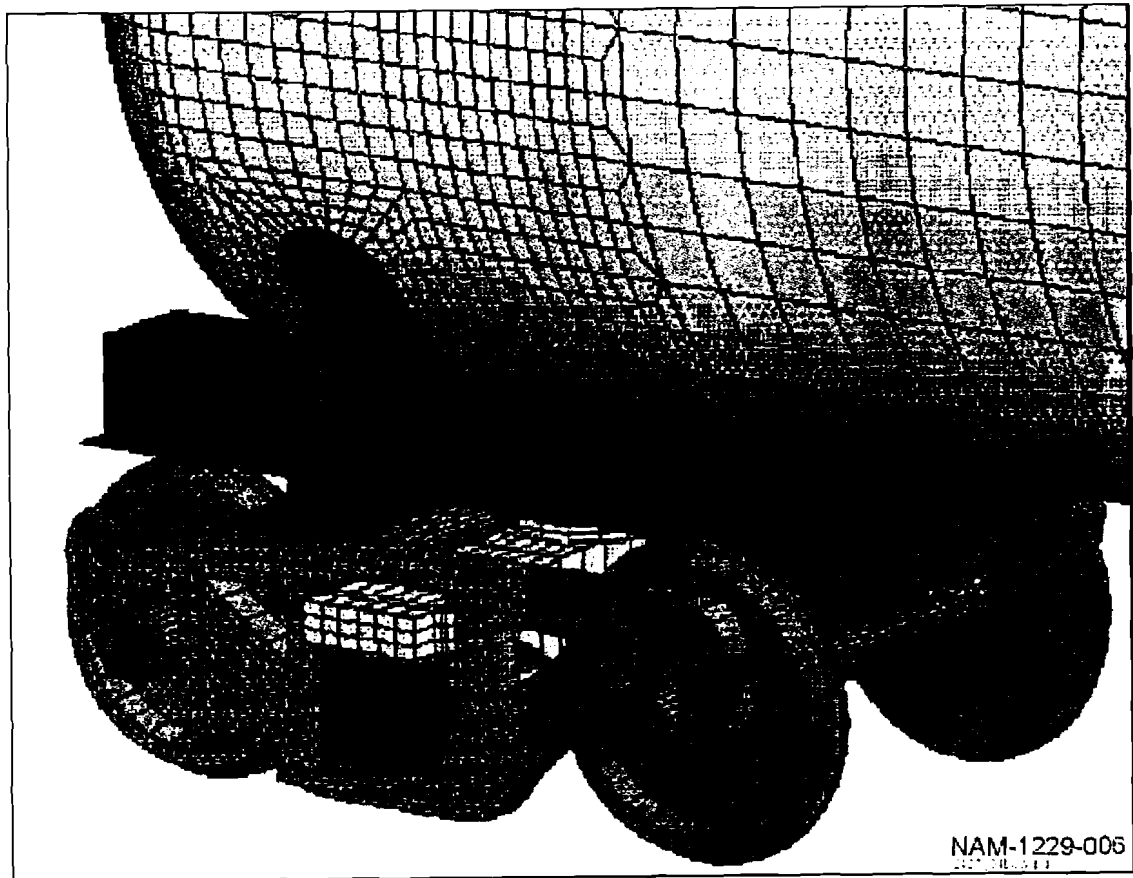
**Figure 4. Detail of the Wheelset, Stub Sill, and Suspension for the Model
Showing Mesh Resolution**

3.3.2 Ring-Section Models

For analysis of dent damage, the long longitudinal dent geometry is of particular interest. To analyze these long dents, a ring model (as shown in Figure 5) was created for the tank car to allow analysis of the tank car denting in a two-dimensional geometry. The ring model is essentially a transverse slice of the tank car. The advantage of this ring model over that of the full tank car is that the calculations can be performed in greater detail with a finer mesh resolution and still have a much shorter run time than a simulation with the full tank model.

Model of tank car ring and impactor

Ring model with mesh resolution shown
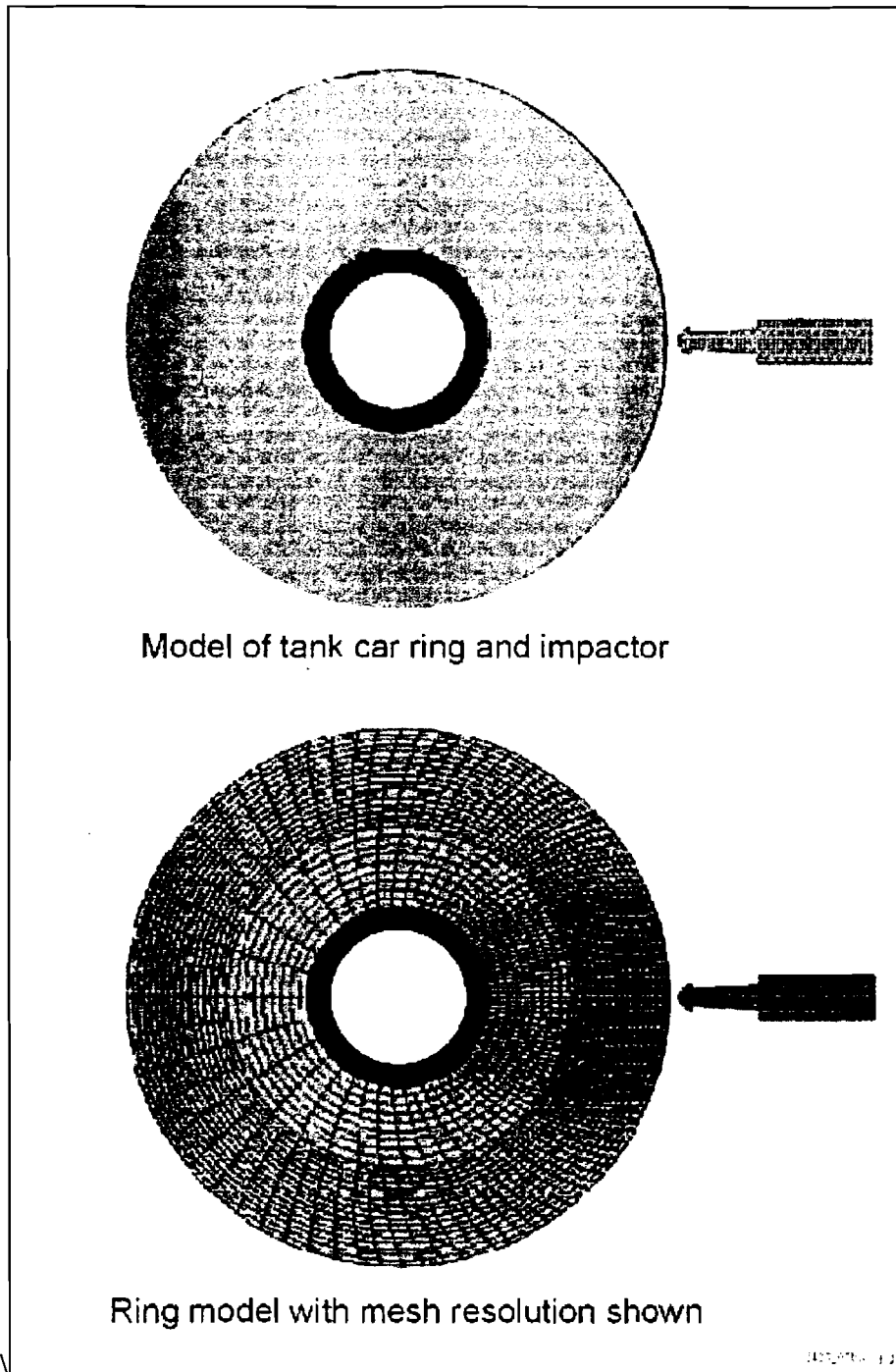
Figure 5. Finite Element Tank Car Ring Model Used to Calculate the Denting Response

In addition to the structural tank ring, we wanted to include the effects of the internal fluid within the tank. In the full tank car model, the internal pressure as well as the hydrostatic pressure gradient were added to the tank wall. However, the inertial effects of the water were not included because of the large computational effort required to model the internal fluid. For the ring models, the water could be included in the model.

When adding the internal fluid to the tank car ring model, an ullage region was needed to prevent the model from being too stiff in any response that would produce a volume change. The addition of a free surface introduces a complexity to the model because the fluid-structure interaction could produce a wave or splashing response at the free surface, which would produce severe deformations in the fluid elements and stop the simulation. To avoid these computational difficulties, the ullage region was modeled as a cylindrical bubble at the center of the tank ring and a rubber liner was added to avoid splashing at the liquid surface. Rings were loaded by impacting with the indenter shown in Figure 5.

3.3.3 Coupon Test Models

Finite element models of the smooth round bar and notched round bar tensile specimens were created as shown in Figure 6. Test data and analyses of these coupon tests were used to determine the appropriate mechanical properties for the material and to calibrate the Beremin cleavage fracture model for the two tank car materials. The finite element models of the tensile specimens had an element size of approximately 400 μm in the gauge section. To reduce the overall computational time, three planes of symmetry were used in these models to reduce the problem size by a factor of eight.

3.3.4 Engineering Test Models

Finite element models of the engineering gouge specimen and cleavage bend specimen tests were created as shown in Figures 7 and 8, respectively. Test data and analyses of these engineering tests were used to validate the Beremin cleavage fracture model. To reduce the overall computational time, two planes of symmetry were used in each of these models to reduce the problem size by a factor of four.

Smooth round bar specimen model
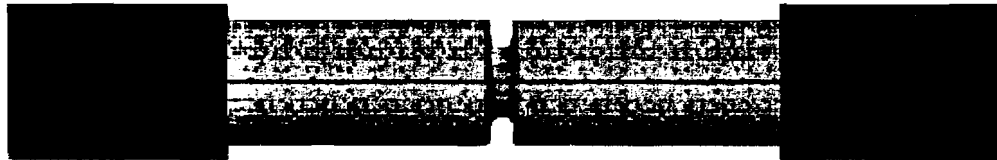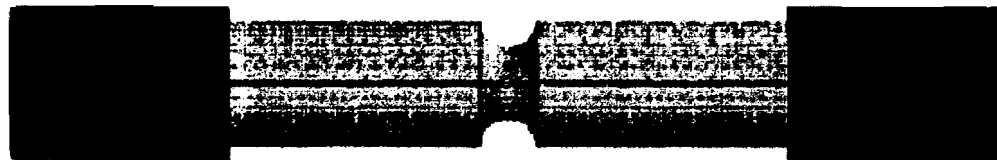
Notched round bar specimen models

Figure 6. Finite Element Models for the Smooth and Notched Tensile Test Specimens
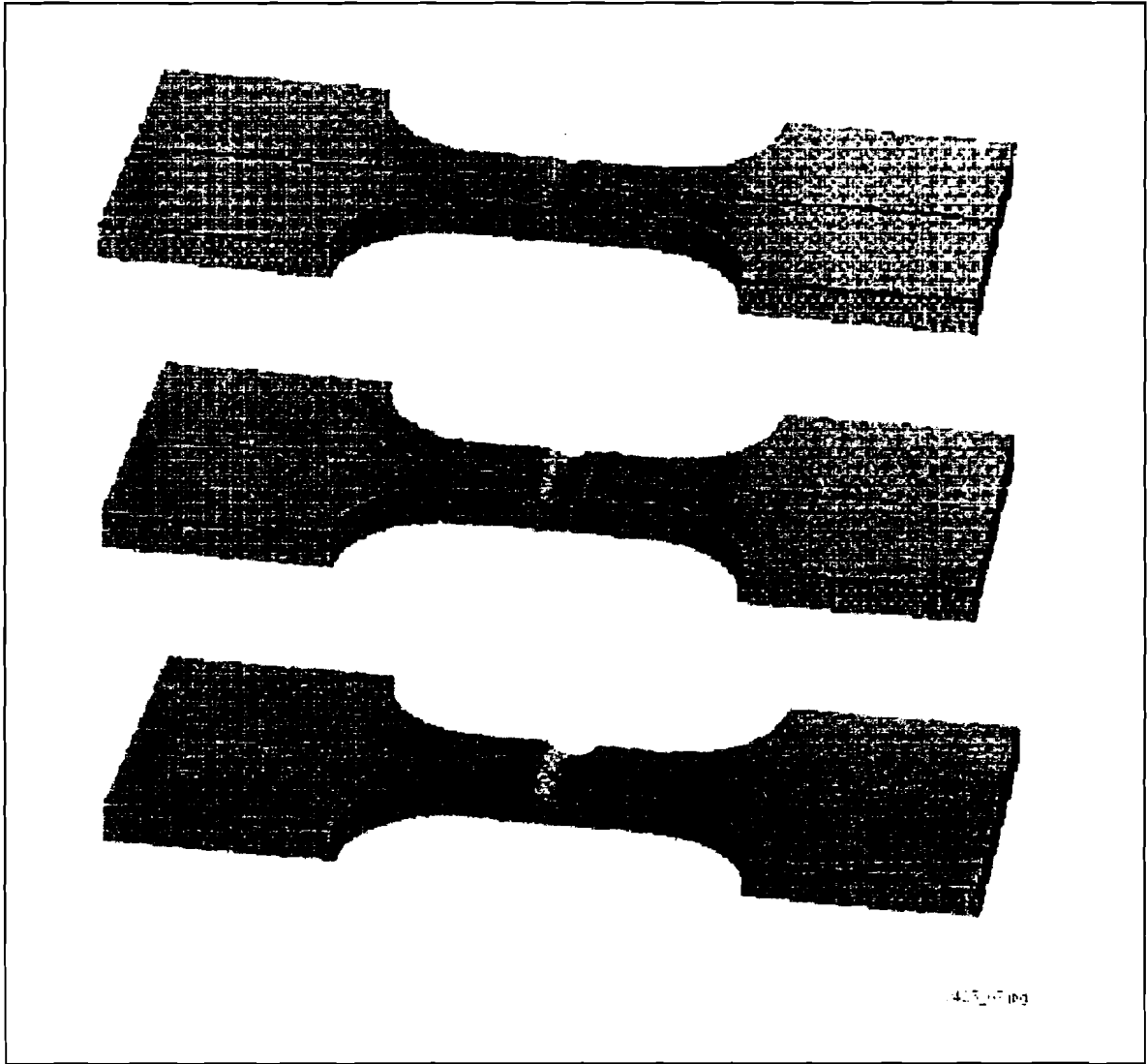
Figure 7. Example Finite Element Models for Analysis of Gouge Specimen Engineering Tests
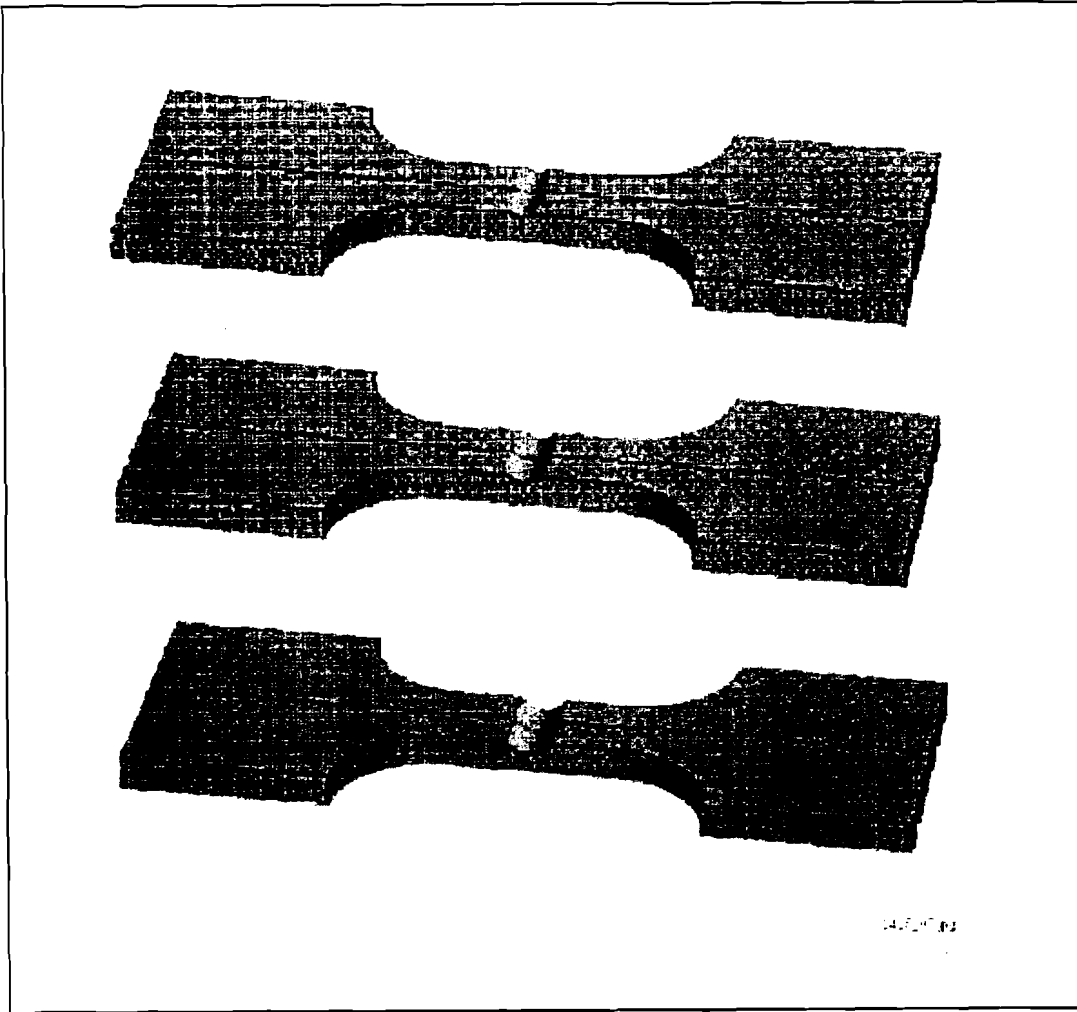
Figure 8. Finite Element Model for the Bend Coupon Engineering Test

3.4 COUPON TESTS FOR MODEL CALIBRATION

All coupon tests were performed using a 100-kip MTS servohydraulic testing machine under displacement control. During the tests, ram displacement, load, extensometer output(s), and thermocouple output were recorded digitally. Thermocouples were welded directly to the coupons near the test section. For low temperature tests, specimens were either immersed in liquid nitrogen and cooled to -321°F (-196°C), placed in the testing machine, allowed to warm to the desired temperature, then tested, or they were placed in an insulated box surrounding the grip area of the testing machine and liquid nitrogen was piped into the box until the desired temperature was reached.

27

3.4.1 Smooth Round Bar Tests

Smooth round bar tensile tests were performed at various temperatures to establish the stress-strain behavior of the steels and the increase in flow strength with decreasing temperature. The smooth round bar test specimen is sketched in Figure 9. During the tests, a 1-inch (25.4-mm) gauge length extensometer was installed to record engineering strain. Post-test, failed neck diameters were measured to provide the final true strain for input to the finite element model. All tests were performed at $\square 10^{-3}$ s^{-1} strain rate.

3.4.2 Notched Round Bar Tests

Notched round bar tensile tests were performed to establish the stress-strain and fracture behavior of the steels under varying levels of triaxial constraint. The tests were also simulated using the finite element model, and model parameters were adjusted until agreement between tests and models was obtained. In this way, both the plastic flow and cleavage failure portions of the models were calibrated to the steels used throughout the program. The notched round bar test specimens are also sketched in Figure 9. TC-128B and A515-70 specimens were machined with three notch root radii: 0.25-in., 0.1-in., and 0.05-in. (6.35 mm, 2.54 mm, and 1.27 mm). Weld specimens were machined with only the two smaller root radii, and the reduced section was machined such that the smallest diameter was in the middle of the heat-affected zone.

During the notched round bar tests, a 1-inch (25.4-mm) gauge length extensometer was again installed such that the gauge length straddled the specimen notch. The extensometer output was used to verify the displacement computed in the finite element model. In a few room temperature tests, a radial extensometer was also applied to measure the change in specimen diameter as necking proceeded. For the tests in the cleavage regime (-238°F or -150°C), however, the radial extensometer was unnecessary because the amount of necking was insignificant. All tests were performed at $\square 10^{-3}$ in./s (25 µm/s) displacement rate.

28
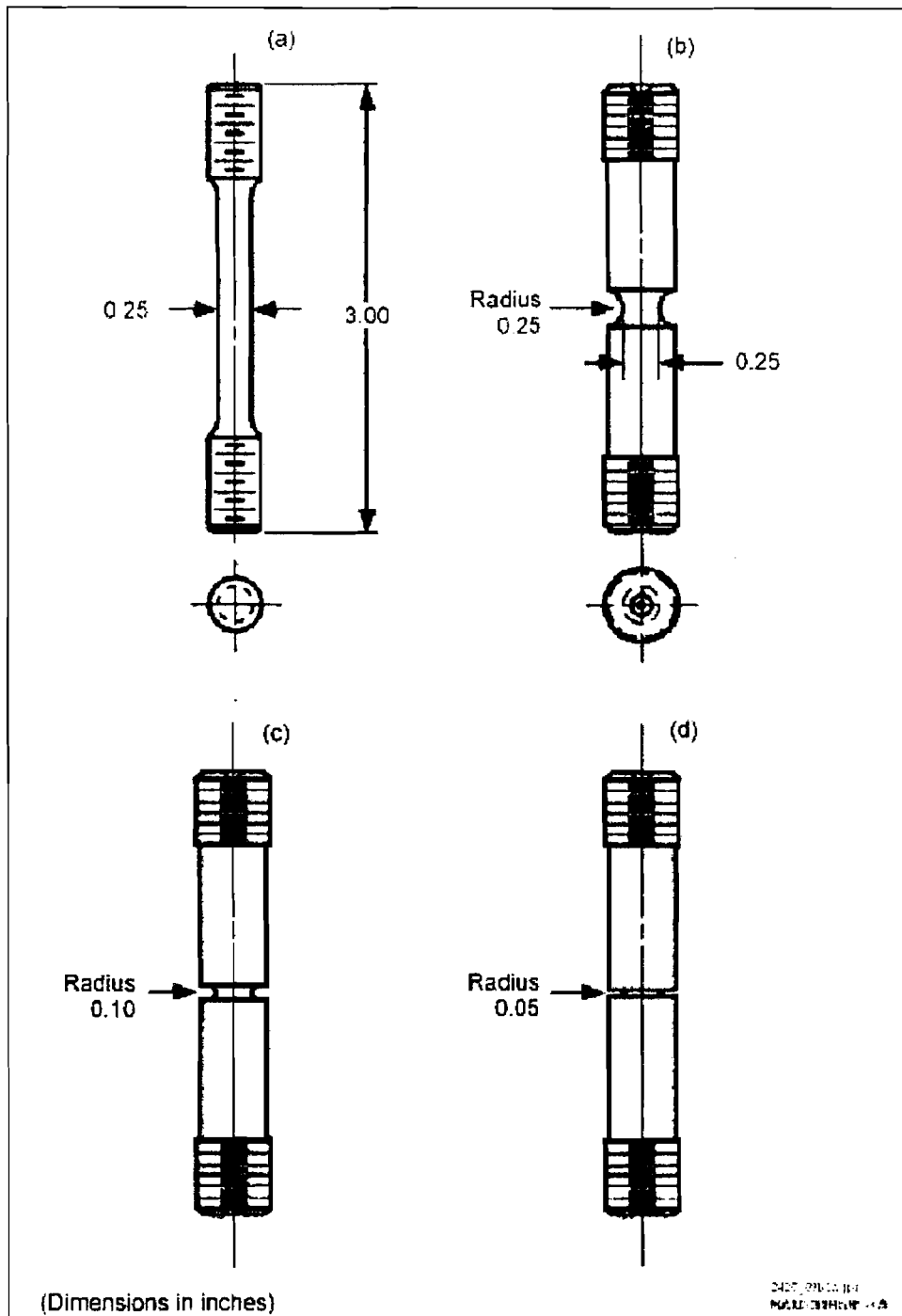
Figure 9. Round Bar Tensile Specimens: (a) Smooth, (b)-(d) Notched

3.5 COUPON TESTS FOR ENGINEERING APPROACH AND MODEL VALIDATION

3.5.1 Gouge Tests

As part of the engineering approach, coupon tests with simulated gouges were performed. These tests provided a direct attempt to validate the gouge Guidelines and to further validate the calibrated finite element models. Gouge specimens and the loading fixture are sketched in Figure 10. The specimens all had the same width (1.75 in or 44.5 mm), the same gouge depth (0.25 in. or 6.35 mm), and were of the as-rolled thickness, but two different gouge root radii, 0.5 in. (12.7 mm) and 0.125 in. (3.2 mm), were tested. All gouge tests were performed in the cleavage regime at a loading rate around 0.1 in./s (2.5 mm/s). Extensometers were installed on the front and back faces of the specimens, bridging the notches, to verify the displacements computed in the finite element models and to measure the amount of bending induced by the asymmetry of the specimen and loading.

3.5.2 Cleavage Bend Tests

As a second part of the engineering approach, three-point bending coupon tests were performed. These tests were meant to simulate dent formation and to provide further validation of the finite element model. As shown in Figure 11, the specimens were 5 x 6.5-in. (127 × 153-mm) plates, 0.596 in. (15.1 mm) thick. The supports were 1-in.-diameter (25.4-mm-diameter) hardened rods spaced 3.30 in. (83.8 mm) apart. The load and deflection were recorded. The plates were ground on both faces to remove the rusty mill finish and to ensure parallelism. In addition, as-received plate edges were cut back at least 0.5 in. (12.7 mm). The edges of the A515-70 were received flame-cut and were particularly hard and brittle; cracks would have initiated there had the edges not been removed. Tests were performed at room temperature, -112°F (-80°C), and -238°F (-150°C), with and without welds. Welds were oriented such that the line of the weld ran from support to support down the middle of the plate.

Figure 10. Simulated Gouge Specimens

1.000 in. D

3.313 in.

0.596

Welded specimens oriented as shown

5 in. 6.5 in.
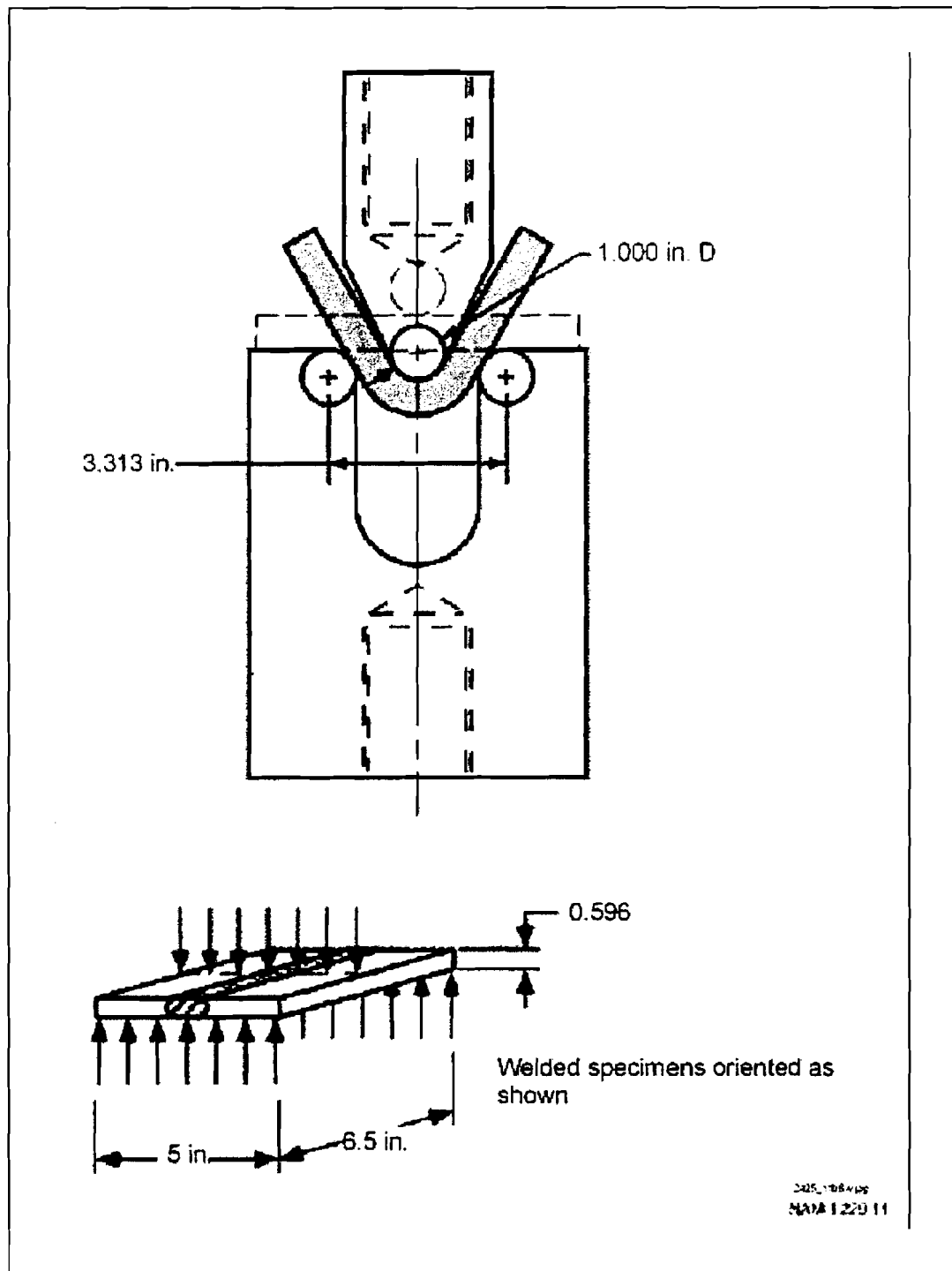
Figure 11. Bend Test Setup

3.5.3 Cleavage Bend Tests

As a second part of the engineering approach, three-point bending coupon tests were performed. These tests were meant to simulate dent formation and to provide further validation of the finite element model. As shown in Figure 11, the specimens were 5 x 6.5-in. (127 x 153-mm) plates, 0.596 in. (15.1 mm) thick. The supports were 1-in.-diameter (25.4-mm-diameter) hardened rods spaced 3.30 in. (83.8 mm) apart. The load and deflection were recorded. The plates were ground on both faces to remove the rusty mill finish and to ensure parallelism. In addition, as-received plate edges were cut back at least 0.5 in. (12.7 mm). The edges of the A515-70 were received flame-cut and were particularly hard and brittle; cracks would have initiated there had the edges not been removed. Tests were performed at room temperature, -112°F (-80°C), and -238°F (-150°C), with and without welds. Welds were oriented such that the line of the weld ran from support to support down the middle of the plate.
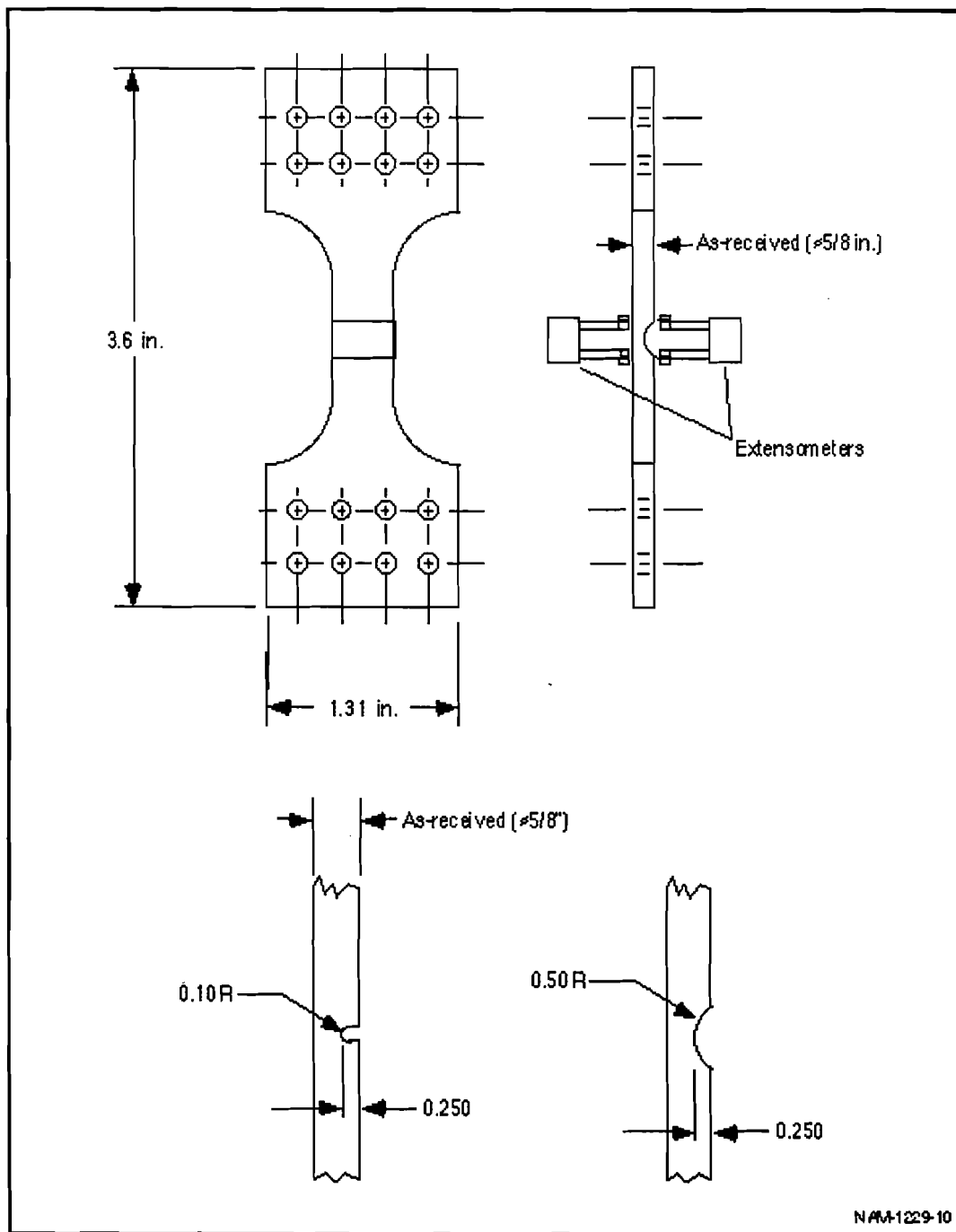
3.5.4 Dent/Undent Tests

To simulate the effects of denting followed by pressurization, we bent samples of tank car plate in three-point bending using the same fixture as in the cleavage bend tests described above (see Figure 12). We then pulled the samples in tension (as shown schematically in Figure 13), which straightened the dents. We continued pulling to failure. Specimens were prepared from spare gouge specimens by grinding the gouged face until the gouge disappeared. Specimens were tested with the ground face in tension and the as-rolled mill scale surface in tension. We recorded load and load-point displacement during both the denting and straightening phases of the tests. Tests were performed at room temperature and at -40° C (-40°F).

3.5.5 Fracture Mechanics Tests

We followed the test methods outlined in ASTM E-813 [15] and E-1152 [16] to obtain J_{IC} and J-R curves. We tested A515 Grade 70 (A212B Grade 70) compact tension specimens cut from undeformed areas of the cleavage bend specimens. We also tested two specimens of TC-128B as-rolled (non-normalized) cut from a tank car that fractured unexpectedly (see Appendix B). We did not test the TC-128B normalized steel, because this steel was expected to have far better fracture properties than A515-70. We tested the A515-70 specimens at room temperature and at -40° F (-40°C). We tested the as-rolled TC-128B at -10° F (-23°C). We used the compliance method to measure the crack lengths during the tests. We cut sidegrooves in the specimens to encourage formation of a straight starting crack front.

Dent/undent test specimen. Thickness is approximately 0.54 in.

Dent test configuration

2425_12b&w.jpg
NAM-1229-34
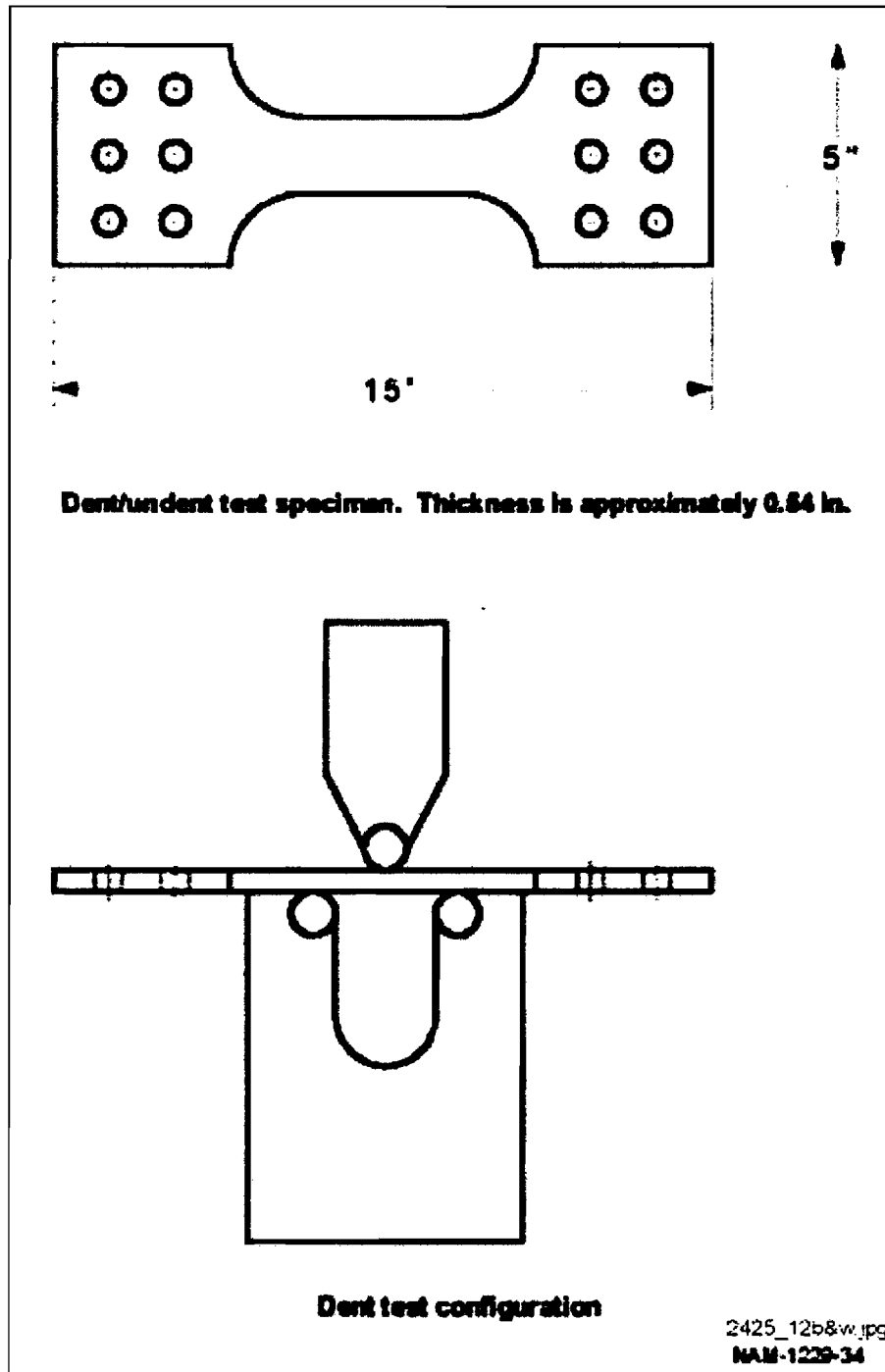
Figure 12. Specimen and Configuration for Dent/Undent Test

34

Typical
failure locations

NAM-1229-35
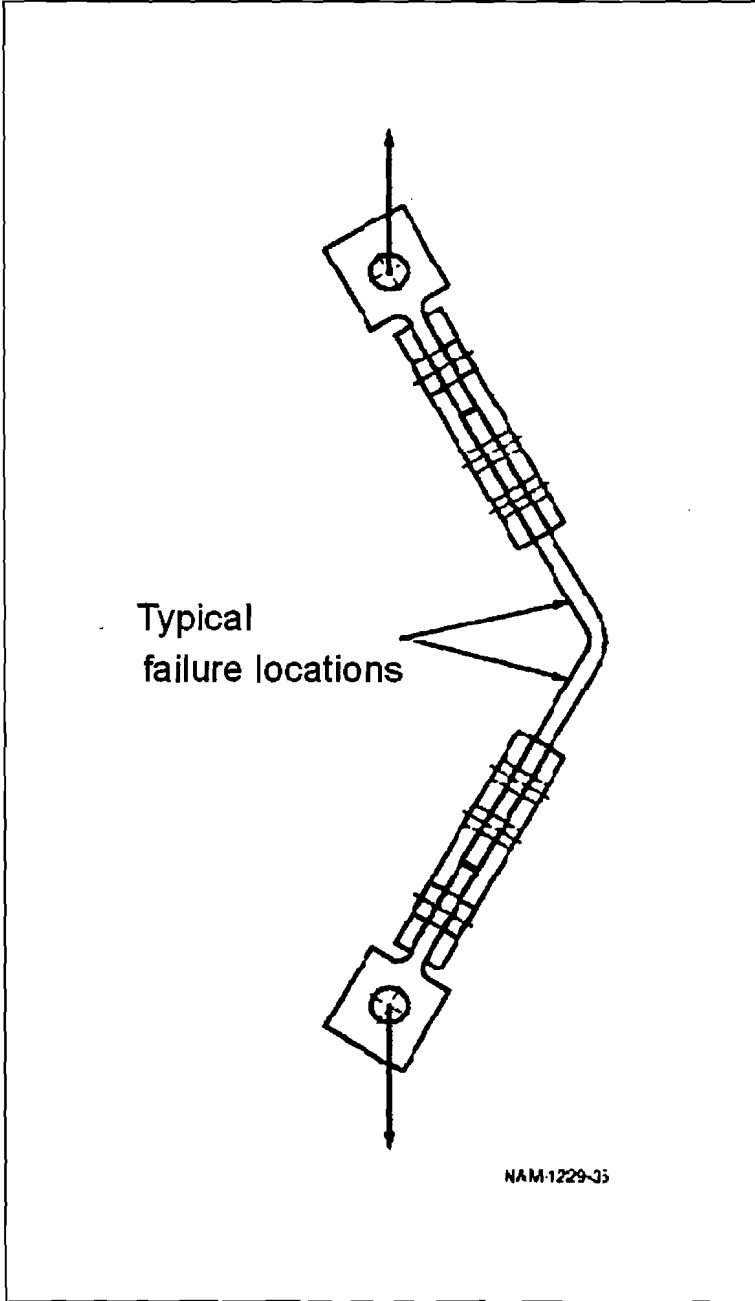
Figure 13. Configuration of Undent Tests

4.0 RESULTS

4.1 LOCAL FRACTURE APPROACH

The smooth round bar tensile stress-strain curves are shown in Figure 14 in terms of engineering stress and engineering strain. The notched round bar tensile stress-displacement curves are shown in Figure 15. The stress value is the load divided by the original diameter at the root of the notch.

The results of the coupon tests were used to calibrate the Beremin cleavage model. The approach is to first use the smooth round bar test to obtain the true stress versus plastic strain curve for the material. This curve can be estimated from the experimental curve from measurements of the necking behavior and measurement of the engineering stress-strain behavior. Performing simulations of the smooth round bar tensile test and making adjustments to the material parameters until the necking behavior is accurately reproduced can further refine the true stress curve. The resulting engineering stress-strain curve for the A515-70 tank car steel is shown in Figure 16. Table 5 gives the effective stress versus plastic strain curves determined for the two tank car steels at -238°F (-150°C).
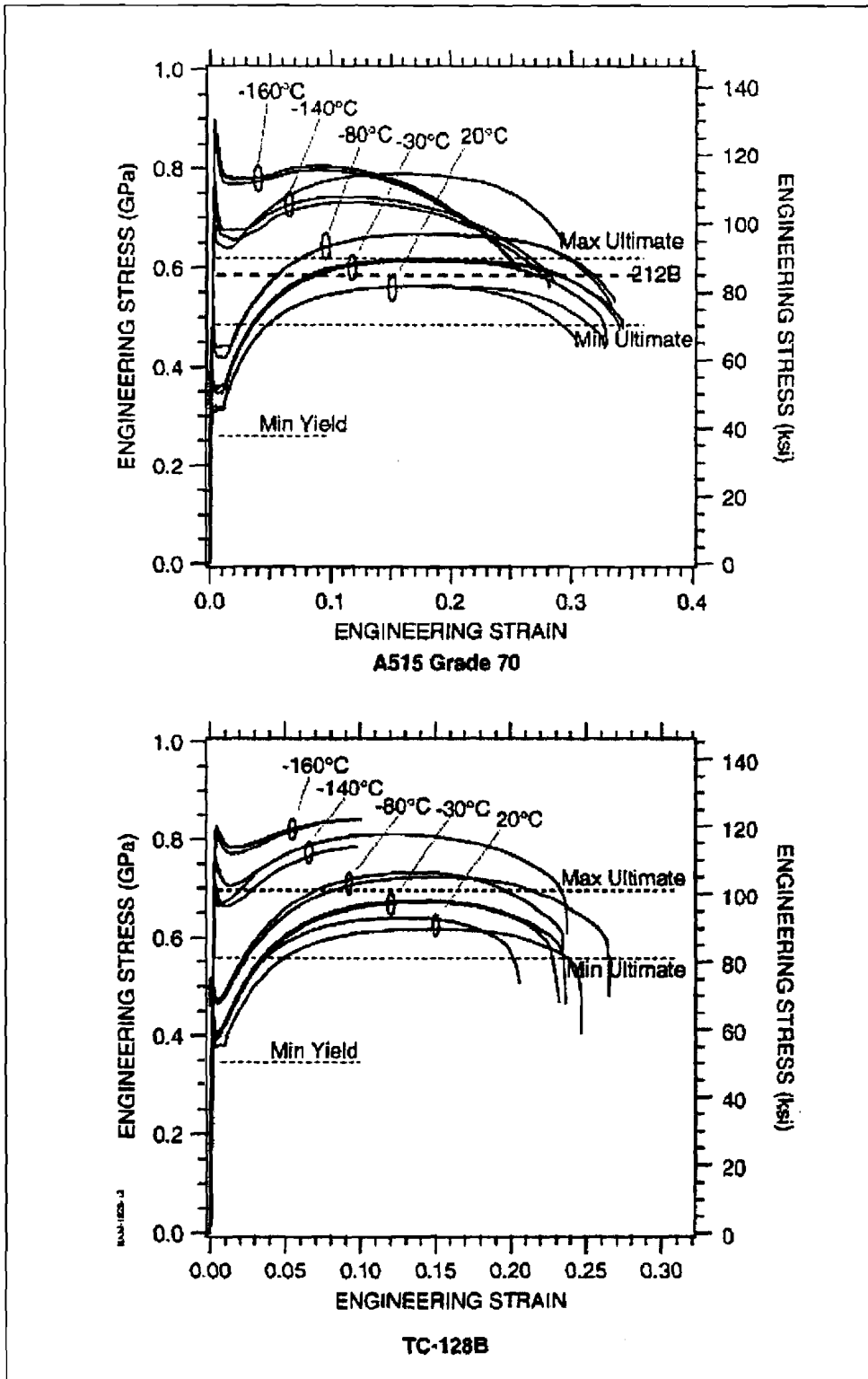
Figure 14. Engineering Stress-Strain Curves from Smooth
Round Bar Laboratory Results
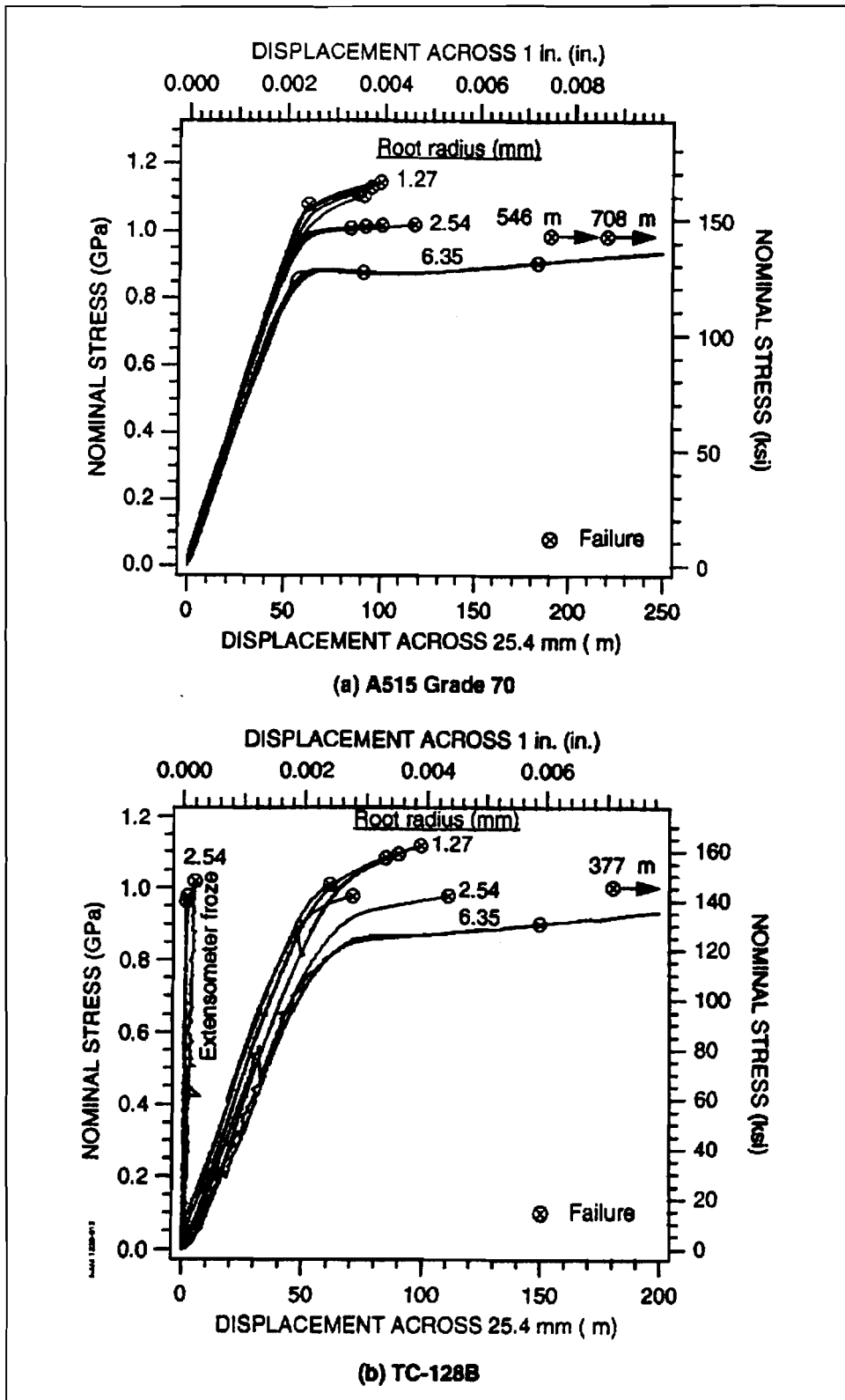
Figure 15. Tensile Stress-Displacement Curves from Notched
Round Bar Laboratory Test Results

38
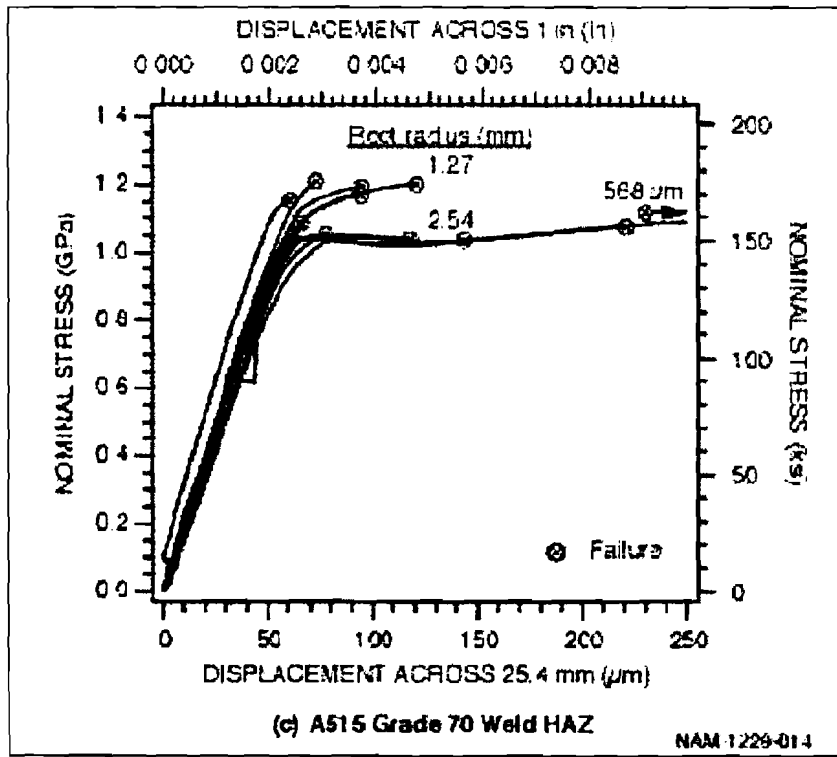
Figure 15 (continued). Tensile Stress-Displacement Curves from Notched Round Bar Laboratory Test Results
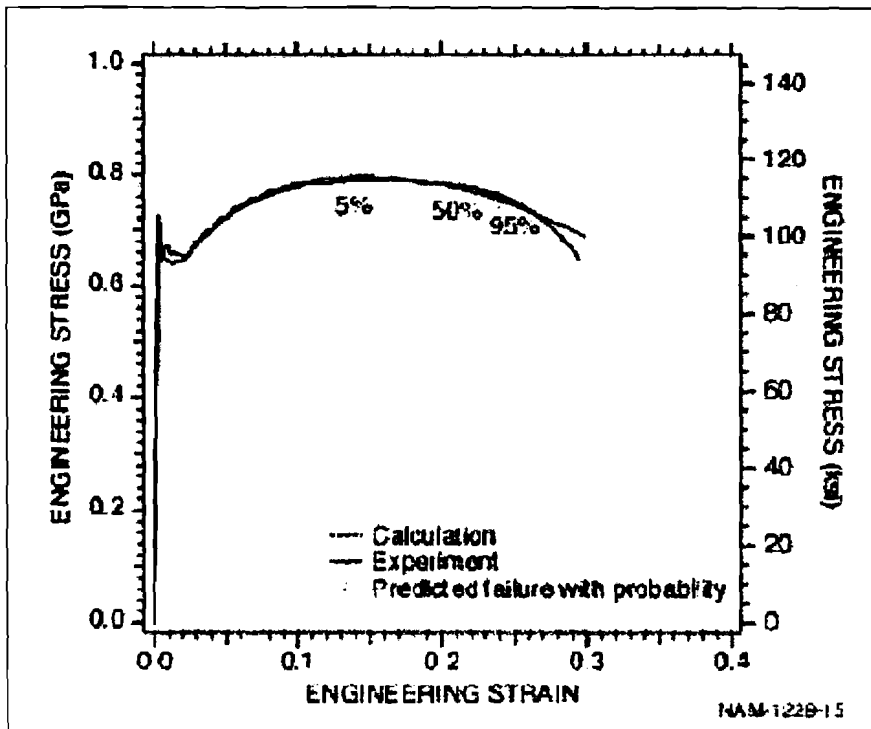
Figure 16. Comparison of Measured and Computed A515-70 Smooth Round Bar Stress Strain Behavior (-238°F or -150°C)

39

Table 5. Stress-Strain Curves for the Tank Car Steels at -238°F (-150°C)

| TC-128B True Stress-Strain Curve		A515-70 True Stress-Strain Curve	
Plastic Strain	Effective Stress (MPa)	Plastic Strain	Effective Stress (MPa)
0.000e+00	625.0	0.000e+00	728.5
5.000e-05	641.0	1.000e-03	702.4
1.030e-04	656.0	2.000e-03	669.3
1.560e-04	669.0	2.500e-03	660.0
2.060e-04	6754.0	3.000e-03	655.9
2.560e-04	679.2	4.000e-03	653.6
2.960e-04	681.0	8.000e-03	648.6
3.510e-04	683.8	9.000e-03	647.6
4.160e-04	686.0	1.000e-02	648.0
4.620e-04	686.4	1.600e-02	655.7
5.140e-04	687.0	1.700e-02	657.8
5.550e-04	686.9	1.800e-02	661.0
6.050e-04	686.6	1.900e-02	664.6
7.070e-04	685.5	2.000e-02	668.5
7.660e-04	684.6	2.200e-02	676.3
8.790e-04	682.6	2.400e-02	683.9
9.940e-04	680.0	2.600e-02	691.8
1.270e-03	674.9	2.800e-02	699.5
1.470e-03	671.8	3.000e-02	706.8
1.840e-03	669.2	3.500e-02	724.4
2.300e-03	667.8	4.000e-02	741.3
3.120e-03	667.9	4.500e-02	756.2
4.600e-03	669.9	5.000e-02	770.9
6.020e-03	672.1	6.000e-02	796.0
7.520e-03	674.7	7.000e-02	817.7
9.030e-03	676.5	8.000e-02	836.4
1.000e-02	678.5	9.000e-02	853.3
1.200e-02	682.7	1.000e-01	868.4
1.400e-02	687.8	1.100e-01	881.4
1.600e-02	693.5	1.200e-01	893.4
1.800e-02	698.6	1.300e-01	904.0
2.000e-02	704.2	1.400e-01	914.0
2.200e-02	711.1	1.500e-01	923.0
2.400e-02	717.2	1.600e-01	931.0
2.600e-02	723.9	1.700e-01	939.0
2.800e-02	731.0	1.800e-01	948.0
3.000e-02	738.7	1.900e-01	954.0
3.500e-02	755.8	2.000e-01	963.0

Table 5 (continued). Stress-Strain Curves for the Tank Car Steels at -238°F (-150°C)

TC-128B True Stress-Strain Curve		A515-70 True Stress-Strain Curve	
Plastic Strain	Effective Stress (MPa)	Plastic Strain	Effective Stress (MPa)
4.000e-02	772.2	2.500e-01	100.0
4.500e-02	786.6	3.000e-01	103.4
5.000e-02	800.8	3.500e-01	106.8
6.000e-02	822.9	4.000e-01	110.0
7.000e-02	841.6	4.500e-01	112.9
8.000e-02	857.3	5.000e-01	115.8
9.000e-02	871.2	5.500e-01	118.7
1.000e-01	884.3	6.000e-01	121.4
1.100e-01	895.8	6.450e-01	124.0
1.200e-01	906.4	—	—
1.300e-01	916.2	—	—
1.400e-01	925.3	—	—
1.500e-01	933.1	—	—
1.600e-01	940.5	—	—
1.700e-01	947.5	—	—
1.800e-01	954.9	—	—
1.900e-01	960.6	—	—
2.000e-01	967.2	—	—
2.500e-01	995.5	—	—
3.000e-01	102.1	—	—
3.500e-01	104.6	—	—
4.000e-01	106.6	—	—
4.500e-01	108.5	—	—
5.000e-01	110.4	—	—
5.500e-01	112.4	—	—
6.000e-01	114.0	—	—
6.450e-01	115.8	—	—
4.000e-01	106.6	—	—
4.500e-01	108.5	—	—
5.000e-01	110.4	—	—
5.500e-01	112.4	—	—
6.000e-01	114.0	—	—
6.450e-01	115.8	—	—

The next step is to use the stress-strain behavior from the smooth round bar to analyze the notched round bar specimens. Figure 17 compares these measured and calculated notched round bar behaviors for the A515-70 steel. With these simulations, the cleavage stress (s_u) can be varied until a good match between predicted and measured rupture stresses is obtained.

For a given value of the cleavage stress, a probability of rupture can be determined at any load level. The notched round bar simulations with the 5%, 50%, and 95% rupture probability loads indicated are shown in Figure 18. The calibrated parameters determined for the Beremin cleavage model for the two tank car steels are given in Table 6.

Figure 17. Calculated and Measured Notched Round Bar Stress-Displacement Curves for A515-70 (-238° F or -150° C)

Figure 18. Calculated Notched Round Bar Stress-Displacement Curves for A515-70 with Rupture Probabilities Indicated (-238°F or -150°C)

Table 6. Tank Car Material Parameters for the Beremin Cleavage Model

Tank Car Material	Characteristic Volume (V_0)	Cleavage Stress (σ_u)	Microcrack Exponent (m)
TC-128B	(200 mm)3	1.65 GPa	22
A515-70	(200 mm)3	1.75 GPa	22

The statistical nature of cleavage fracture can be seen by normalizing all the notched round bar failure stresses by the predicted 50% probability load level. These normalized failure stresses can then be plotted against a normalized rupture probability curve as shown in Figure 19 for the A515-70 steel. This fit is good over the full range of tests performed.

The comparable tensile coupon test measurements and cleavage model predictions for the calibrated TC-128B tank car steel at -238°F (-150°C) are shown in Figures 20 through 23.

43

Figure 19. Summary of A515-70 Notched Round Bar Tests at -238° F (-150°)
Compared with the Normalized Cleavage Probability Curve
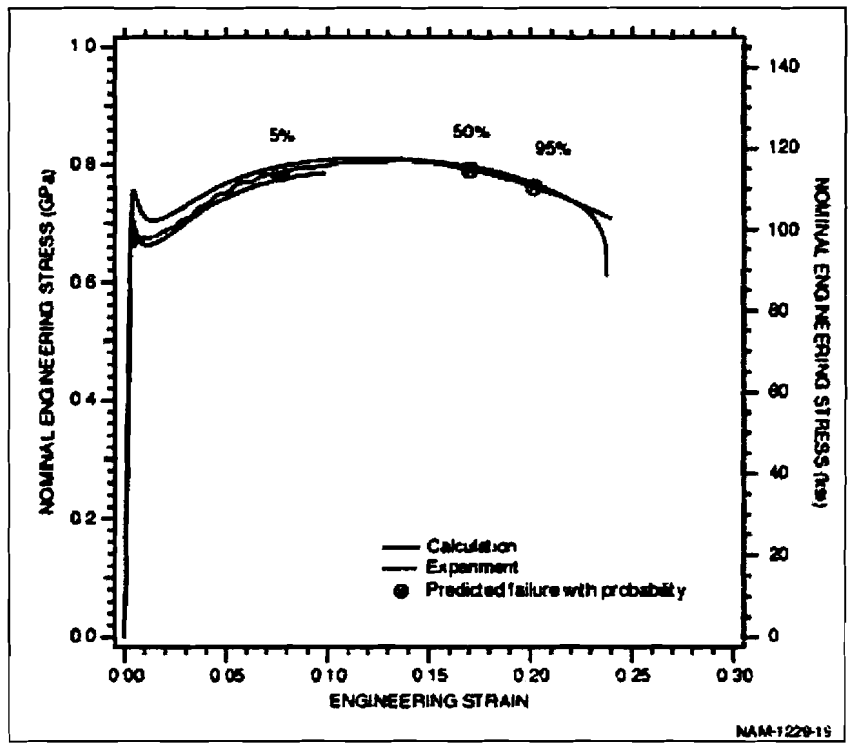
Figure 20. TC-128B Smooth Round Bar Stress-Strain Behavior with
Calculated Cleavage Rupture Probabilities Indicated (-238° F or -150° C)
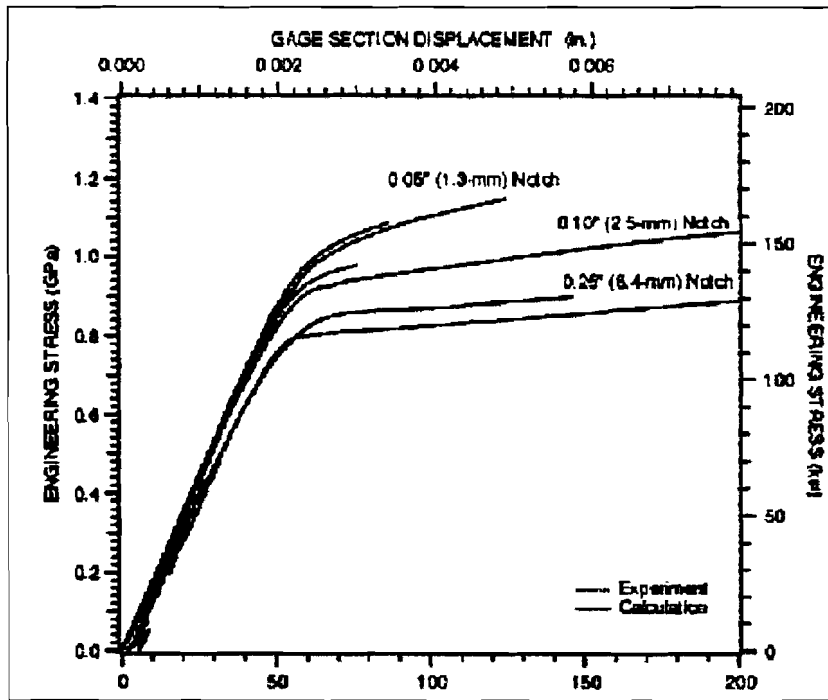
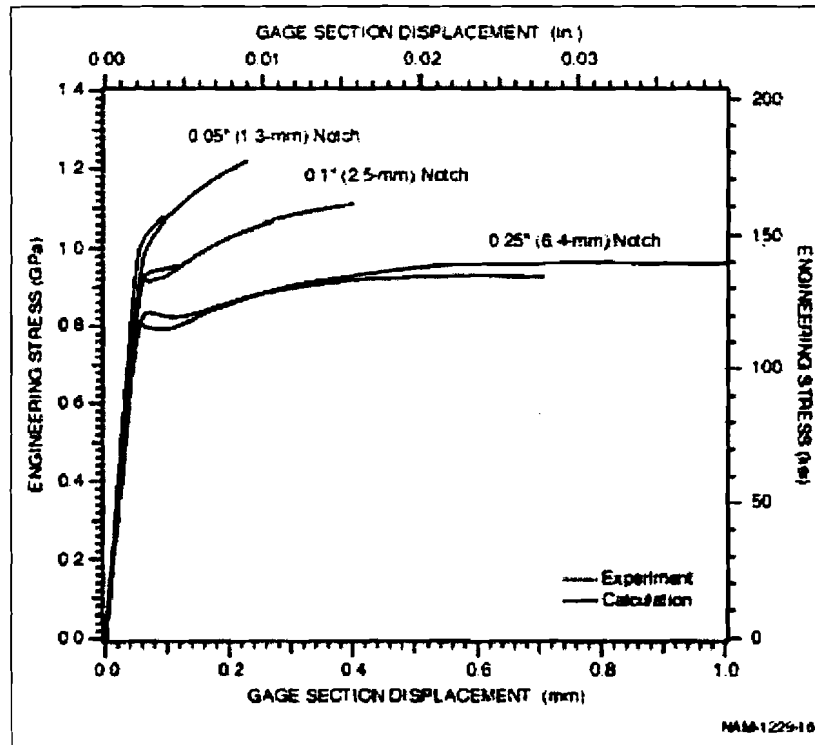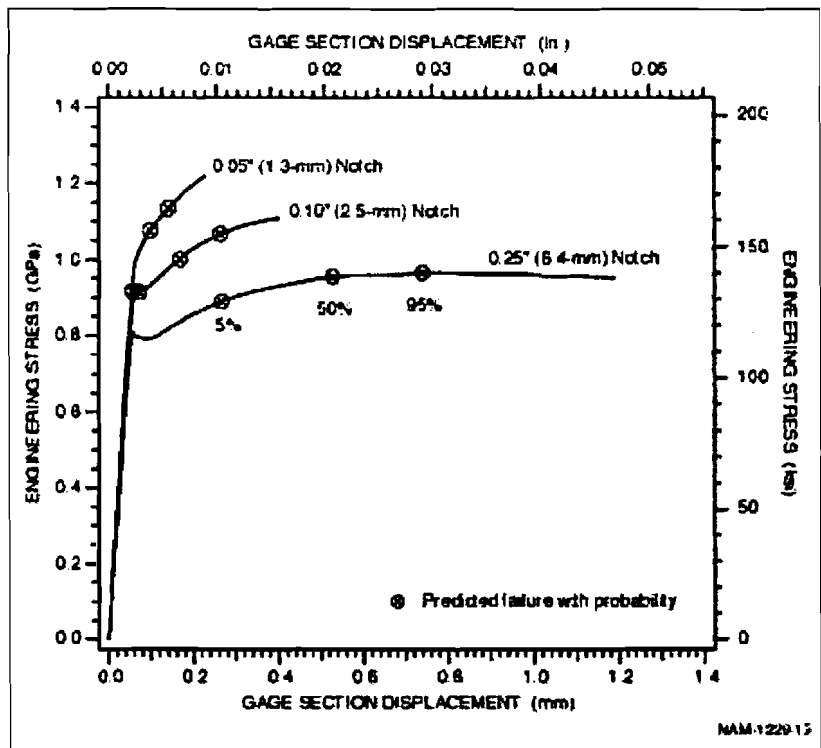**Figure 21. Calculated Notched Round Bar Stress-Displacement Curves for TC-128B (-238°F or -150°C)**
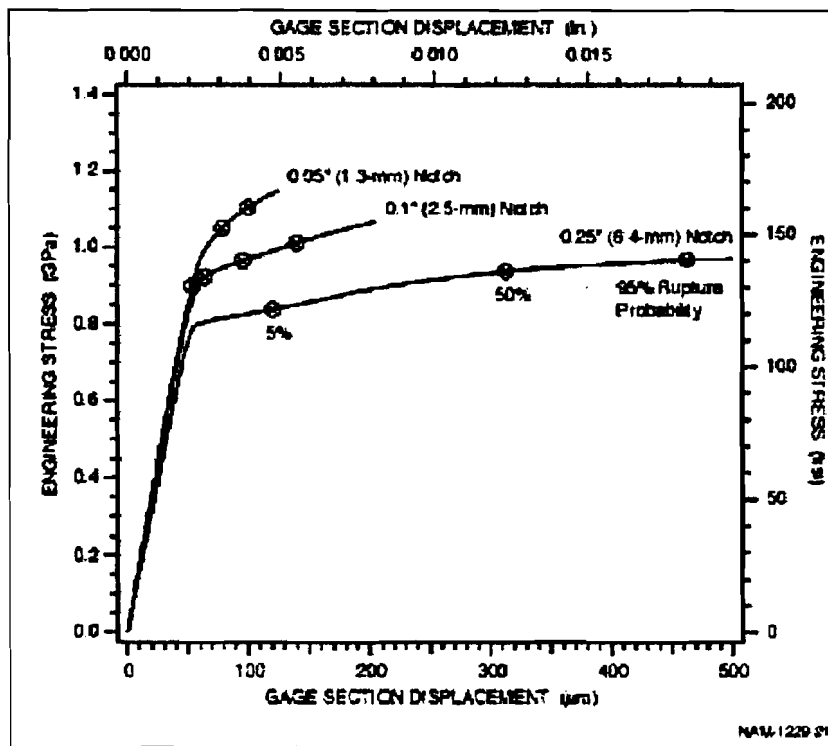
Figure 22. Calculated Notched Round Bar Stress-Displacement Curves, for TC-128B with Rupture Probabilities Indicated (-238° F or -150° C)
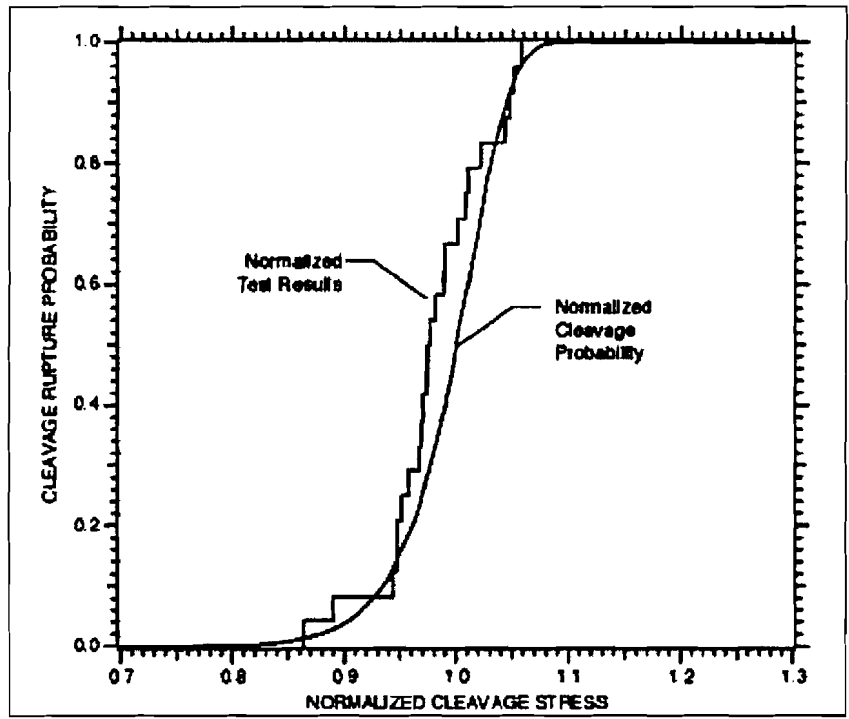
45
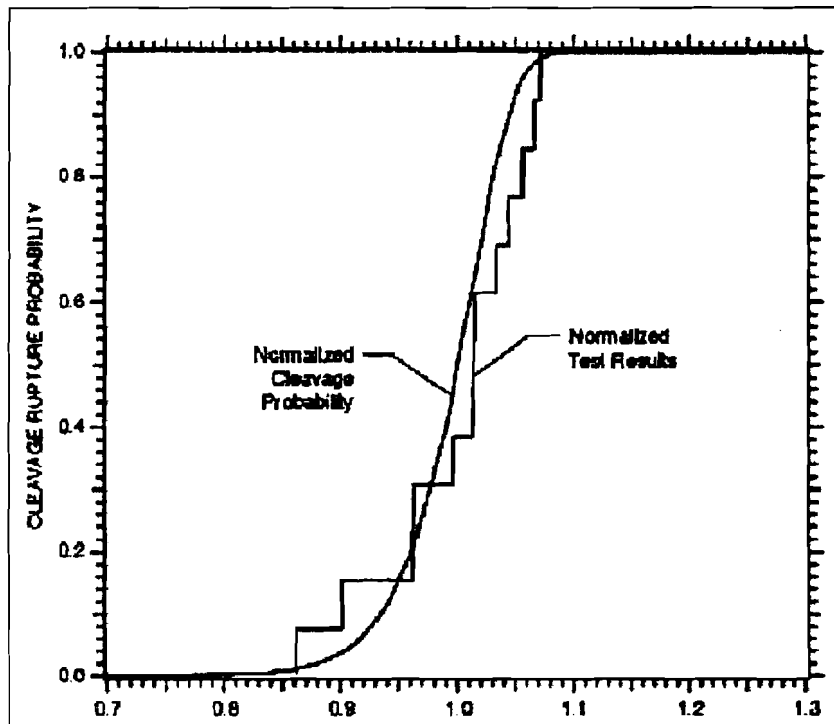
Figure 23. Summary of TC-128B Notched Round Bar Tests at –238° F (-150° C) Compared with the Normalized Cleavage Probability Curve

4.2 ENGINEERING APPROACH

4.2.1 Coupon Test and Finite Element Modeling Results

Figure 24 summarizes the gouge test results. Included in the figure are allowable levels of hoop stress from Table 1 of the Guidelines. Hoop stresses are obtained from Table 1 pressures by assuming a tank radius of 60 in. (1.52 m) and a wall thickness of 5/8 in. (15.9 mm).

The finite element simulations of the gouge tests on the A515-70 and TC-128B materials are shown in Figures 25 and 26, respectively. The predicted load displacement behavior for the bend tests agrees well with the measured values. The discrepancies between measured and predicted stress-displacement behaviors can be attributed to slight temperature variations between specimens and the small increase in temperature that occurs during the experiment.

The cleavage model does a good job of predicting the cleavage rupture of the gouge specimens with the exception of the 1/8-in. gouge radius with the TC-128B tank car material, for which the model is conservative. The reason for this discrepancy cannot be determined without additional testing to provide a greater statistical database for calibration and validation of the cleavage

46

model. However, the overall agreement of the model and testing is good and, as shown below, the nonconservative nature of the 1/8-in. TC-128B gouge results does not affect the validation.

4.2.2 Cleavage Bend Tests

Figure 27 summarizes the results of the cold bend tests on A515-70, welded A515-70, and TC-128B performed around -238°F (-150°C). In all cases, cleavage fracture initiated at relatively large (≈30-in. or 760 mm) radii of curvature. Figure 27 also includes the bending moment per unit width on the right-hand axis. Bend tests were also performed at room temperature on a welded A515-70 plate and at -112°F (-80°C) on TC-128B as-rolled plate. In both cases, bends sharper than 1-in. (25.4-mm) radius of curvature were reached without fracture.

The finite element simulations of the bend tests on the A515-70 and TC-128B materials are shown in Figures 28 and 29, respectively. The predicted load displacement behavior for the bend tests is significantly different from those measured in the experiments. We believe that this difference is a result of the changes in temperature level and distribution in the specimen during the experiment due to heat conducting in from the supports.
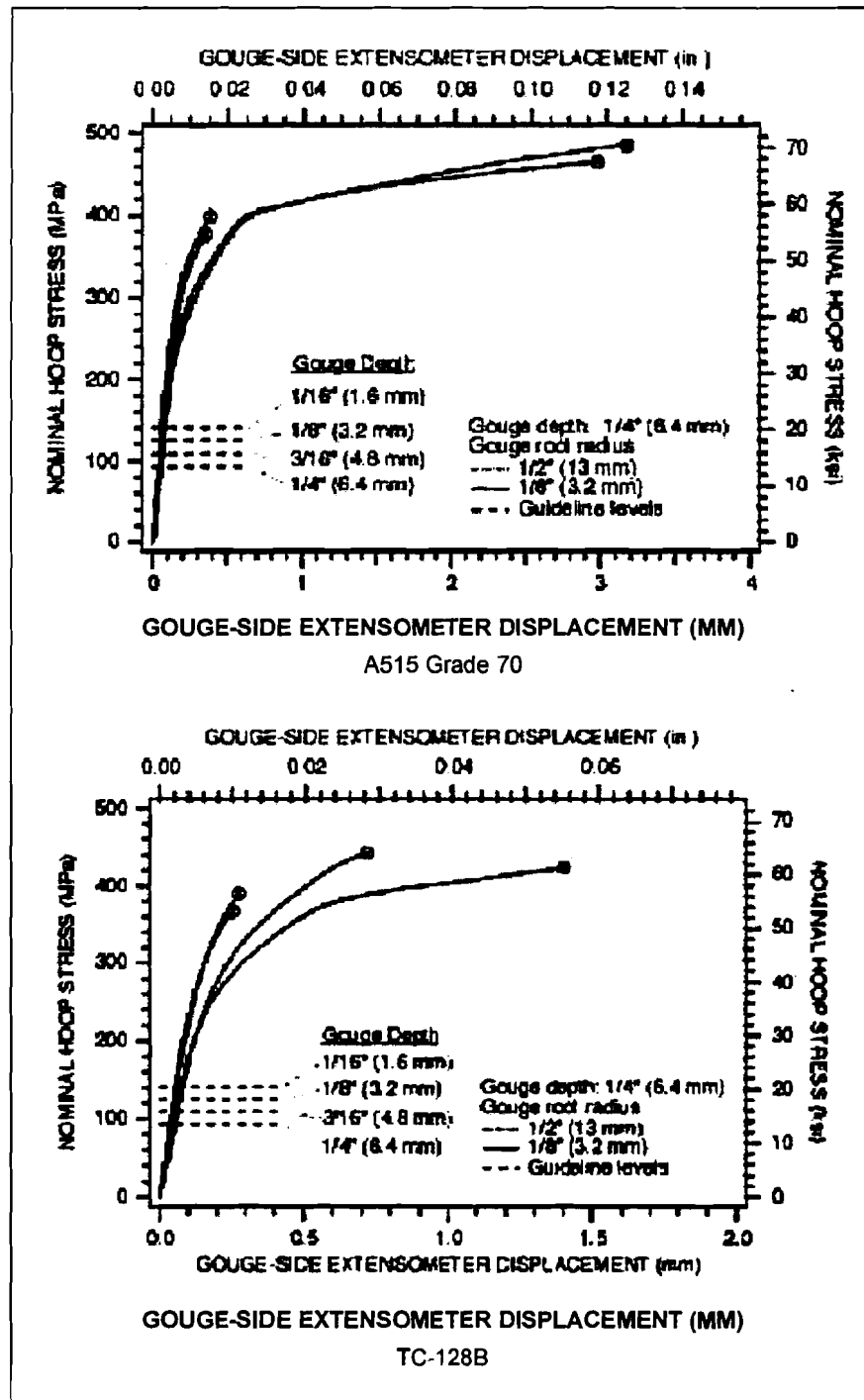
Figure 24. Results of Simulated Gouge Tests

48
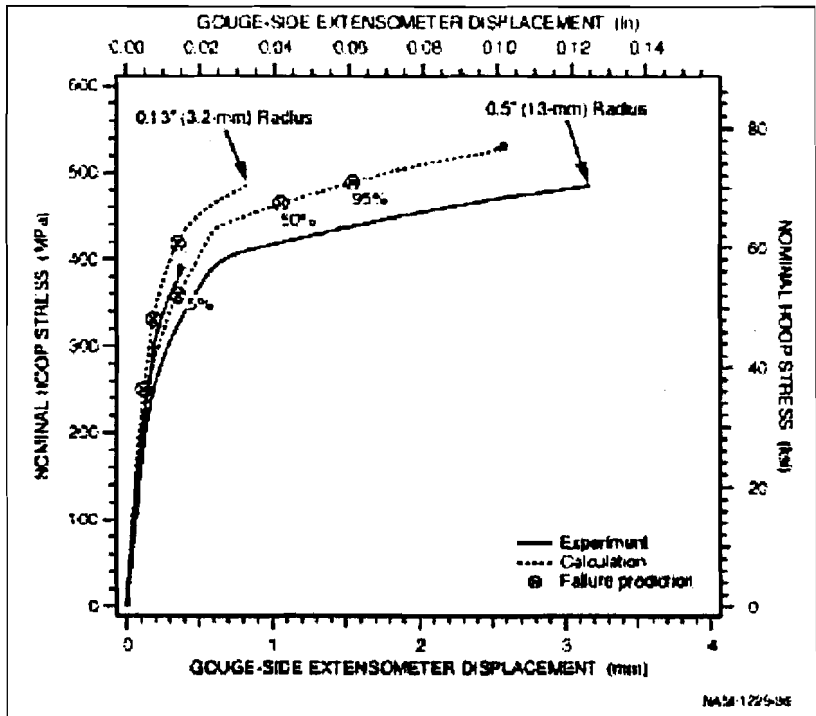
Figure 25. Summary of A515-70 Gouge Test Measurements at -238 F (-150° C) Compared to Calculated Response
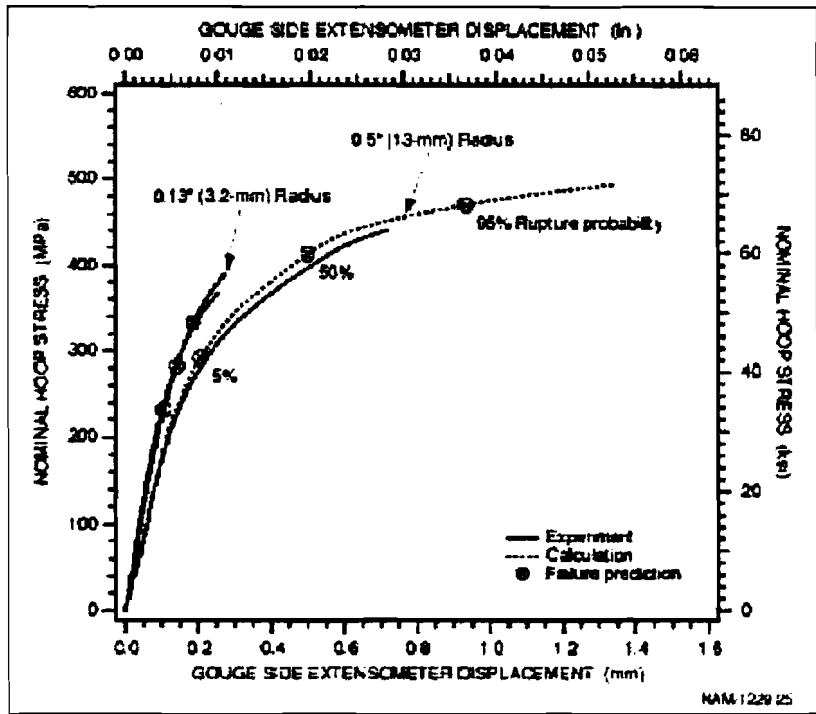
Figure 26. Summary of TC-128B Gouge Test Measurements at -238° F (-150° C) Compared with Calculated Responses

49
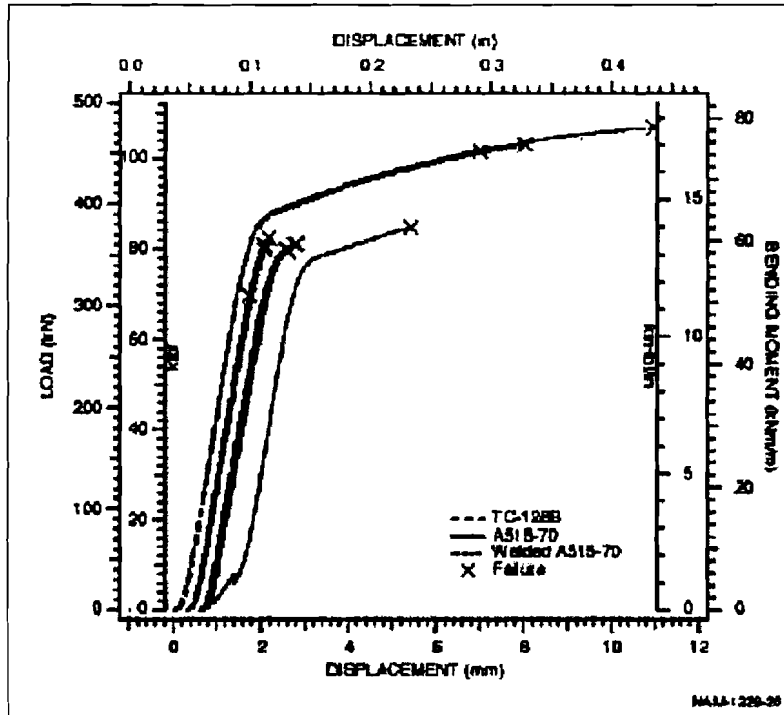
Figure 27. Results of Laboratory Cleavage Bend Tests
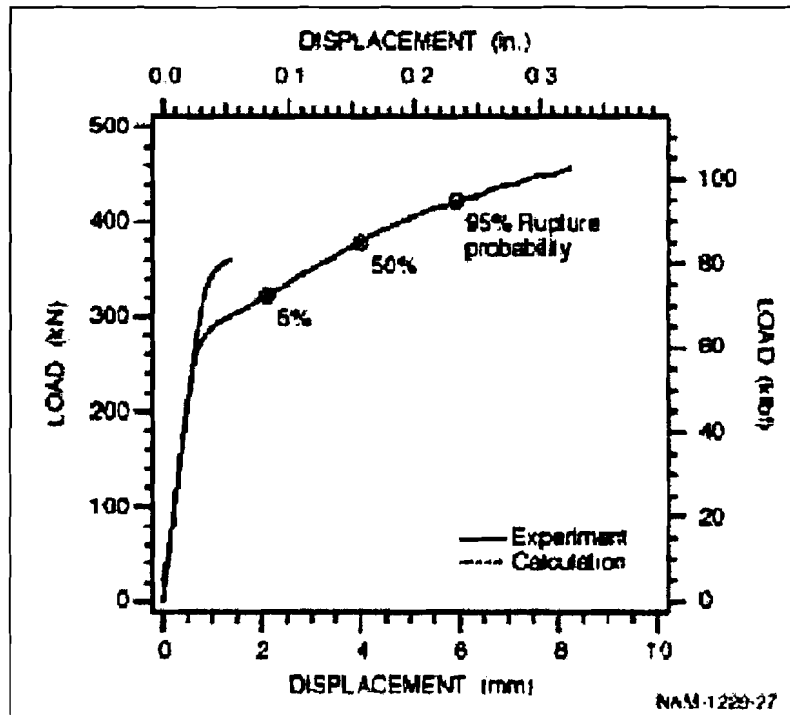
Figure 28. Comparison of Measurements and Analyses for the Engineering Bend Test with the A515-70 Tank Car Steel at –238°F (-150° C)

50
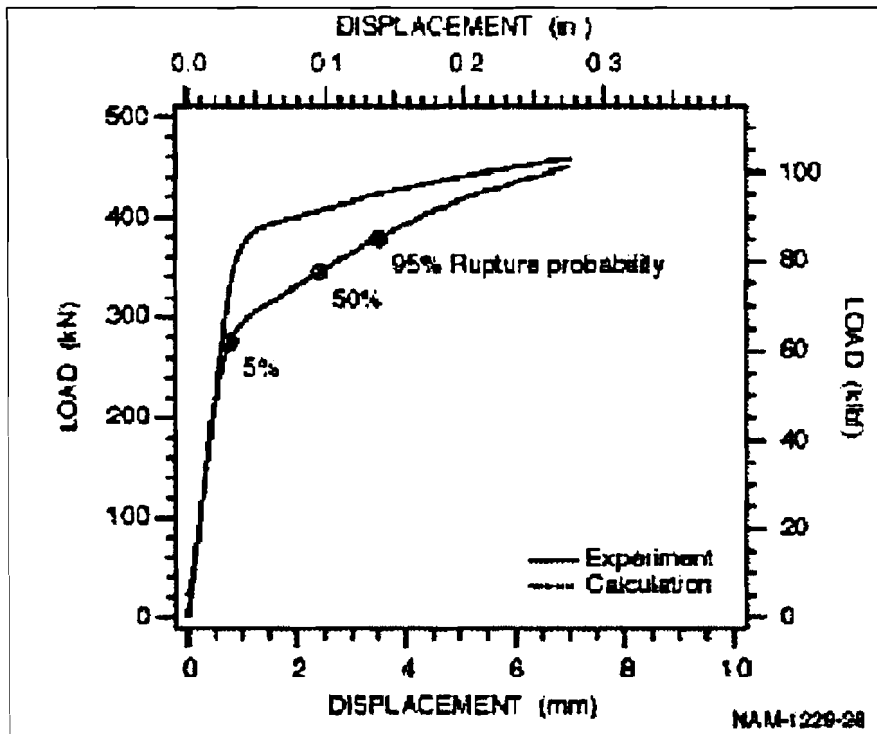
Figure 29. Comparison of Measurements and Analyses For the Engineering Bend Test with the TC-128B Tank Car Steel at -238°F (-150° C)

This variable temperature distribution makes a direct comparison of the bend experiment and computations difficult. For the A515-70, the measured cleavage load is consistent with the predicted rupture loads. For the TC-128B, the predicted cleavage load is somewhat conservative compared with the measured failure loads. However, for both these materials, a variable temperature distribution could significantly alter the stress and plastic strain distributions and thus change the cleavage behavior.

4.2.3 Dent/Undent Tests

Figure 30 shows the results of the denting portion of the dent/undent laboratory tests. The curves show the applied load versus load-point displacement at the center of the three-point bend span. The yield point is clearly discernible, as is the substantial effect of work hardening. There is no indication that the load has reached a peak and therefore no indication that failure is imminent. The final displacements correspond to a bend angle of about 140 degrees.

Figure 31 shows the behavior of the bent specimens when they are placed in tension as shown in Figure 13. The initial, low load portion of the curves corresponds to the straightening of the bend. The steep

51

rise in load occurs once the plate becomes straight. The portion of the curves beyond maximum load corresponds to the formation of a neck in the specimen on one or the other side of the original dent root. The ends of the curve correspond to final fracture of the neck. In all cases, final failure occurred in material away from the initial dent root. These failure sites are indicated in Figure 13.

4.3 EFFECTS OF LIFTING METHODS AND PRESSURIZATION

The full-up tank car model (Figure 3) was used to investigate the effects of service and salvage loading on the stresses in the tank wall that could lead to a cleavage rupture. In addition, the full tank car model and the corresponding ring model (Figure 5) were used to calculate the behavior of dents in a tank car caused by impact in combination with the internal pressure. The results of these analyses are presented in the following sections.

4.3.1 Effects of Lifting Methods and Pressurization

The initial calculations with the tank car structural model were performed to determine the tank wall stress magnitudes from service and salvage loading conditions. For these simulations, the tank car is in an undamaged condition. Although damage could be added to the car by simulating an impact with another structure, then applying simulated pressure and lifting loads, we chose the simpler approach of extracting the stress conditions computed in an undamaged car and applying them to small regions of plate containing damage. For example, we used hoop stresses computed in an undamaged car to apply to the simulations of the gouge specimen tests and to validate the gouge depth table in the Guidelines.

A pressure distribution was specified on the inside of the tank wall to simulate the combined effects of an internal pressure and the hydrostatic pressure from the lading. In addition, a gravitational acceleration was specified to include the dead weight loading of the tank car structure. The resulting stresses in the tank car were analyzed to determine the magnitude of the stresses under various conditions.

The first simulation performed corresponds to the loading conditions of an unpressurized tank with a lading load from a full tank of fluid of density equal to water. Figure 32 shows the calculated maximum principal stresses in the tank for this condition. The model predicts some stress concentrations around the bolster and stub sill doubler plate, but the majority of the tank wall has stresses below approximately 6 ksi (41 MPa).

The expected stresses for this condition can be estimated by considering the tank car as a simply supported beam with a uniform load (P_o). From simple beam theory, we can determine the

maximum moment M_{max} and stress σ_{max}. Using a tubular cross section equal to the tank dimensions we obtain

$$M_{max} = \frac{P_o L^2}{8} = \frac{W L}{8} \qquad (5)$$

and

$$\sigma_{max} = \frac{M_{max} c}{I} = \frac{W L}{8 \pi R^2 t} \qquad (6)$$

where L is the length between bolsters, W is the weight of the tank car and lading, R is the tank radius, and t is the tank thickness. Using the appropriate values for the tank, we would expect stresses from beam bending to be approximately 3000 psi (21 MPa).

The second simulation performed corresponds to the previous loading conditions with the addition of a 130 psi (896 kPa) internal pressure. Figure 33 shows the calculated maximum principal stresses in the tank for this condition. The model again predicts some stress concentrations around the bolster and stub sill doubler plate and near the tank head corner. The high stresses in the tank head are probably not characteristic because the increased head thickness that usually occurs in practice and would reduce stresses was not included in the model. The addition of the internal pressure has now increased the stress in the majority of the tank wall to approximately 12 ksi (82.7 MPa).

The expected stresses for the pressure loading can be estimated from the simple formulas used to analyze pressure vessels and pipelines. From this simple approach, the maximum stress in the tank wall is the hoop stress equal to

$$\sigma_{max} = \frac{P_i R}{t} \qquad (7)$$

Using the tank car pressure and tank dimensions in the above equation gives a maximum stress of 12.5 ksi (86.2 MPa), which is consistent with the calculation.
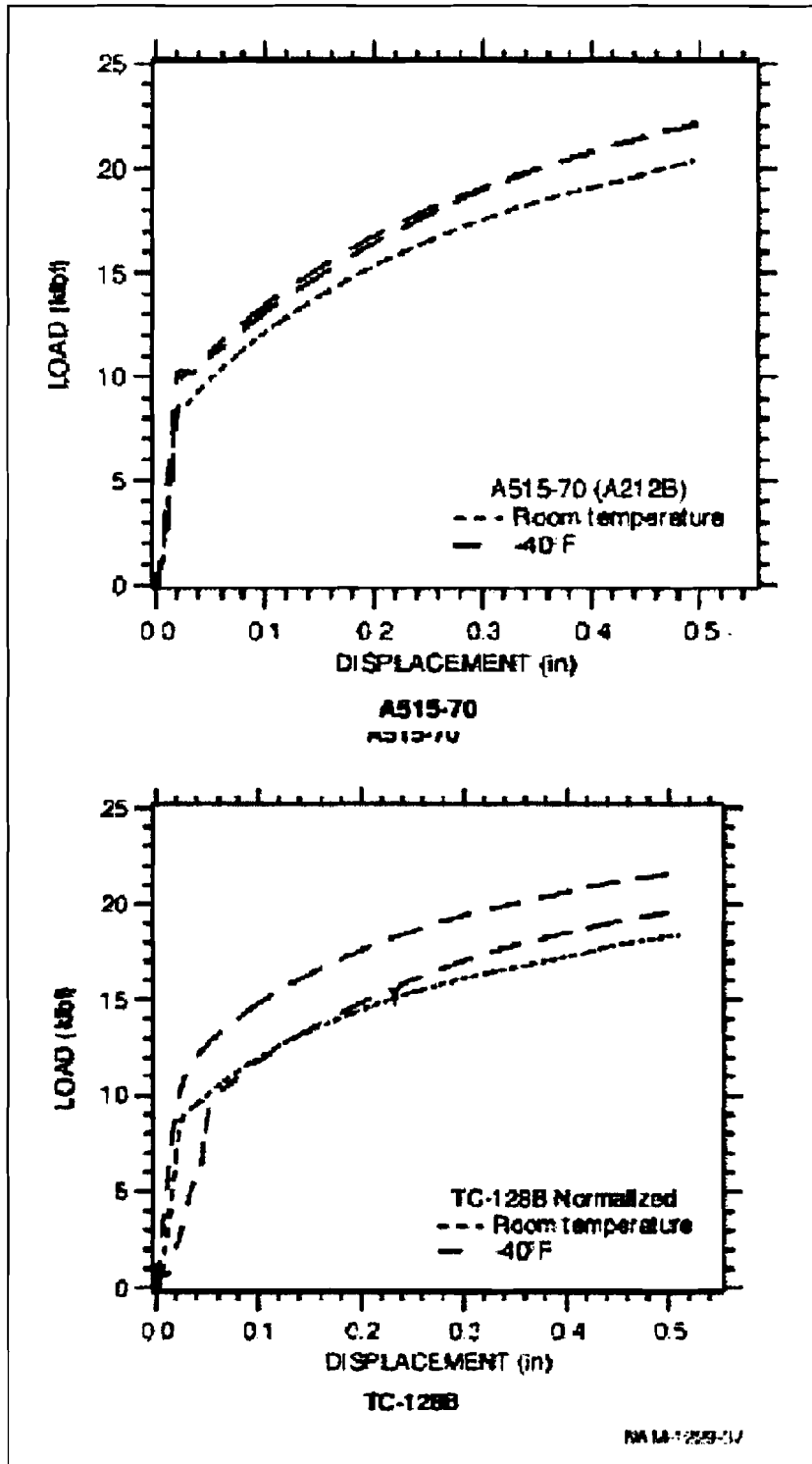
Figure 30. Results of Denting Portion of Dent/Undent Tests

54
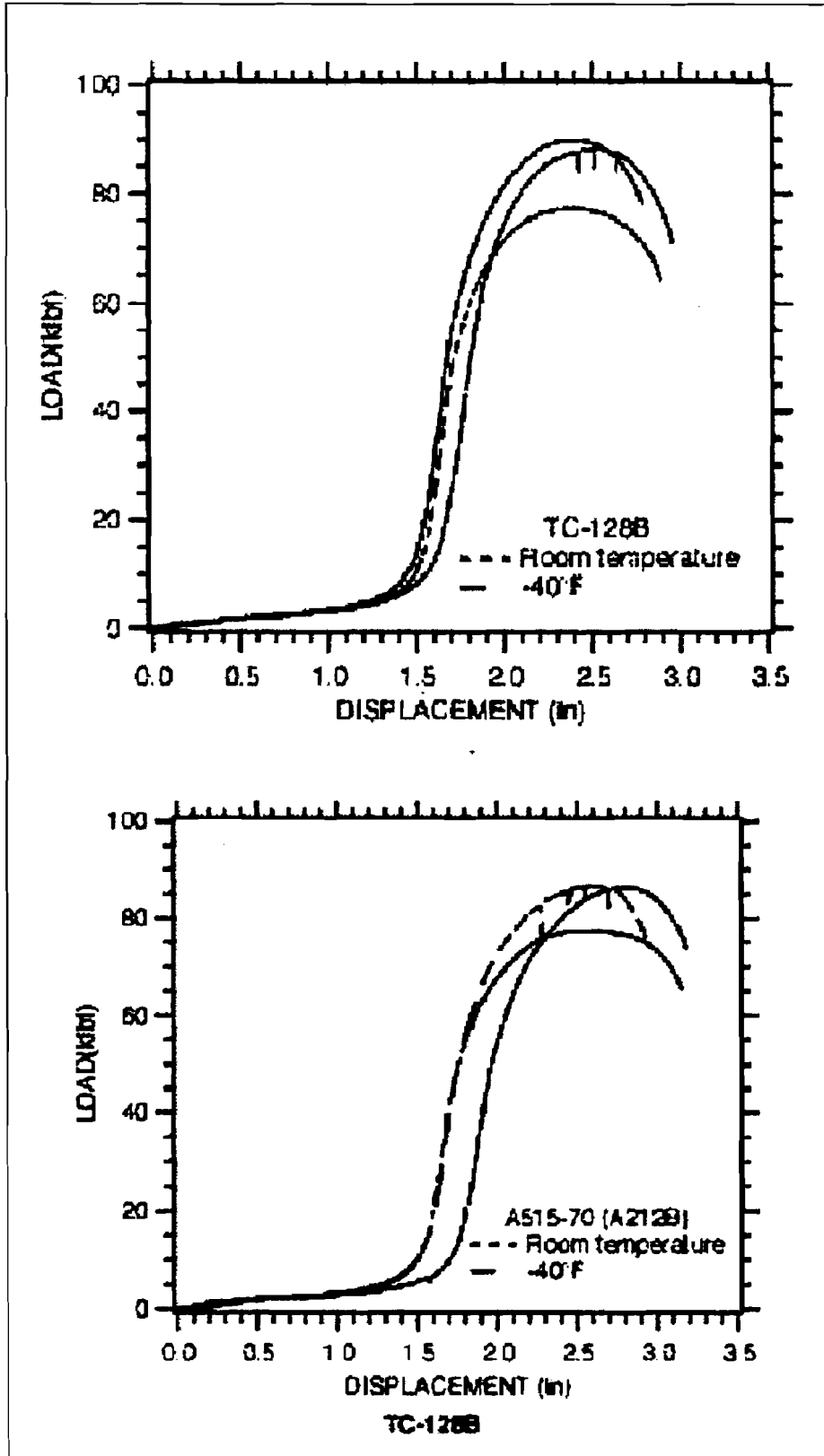
Figure 31. Results of Undenting Portion Of Dent/Undent Tests

55

(ksi) (MPa)

12.0 82.7

9.00 62.1

Max. Principal
Stress

6.00 41.4

3.00 20.7

0.00 0.00

NAM-1229-029
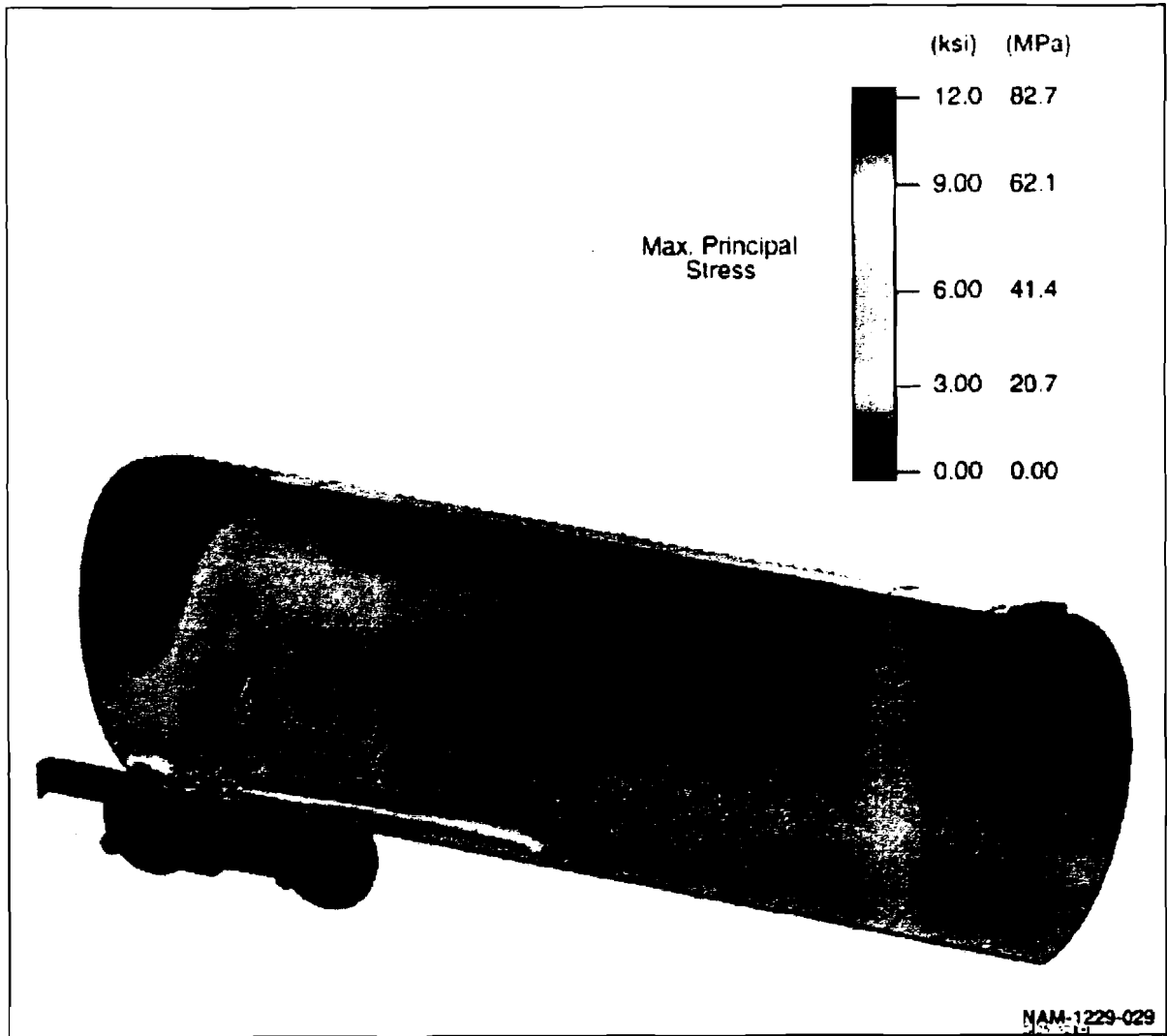
**Figure 32. Maximum Principal Stress Distribution of the
Unpressurized Tank Car with Lading Loads**
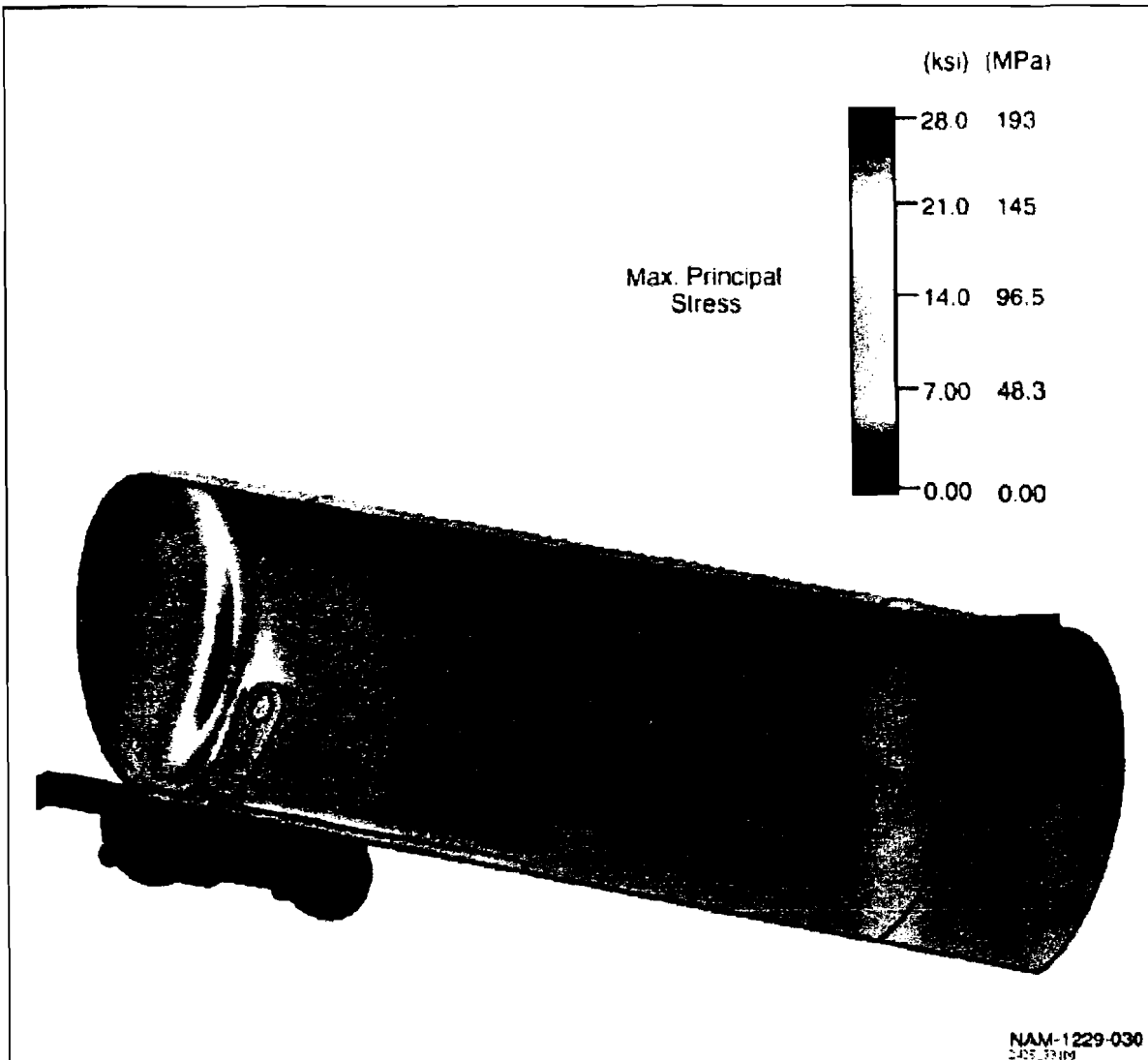
Figure 33. Maximum Principal Stress Distribution from 130-psi Internal Pressure and Lading

The third simulation performed corresponds to the previous loading conditions with the internal pressure increased to 255 psi (1.76 MPa). Figure 34 shows the calculated maximum principal stresses in the tank for this condition. The distribution of maximum principal stresses is very similar to the previous simulation, but with the magnitude scaled up proportionately with the pressure level. This pressure level increases the stress in the majority of the tank wall to approximately 24 ksi (166 MPa).

The above approach of applying stresses for undamaged cars to small regions with damage is approximate, but it is accurate enough for two reasons. First, as we have shown, stresses induced by lifting are small relative to stresses induced by tank pressure. Second, the types of damage that we are considering are relatively localized such that the tank globally maintains its undamaged shape. The shape determines the hoop and longitudinal stresses. We caution, however, that the lifting stresses, no matter how small, could be additive to the pressure stresses and could put critical pressure stresses over the rupture limit. We also caution that our simplified approach may not be accurate when the tank is grossly deformed from the shape of a straight, circular, thin shell.
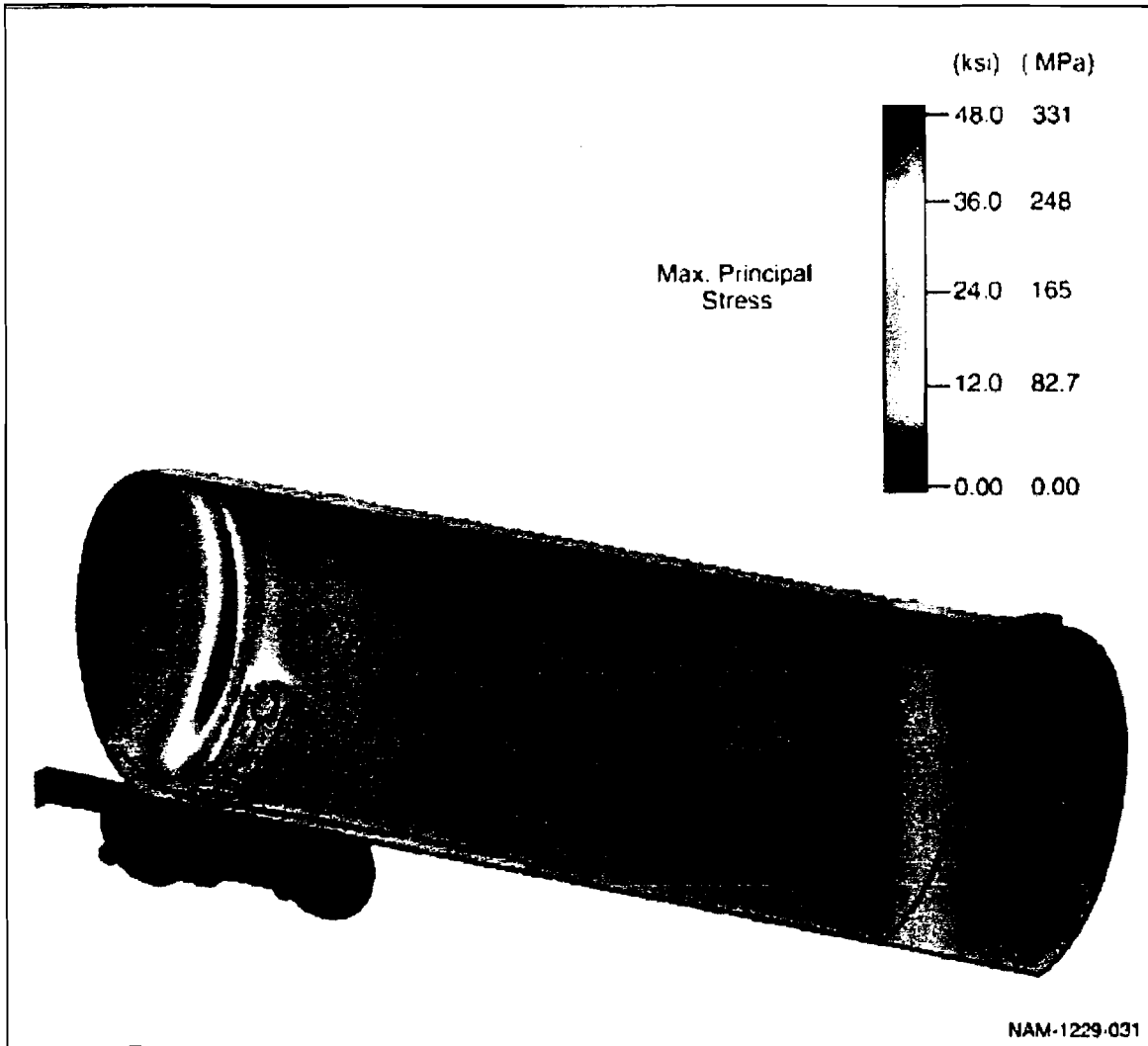
Figure 34. Maximum Principal Stress Distribution from 255-psi Internal Pressure and Lading

4.3.2 Effects of Tank Pressure on Dent Behavior

Additional calculations were performed with the tank car structural model to investigate dent damage and the interaction of the internal pressure with a dent. The concern is that the pressure in a tank car can push out the dent such that the final dent shape shows little evidence of the full extent of deformation in the tank wall. In addition, a tank car with dent damage could be at risk of further plastic deformation if the internal pressure within the tank were to increase during the salvage operation.

The first simulation performed to investigate the dent response with internal pressure used a vertical pole indenter with an impact velocity of 20 mph (9 m/s). The indenter nose is a rigid pole with a radius of 4.0 in. (10 cm). The model used in this simulation is shown in Figure 35. The impact produces a dent geometry with the primary axis of the dent in the tank's circumferential direction. The simulation performed calculates the dent formation with an unpressurized tank, then smoothly increases the internal pressure to a maximum level of 255 psi (1.76 MPa).

The calculated response for the vertical pole impact is shown in Figure 36. The formation of the dent in the tank car side is shown in Figure 36(a). The maximum dent depth is approximately 5 in. (13 cm) at the center in the unpressurized tank. After pressurization to 255 psi (1.76 MPa), the dent depth is significantly reduced with a depth of approximately 2 in. (5 cm) as shown in Figure 36(b). However, the dent is still clearly visible in the final state.

The second simulation performed to investigate the dent response with internal pressure used a longitudinal pole indenter with an impact velocity of 40 mph (18 m/s). For this simulation, the indenter has a rigid pole impact nose with a radius of 3.0 in. (8 cm) and a length of 120 in. (3.0 m). The ends of the indenter pole were rounded away from the tank to avoid localized damage from the impact of sharp corners at the ends of the dent. The model used in this simulation is shown in Figure 37. The indenter produces a dent geometry with the primary axis of the dent in the tank's longitudinal direction. Again, the simulation performed calculates the dent formation for an unpressurized tank then smoothly increases the internal pressure to a maximum level of 255 psi (1.76 MPa).
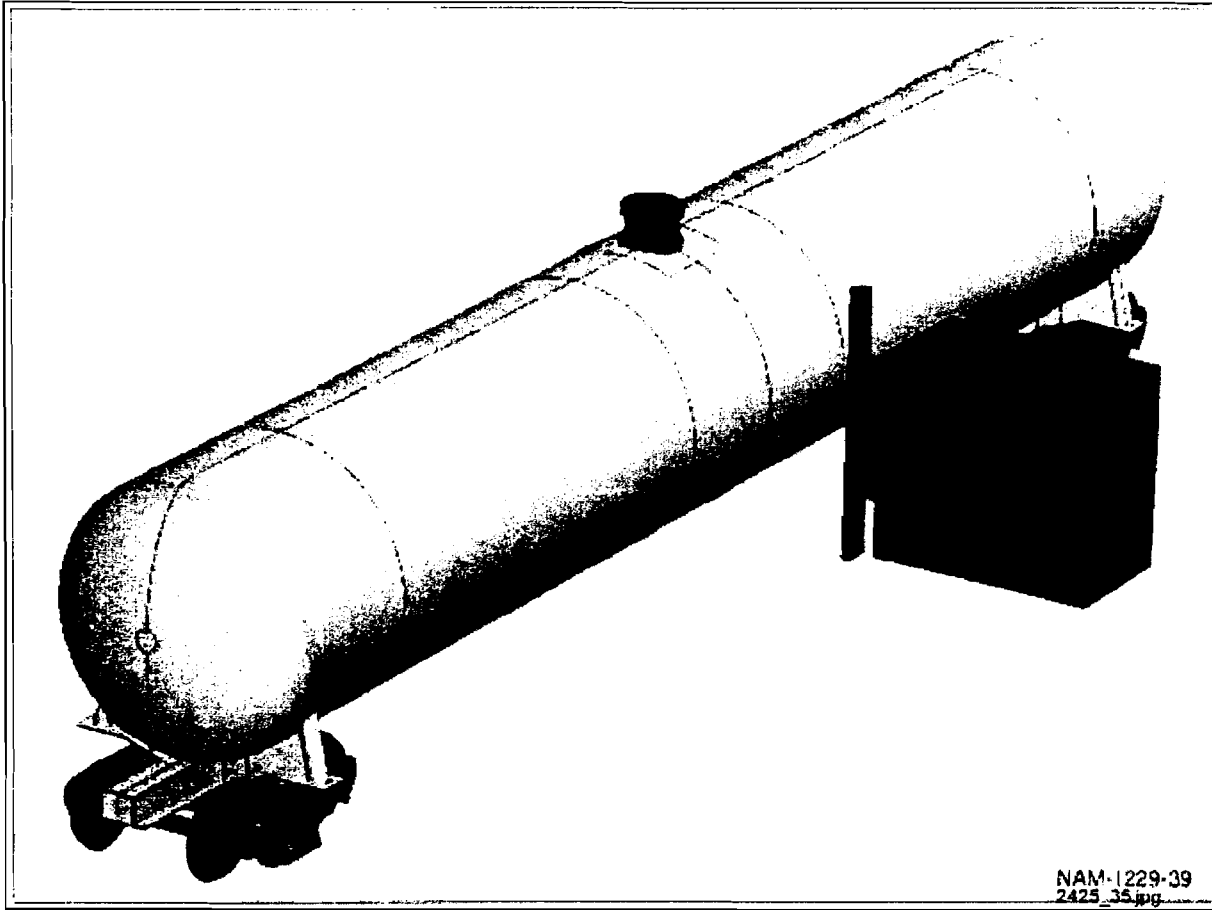
Figure 35. Model Used for Analysis of a Vertical Dent Response with Internal Pressure
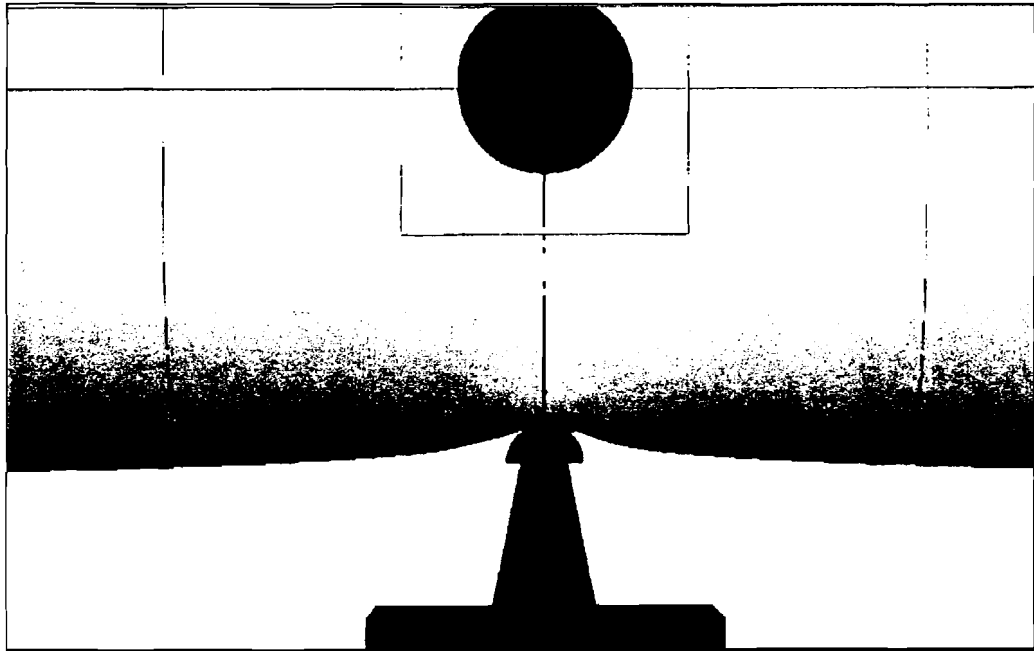
Dent formation in the tank car.

Figure 36a. Model Used for Analysis of a Vertical Dent Response with Internal Pressure
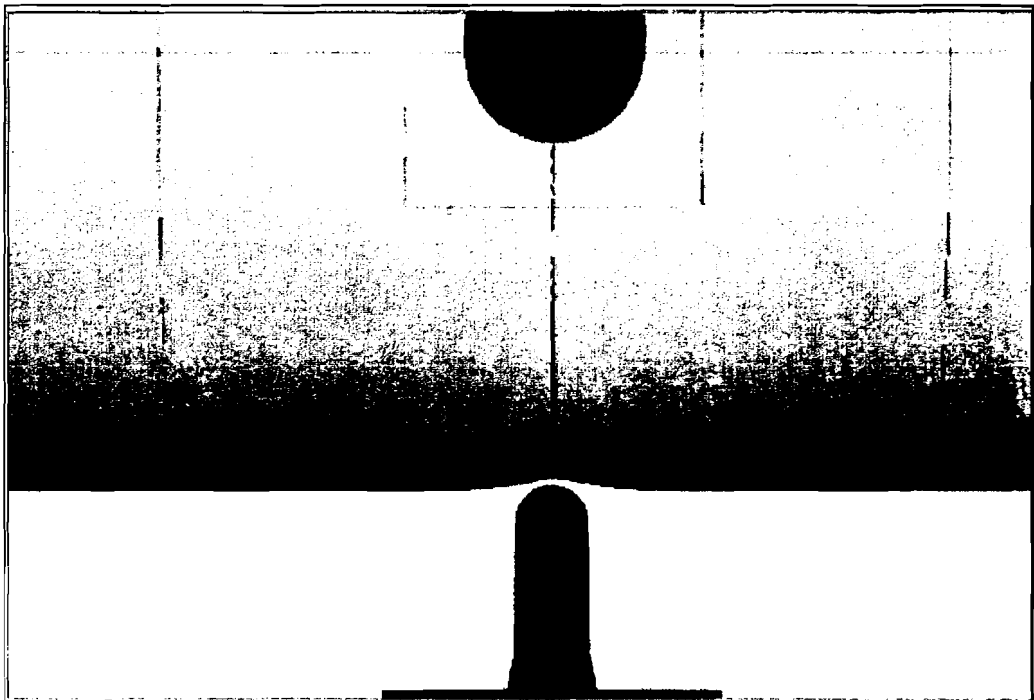
Dent after pressurization to 255 psi

Figure 36b. Analysis of a Vertical Dent Response with Internal Pressure
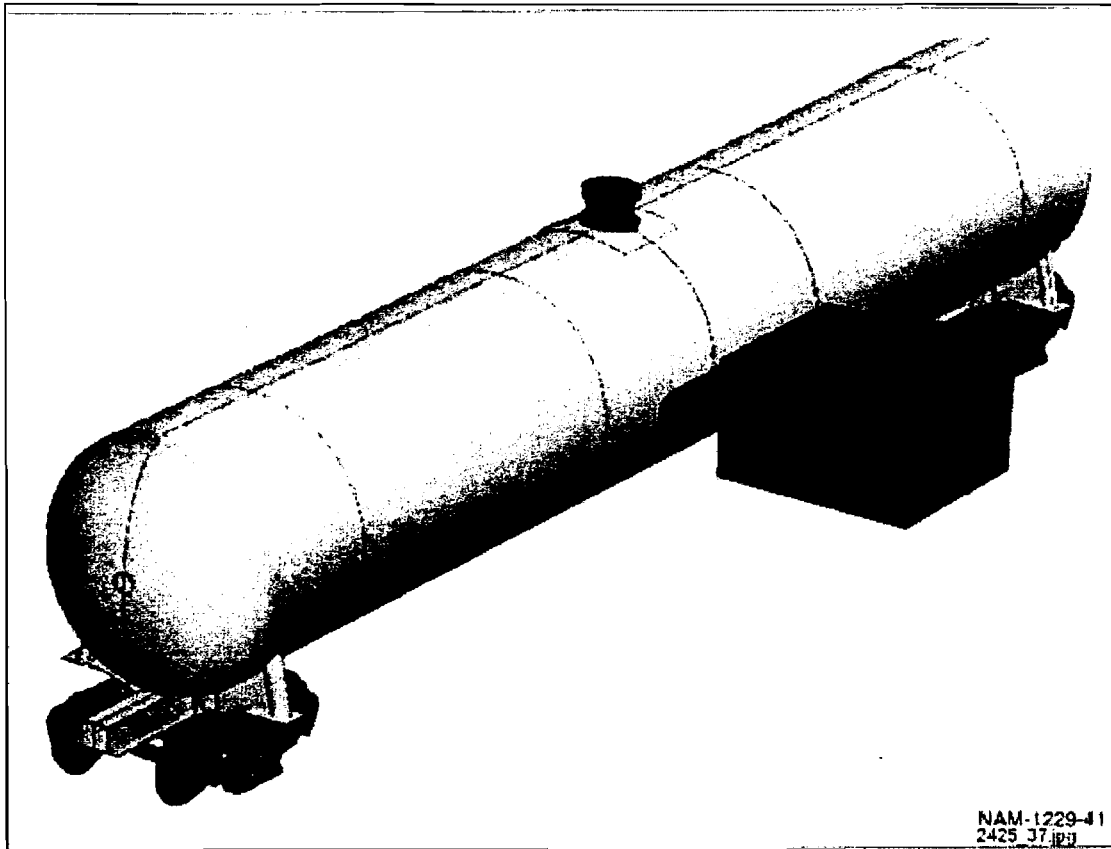
Figure 37. Model Used for Analysis of a Longitudinal Dent Response with Internal Pressure

The calculated response is shown in Figure 38. The formation of the dent is shown in Figure 38(a). For visualization, only one-half of the tank car model is shown in the figure. The maximum dent depth is approximately 6 in. (15 cm) at the center in the unpressurized tank. However, as the tank car is pressurized to 255 psi (1.76 MPa), the dent is pushed outward to the point where the original dent is no longer visible at the tank centerline. Therefore, the internal pressure clearly has a greater influence on this longitudinal dent geometry. This geometry effect is expected because the pressure stresses in an undamaged tank car are twice as large in the circumferential direction than in the longitudinal direction. Thus, the stresses normal to the major dent axis are larger with the longitudinal dent configuration.

(a) Dent formation in the tank car

(b) Dent after pressurization to 255 psi
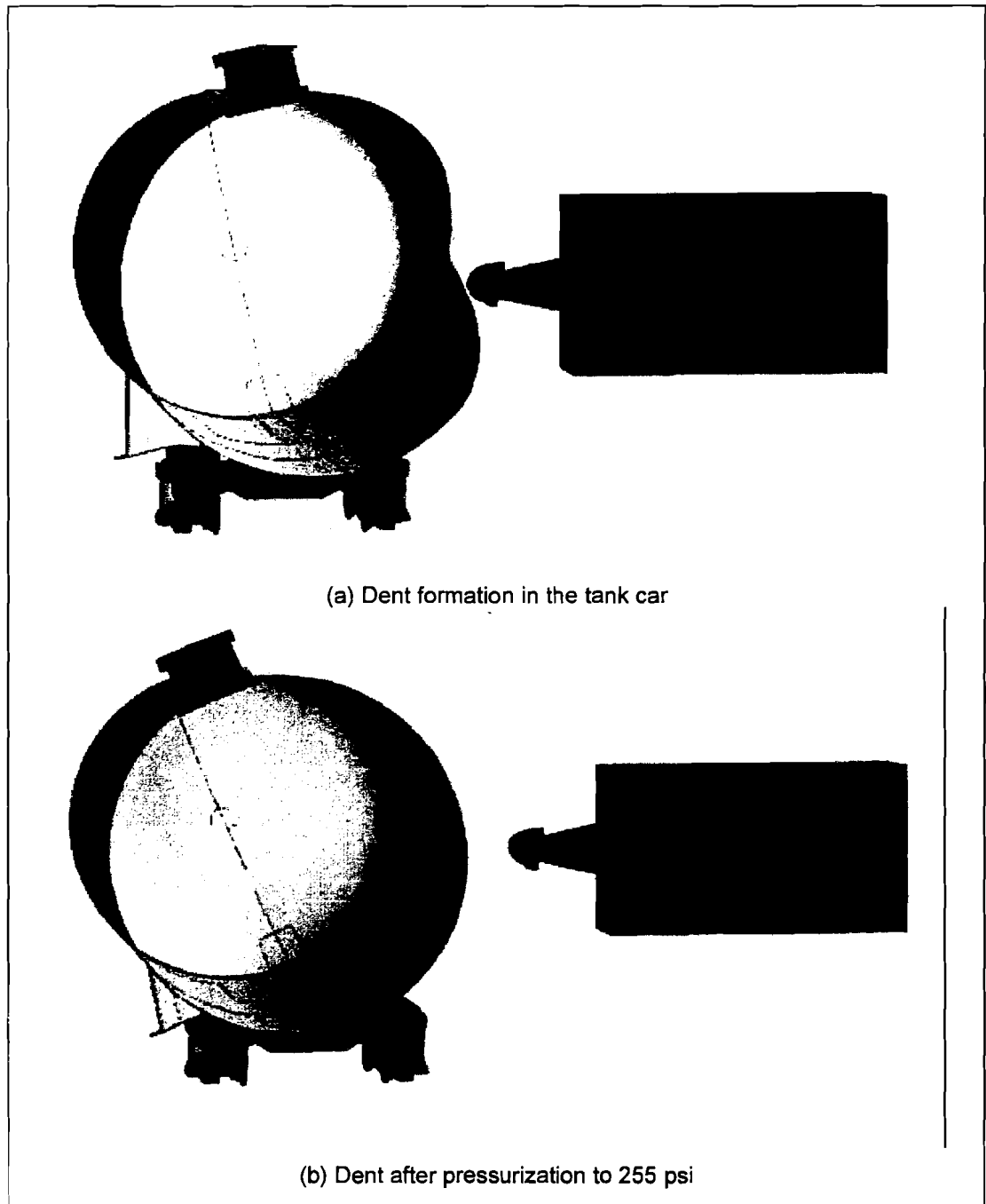
Figure 38. Analysis of a Longitudinal Dent Response with Internal Pressure

From the above simulations, the longitudinal dent is seen to be the more critical dent geometry in the presence of internal tank pressure. To further investigate the behavior of a longitudinal dent, a series of two-dimensional ring analyses were performed as will be described in Section 4.3.3.

A final impact calculation was performed with the full tank car model to investigate a set of impact conditions that could produce damage similar to that of the 112T340W tank car damaged in the May 25, 1995, Flomaton, AL, collision. In that collision, the tank car was impacted end-on by a locomotive. To approximate the collision, a 133-ton mass (121 Mg) was impacted into the tank car end at 40 mph (18 m/s). The tank car in the simulation was pressurized to 145 psi (1.00 MPa).

The end-on impact response of the tank car is shown in Figure 39. The impact of the stub sill, tank end, and bogie against the rigid block produces damage that is concentrated mainly in the bolster and stub sill regions. The load on the sill and bogie produces a response that rotates the bolster away from the impact and forms a maximum dent in the tank approximately 3 feet (1 meter) behind the bolster location as seen in Figure 39(b). The presence of the stub sill and doubler plate at this location reinforces the tank structure such that the internal pressure does not significantly push the dent back out after the collision. This deformation mode and dent location are similar to those observed in the Flomaton collision.

4.3.3 Ring Analyses of Dent Behavior

The finite element analyses of the two-dimensional ring sections provided results on the deformation and stress history near a longitudinal dent. The overall shape of the tank at the innermost denting is shown in Figures 40 and 41 for room temperature and -40°F (-40°C). The progression of the dent shape as the tank rebounds away from the indenter is shown in Figure 42 for the room temperature case. The variable spacing between the traces of the dent shape is due to oscillation of the overall shape of the tank as it moves. At -40°F (-40°C), the dent is not as sharp or deep. This is illustrated in Figure 43, which compares the profiles of room-temperature and -40°F (-40°C) dents at their peak deformation.
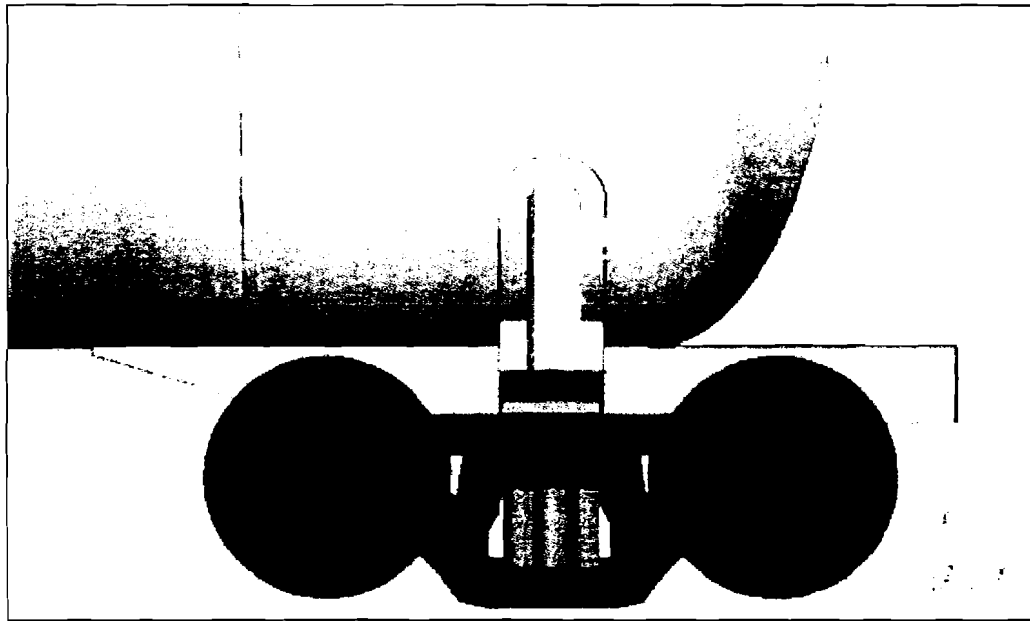
(a) Initial stub sill and bolster geometry
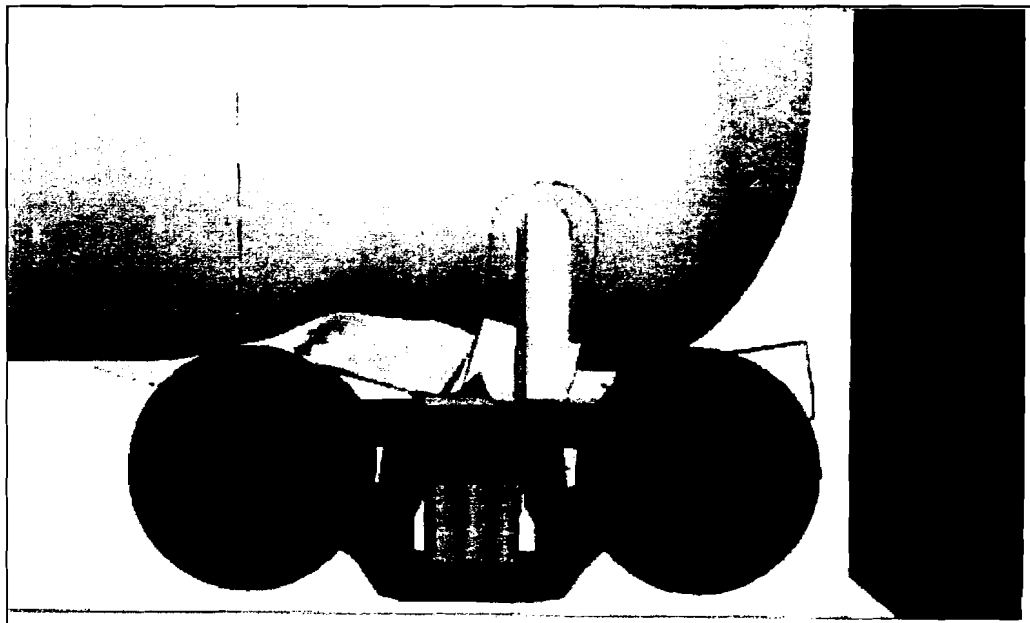
(b) Sill and bolster deformations from axial impact

Figure 39. Analysis of a Longitudinal Impact Response of the Tank Car

Overall deformation

Indentation detail
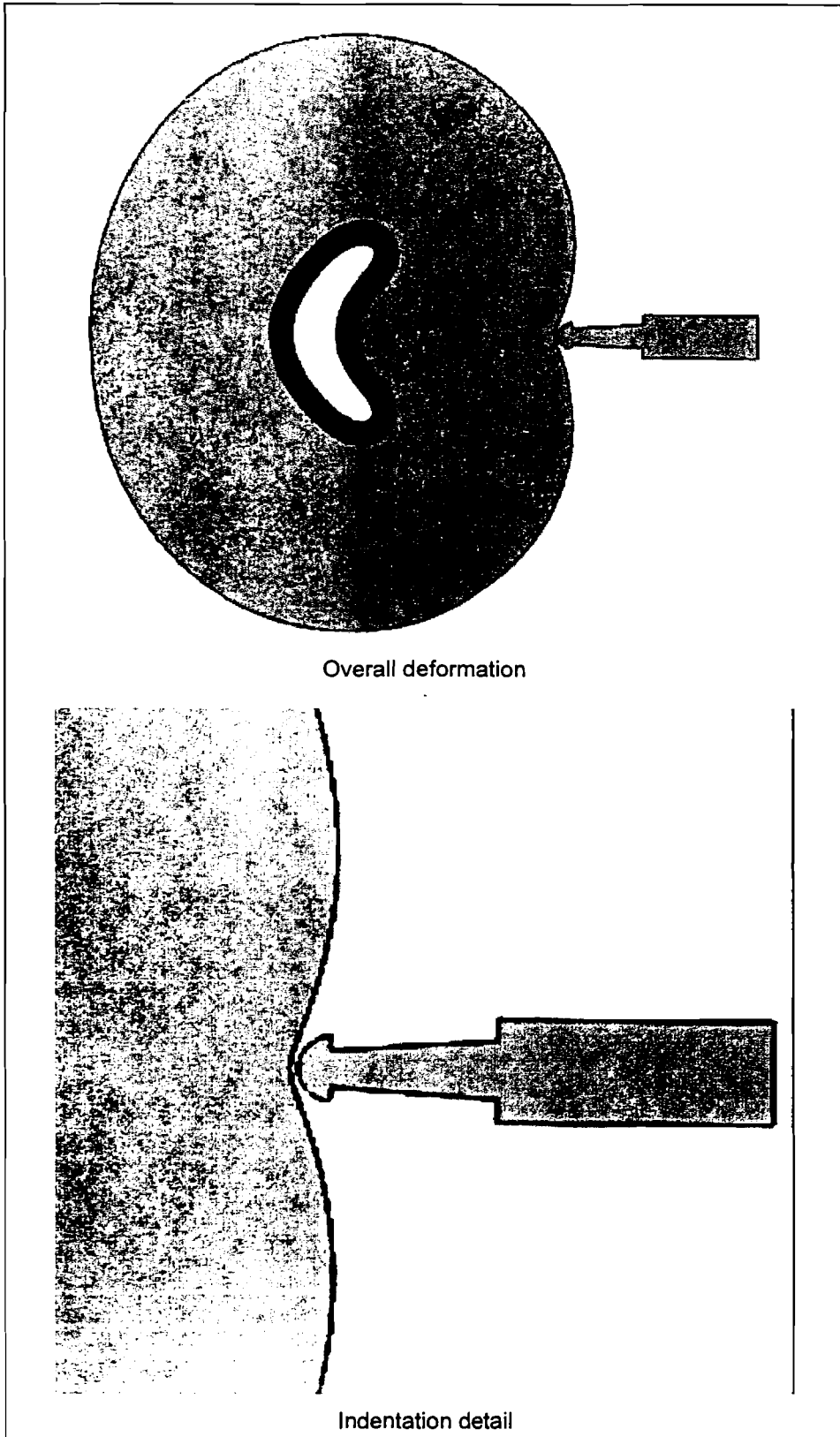
Figure 40. Unpressurized Indentation at 40 mph for an A515-70 Ring at 100° F

Overall deformation

Indentation detail
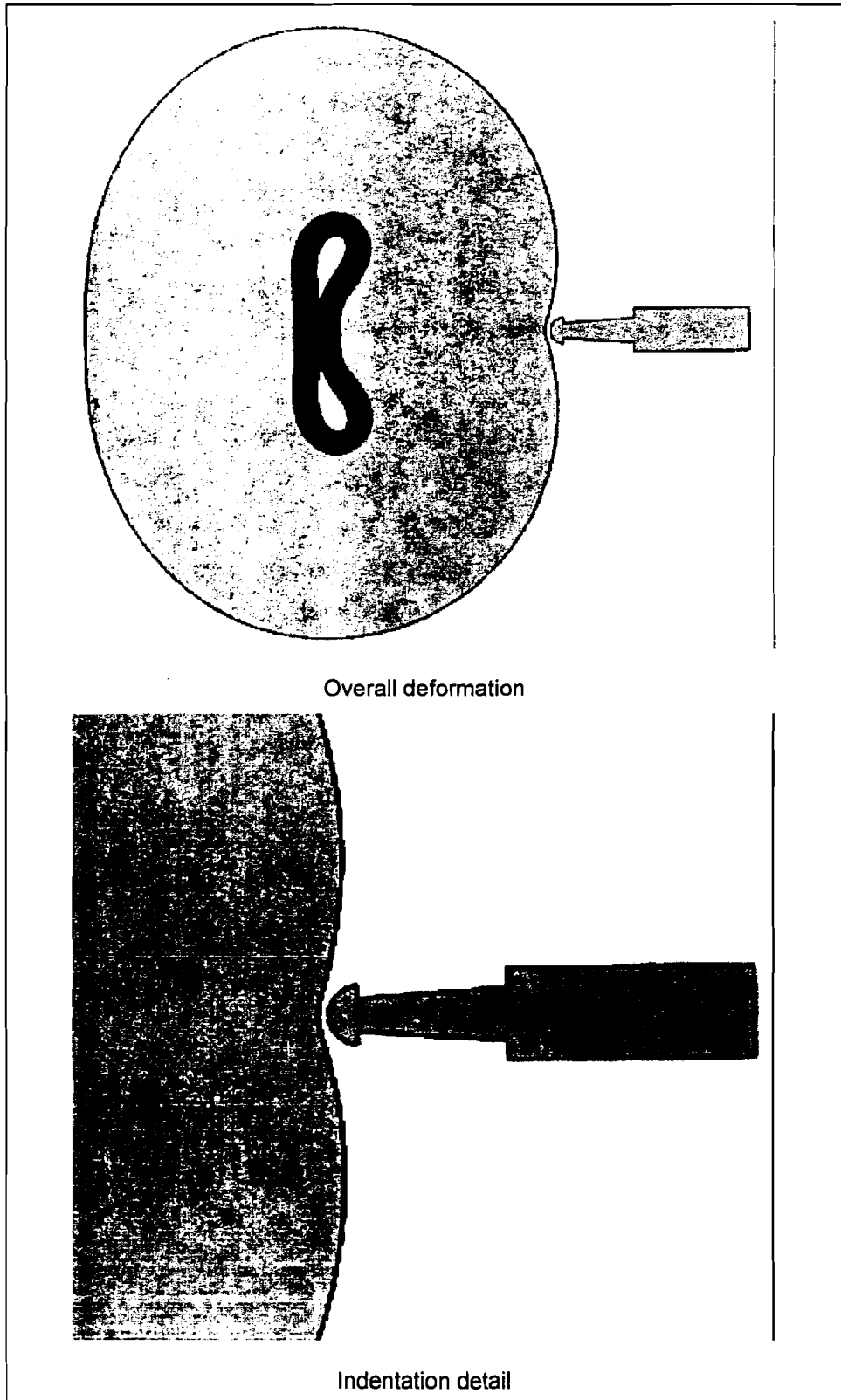
Figure 41. Unpressurized Indentation at 40 mph for an A515-70 Ring at -40° F

68

In the simulations, the tank pressure is increased from 0 to 255 psi following impact. The pressure is included as a parameter along the bottom of the dent traces in Figure 42. The variations with pressure of dent depth, dent angle, dent root net tensile force per unit length, and dent root bending moment per unit length are shown in Figures 44 and 45, for both room temperature and -40°F (-40°C). From Figure 44, we conclude that, independent of temperature, dent depth and dent angle diminish significantly once tank pressure reaches 100 psi. We also conclude that dent depth and angle are relatively independent of temperature for pressures beyond about 100 psi.

Figure 45(a) shows that dent root net tensile force per unit length is essentially the same as the hoop stress in an undeformed tank times the shell thickness. This force is proportional to the tank pressure and is little affected by the impact or subsequent oscillatory motion of the tank. Figure 45(b) shows, however, that dent root bending moment is largely independent of pressure for pressures beyond about 100 psi. This result is expected because the dent root is fully plastic, and the plastic moment of the plate is roughly constant at ≈10,000 lbf-in./in.
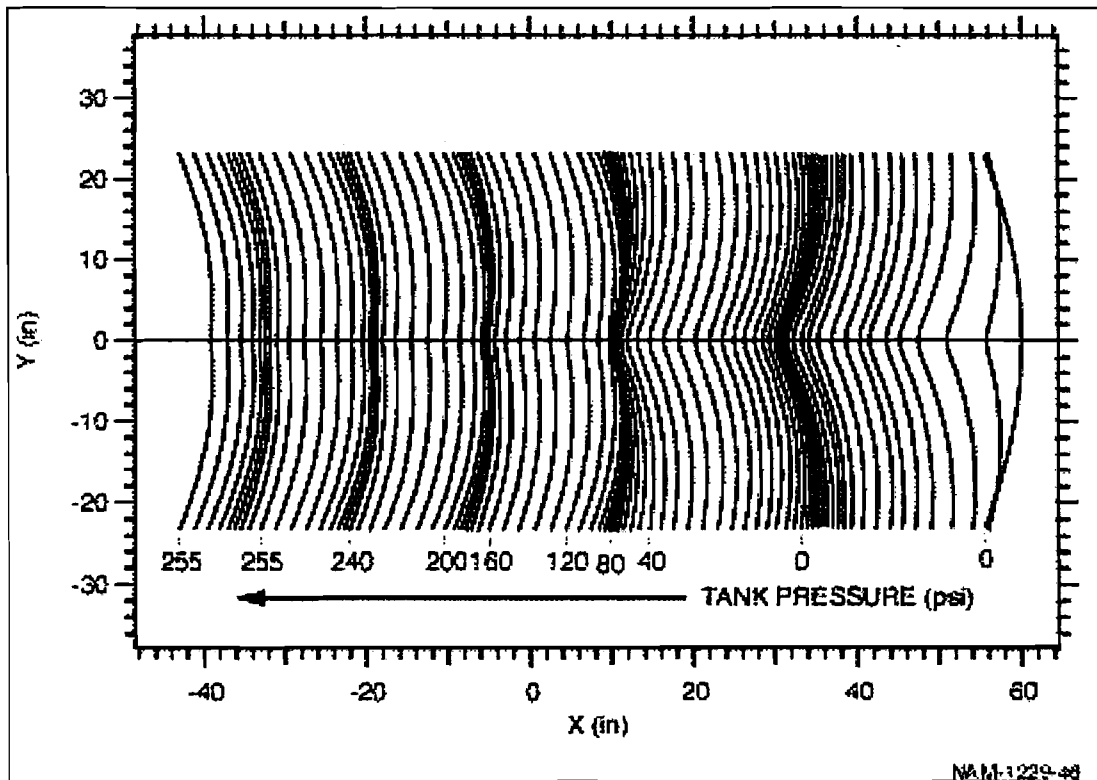
Figure 42. Progression of Dent Profile Following Impact from the Right and Subsequent Pressurization

NAM-1229-47
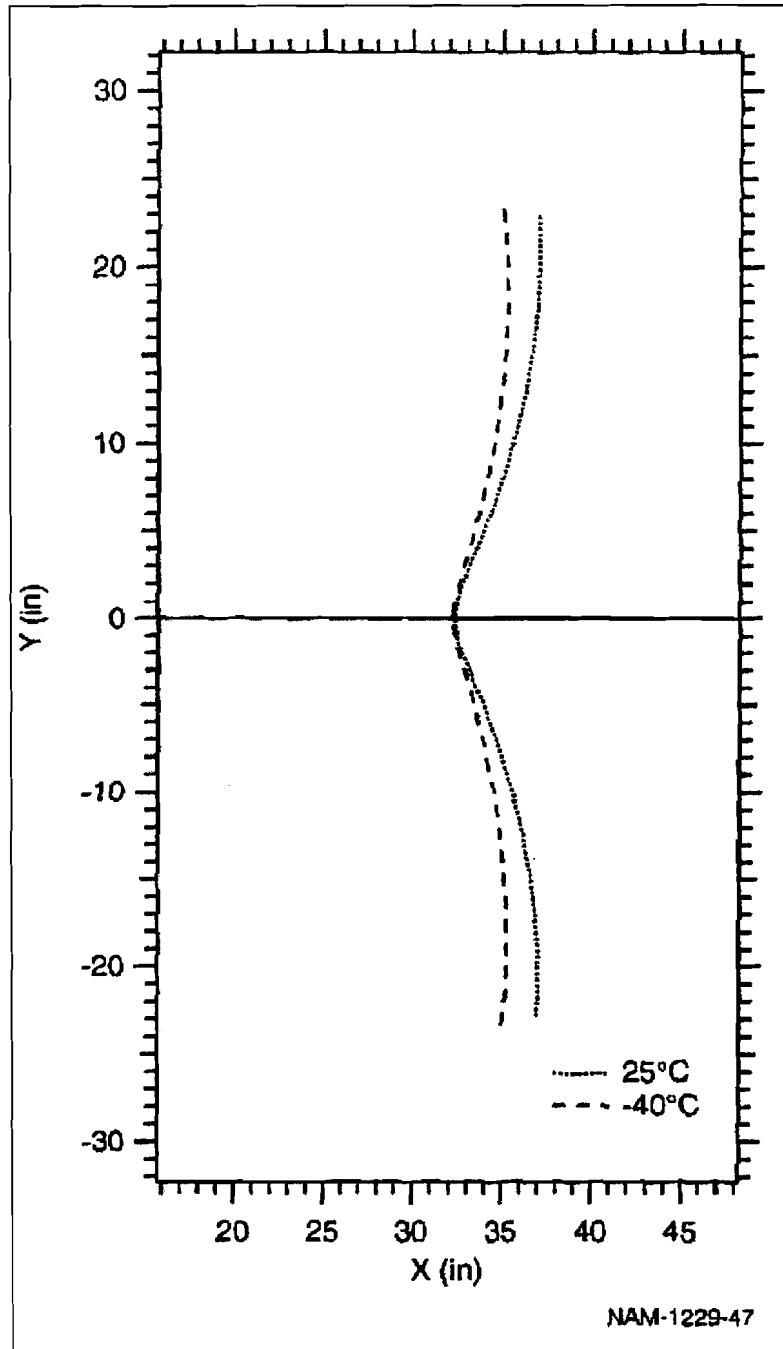
Figure 43. Comparison of Room Temperature and Cold Dent Profiles at Peak Indentation
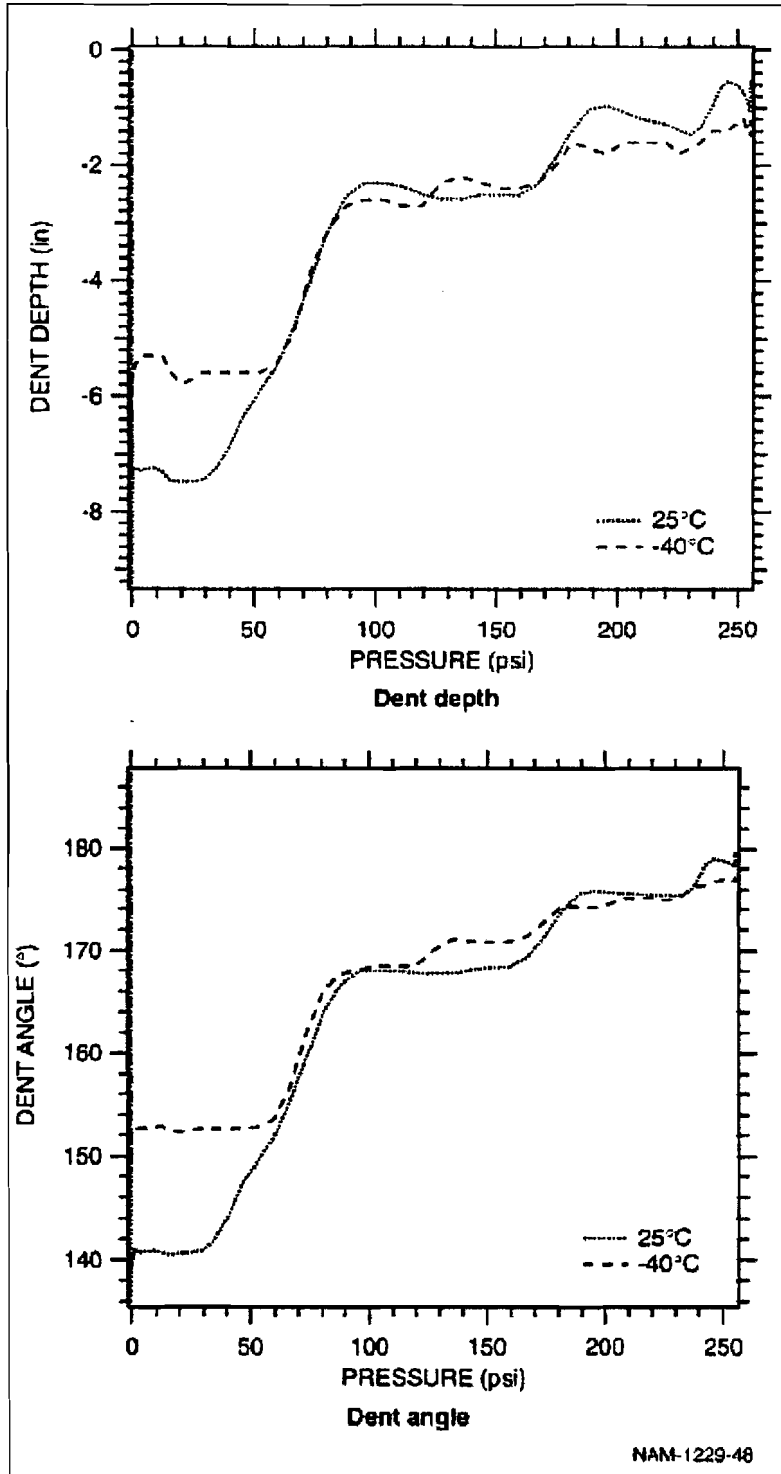
Figure 44. History of Dent Geometry with Increasing Pressure Following Impact

71
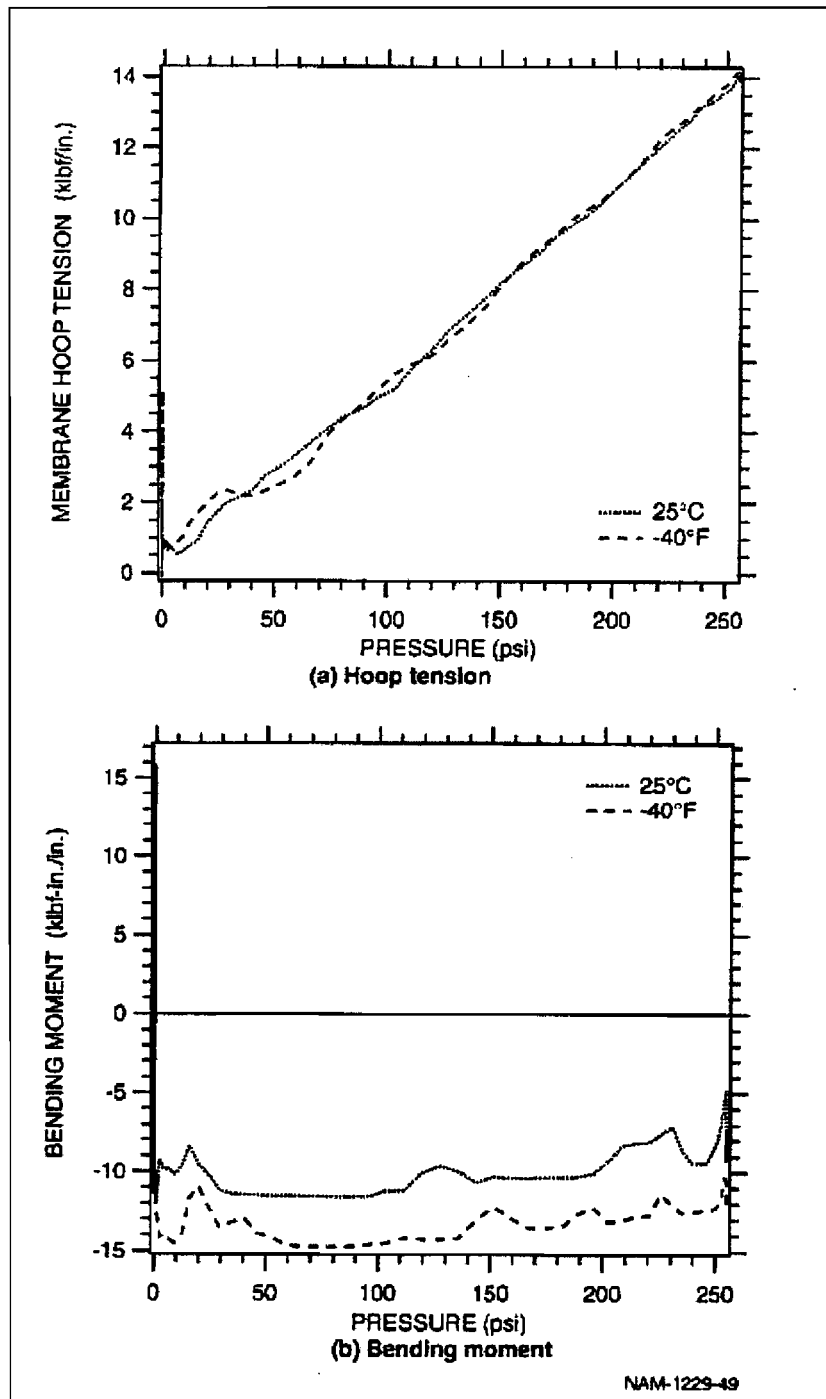
Figure 45. Dent Root Tensile Force Resultant and Bending Moment History following Impact and Subsequent Pressurization

The ring section modeling shows that a crack at a longitudinal dent root would be subjected to a tensile hoop stress equal to that for an undented tank and a bending moment equal to the yield moment of the plate, 10,000 lbf-in./in.

4.4 CONVENTIONAL FRACTURE APPROACH

4.4.1 Fracture Mechanics Test Results

J-resistance (J-R) curves and J-crack-mouth opening displacement (CMOD) curves resulting from the fracture mechanics tests are shown in Figures 46 and 47. As shown in the J-R curves, three of the specimens sustained several hundredths of an inch of stable crack growth, and three of the specimens had negligible stable crack growth prior to instability. The tests in which the three specimens sustained stable crack growth were interrupted prior to instability. For the A515-70 (A121B) steel, the lowest value the J integral at crack initiation was 51 lbf-in./in.^{2} (8.9 kJ/m^2), and the lowest value of J at instability was 132 lbf-in./in.^{2} (23.1 kJ/m^2). Test temperature was -40°F (-40°C) in both cases. For the as-rolled TC-128B (Flomaton) steel, the lowest value of J at instability, which occurred at crack initiation, was 225 lbf-in./in.^{2} (39.4 kJ/m^2). The highest value of J achieved in any test was 312 lbf-in./in.^{2} (54.6 kJ/m^2). Test temperature for the TC-128B was nominally 10°F (-12°C).[17]

4.4.2 Stability Analysis Results

To perform the stability analysis, we first determined the applied J due to the pressure for various crack lengths. For the case of a thumbnail crack at the root of the dent, we assumed that the membrane stress was the hoop stress proportional to the pressure, and we assumed that the bending moment was constant and equal to the plastic moment of the plate, 10,000 lbf-in./in. For the thumbnail crack, we also assumed that the crack shape was such that the stress intensity was the same all along the crack front. This required that the crack grow wider faster than it grew deeper. A sequence of cracks that met this requirement is shown in Figure 48. Formulas for the applied J-integral as a function of load and geometry were derived from formulas for the stress intensity factors, which were in turn obtained from Tada's handbook [18] for the case of through-wall cracks and Newman and Raju [19] for the case of the thumbnail crack.
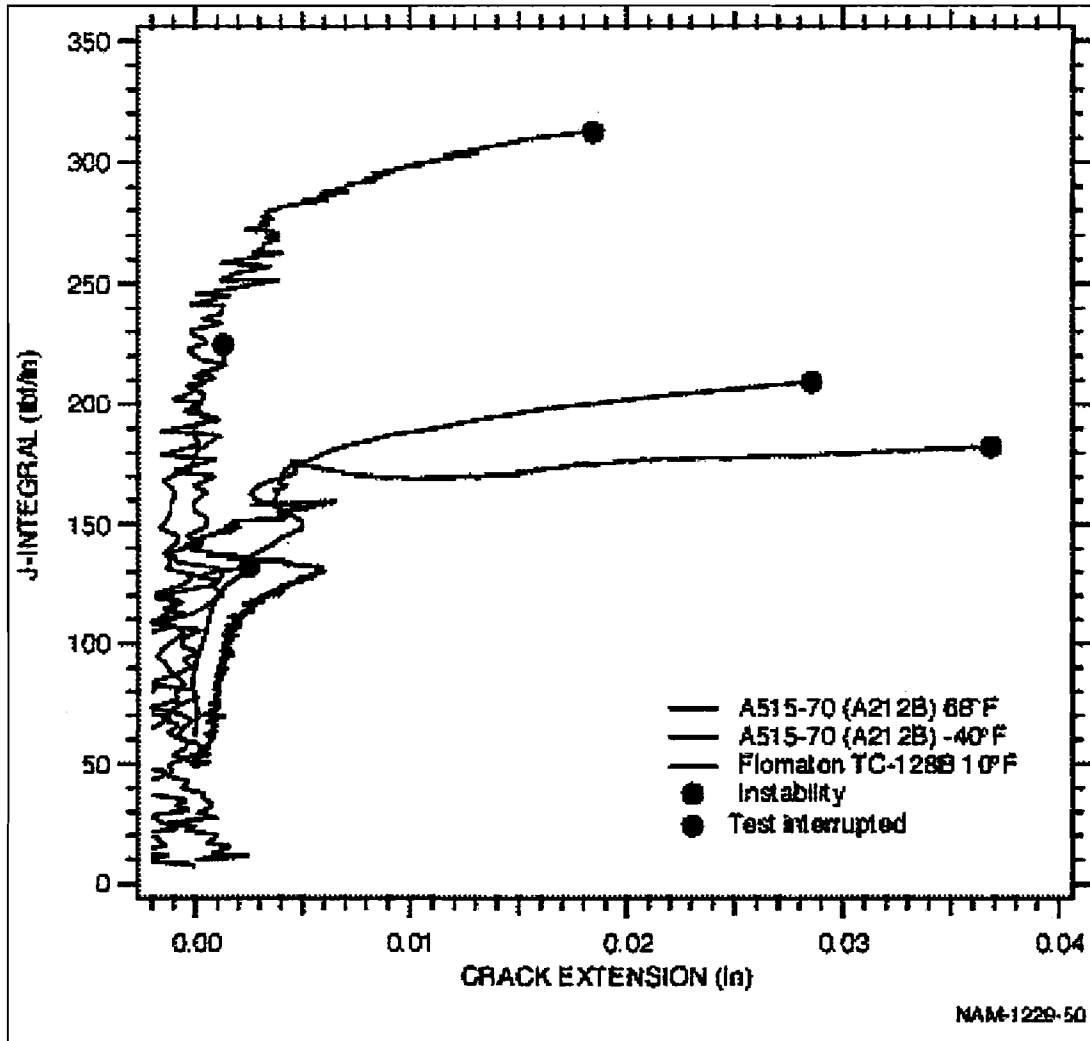
Figure 46. Results of J-R Curve Tests on Pressure Tank Car Steels
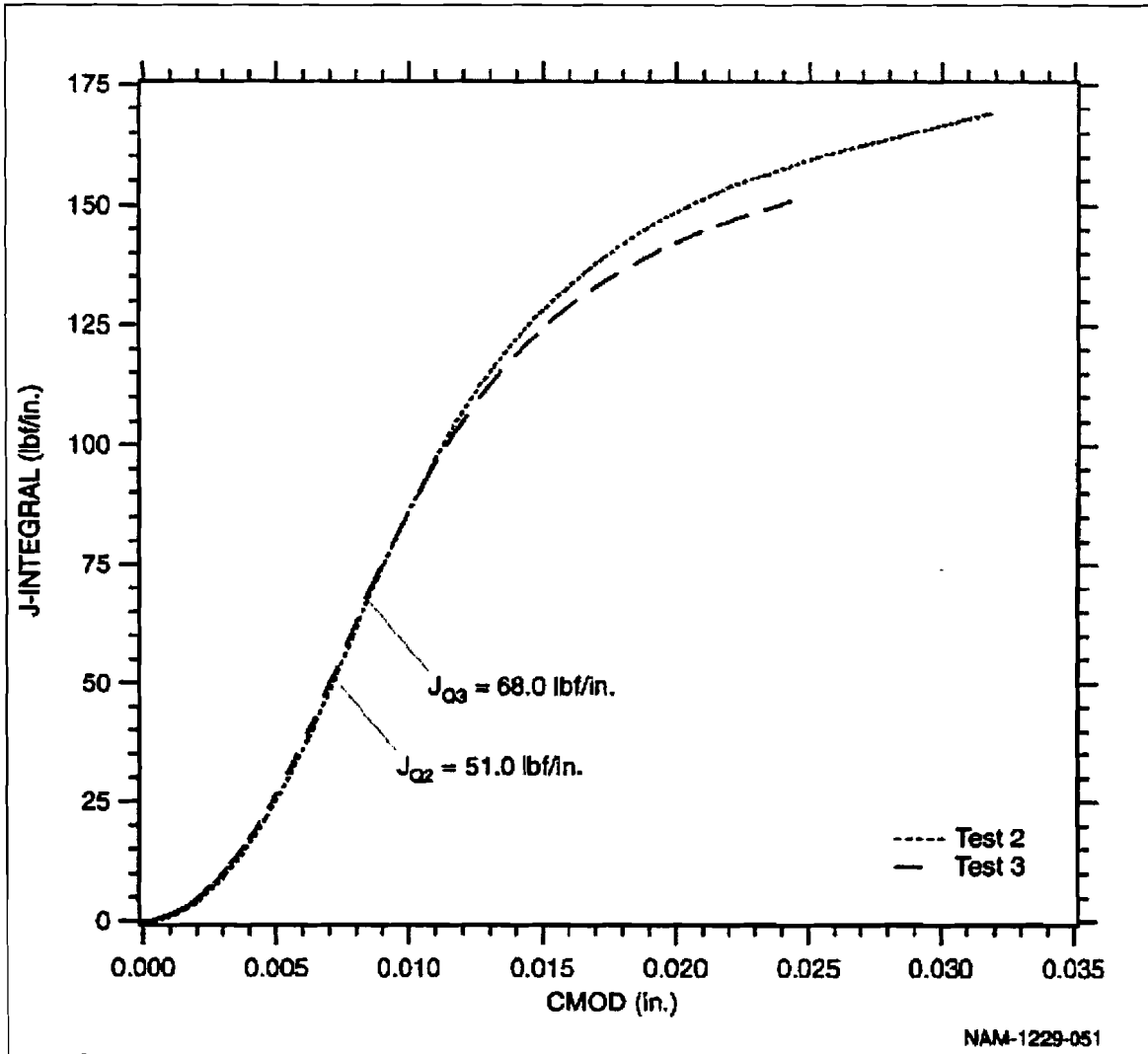
Figure 47. Results of Monotonic J_{ic} Tests on A515-70 (A212B) at -40°F
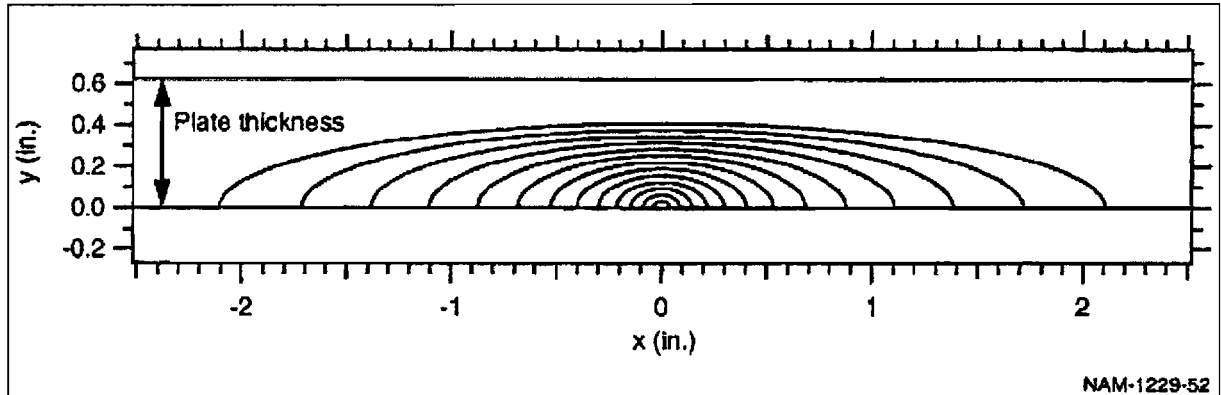
Figure 48. Profiles of Dent Root Thumbnail Cracks Growing with Constant Stress Intensity along the Crack Front for the Case of 285 psi Pressure and 15 klbf-in./in. Bending Moment

The resulting curves of applied J versus crack size for various tank pressures is shown in Figure 49 for the case of a through-wall crack in an undented tank and in Figure 50 for the case of a thumbnail crack in a dented tank. Figure 50 shows results for both crack length along the surface and for crack depth into the plate. The levels of the lowest and highest values of J observed in the fracture toughness tests are indicated. The intersection points with the applied J curves gives the expected crack length for fracture initiation and propagation for the extremes of steel behavior that we observed.

To obtain the stability of through-wall and thumbnail cracks, we superimposed the measured J-R curves for the tank car steels onto the curves for applied J versus crack length and pressure. An example is shown in Figure 51.

For those materials in which we measured no stable crack growth prior to instability in the laboratory fracture mechanics tests described above, the stability analysis is simple: instability occurs as soon as the applied J reaches the J value measured at instability. For those materials that sustained stable crack growth, instability for a given pressure occurs at the point where the derivative of the applied J with respect to crack length (at fixed pressure) is equal to the derivative of the J-R curve with respect to crack length. In other words, instability occurs where the two curves are tangent, as illustrated in Figure 51, and the initial crack length that leads to this unstable situation is the place where the J-R curve intersects the crack length axis. To find the tangency point for a given pressure, the J-R curve is slid back and forth horizontally until it is tangent to the applied J versus crack length curve.
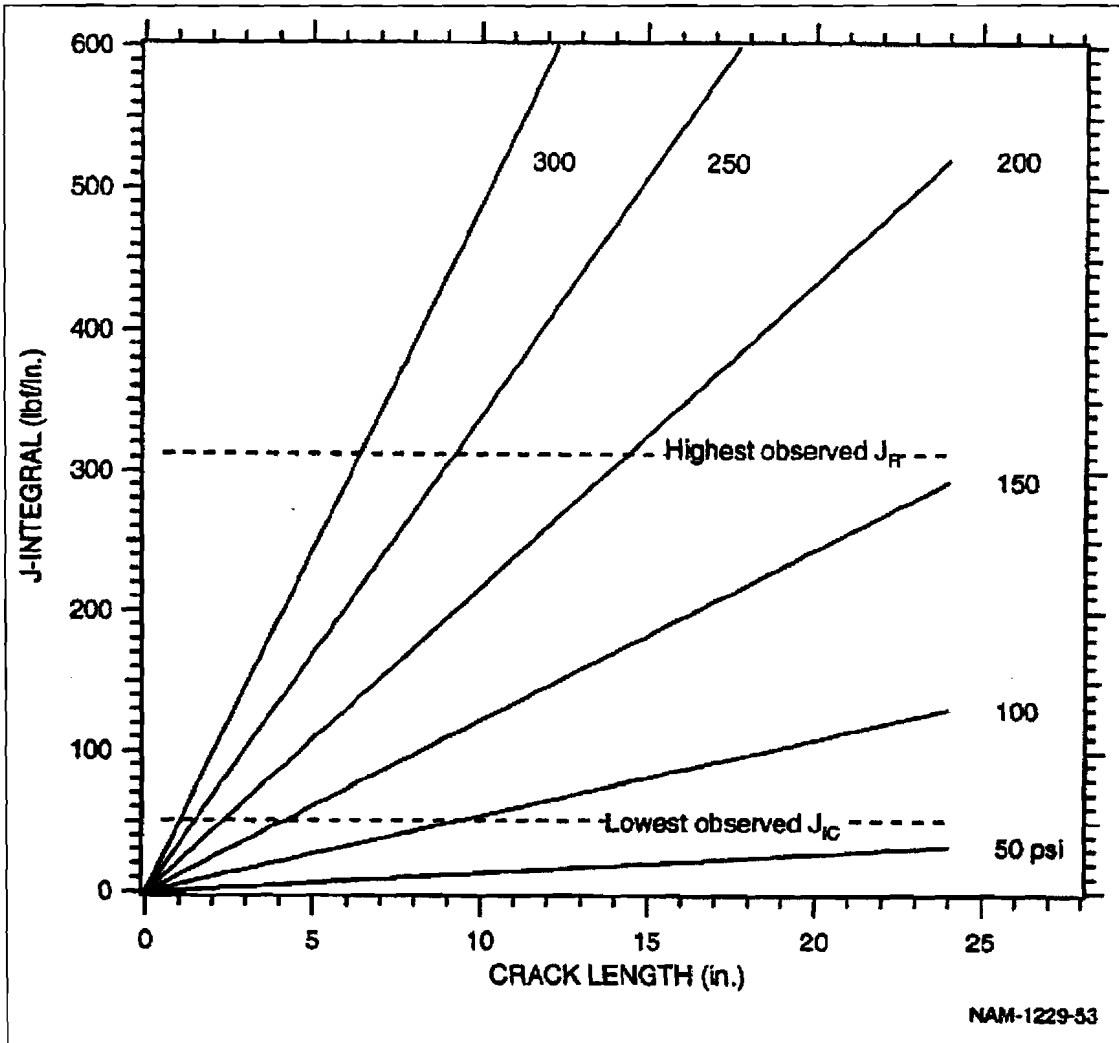
Figure 49. Applied J Versus Crack Length for Through-wall Crack

NAM-1229-53
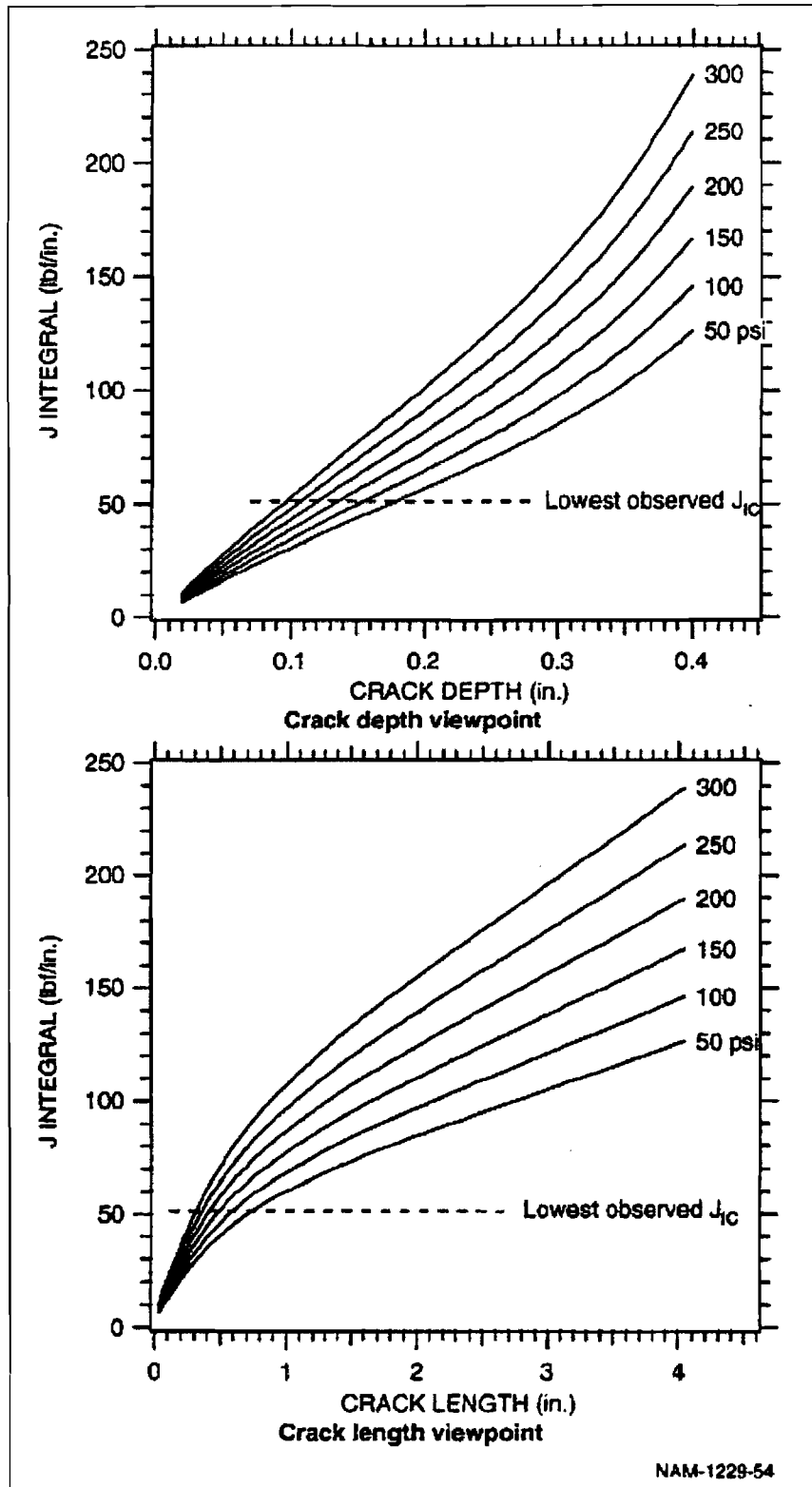
Figure 50. Applied J Versus Crack Length for Thumbnail
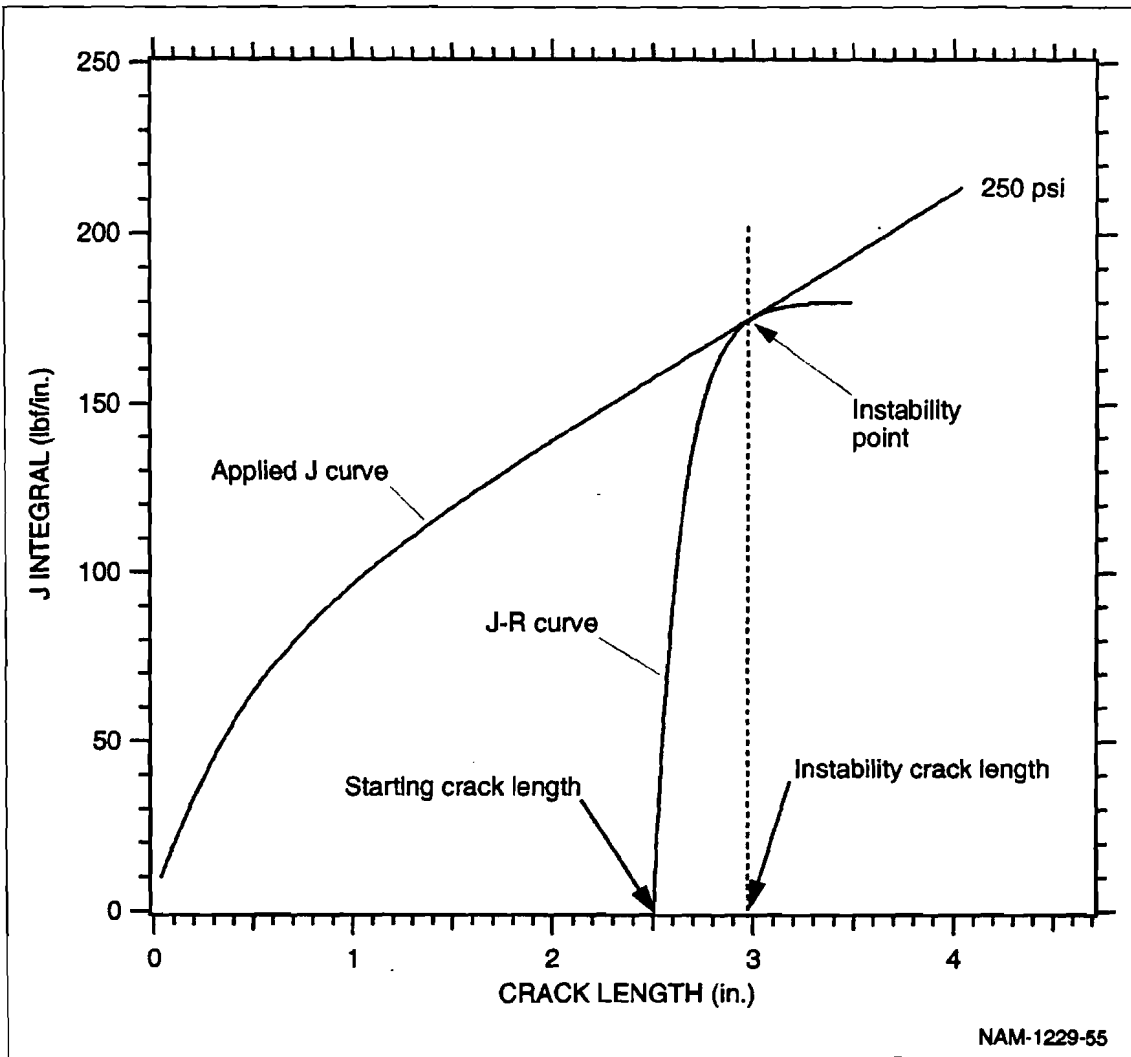
Figure 51. Graphical Representation of the Instability Crack Length

Recall that the J-R curve describes crack growth starting from a preexisting sharp crack of some initial length. The initial length is on the abscissa where the J-R curve intersects. The act of sliding the J-R curve back and forth simply adjusts this initial crack length.)

In all cases considered here, the point of tangency was at or beyond the end of the laboratory data, because the ASTM E1152 test specifications limited the amount of crack growth that could be accommodated in the tests.

Figure 52 shows an example and illustrates that the instability lengths that we derive are lower bounds for the true instability lengths. The fact that we were unable to grow cracks sufficiently to reach the true tangency points is immaterial, because we based our conclusions regarding crack and dent Guidelines on the cases in which there was no stable crack growth at all.
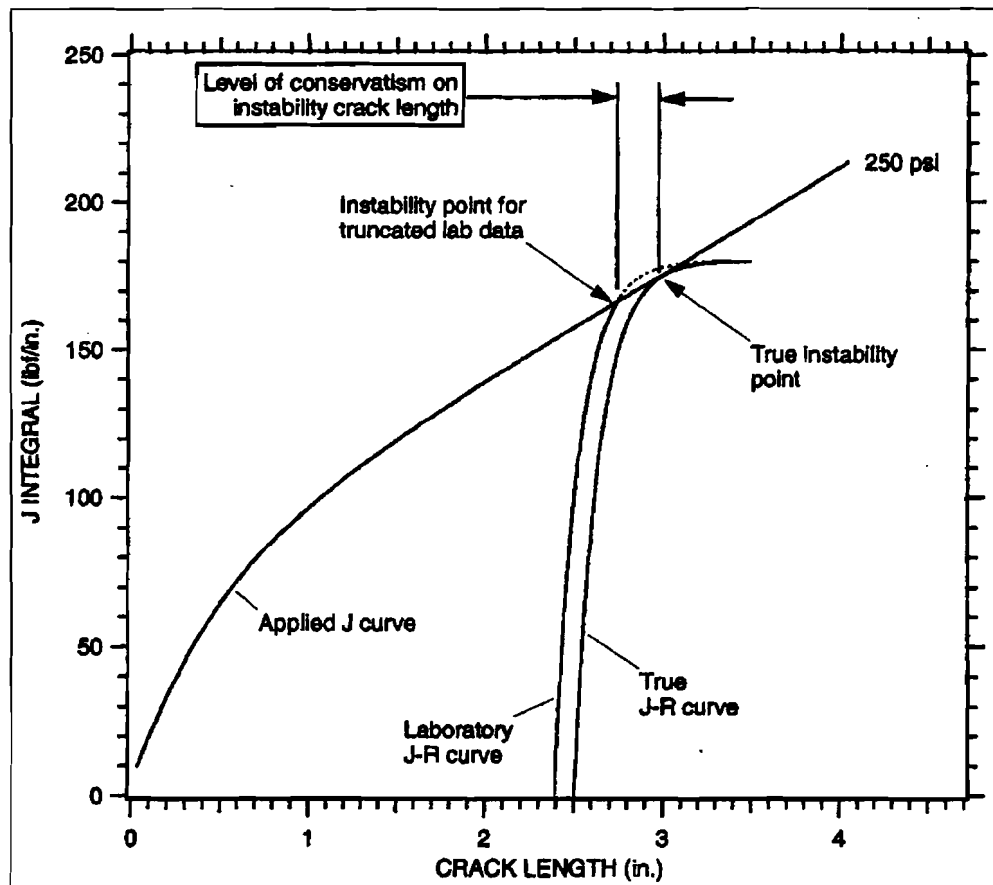
Figure 52. Example Showing How Truncating Laboratory J-R Curve
Introduces Conservatism on the Predicted Instability Crack Length

In addition, we estimate that the amount of truncated crack growth that is the level of conservatism amounts to a few hundredths of an inch (a few tenths of millimeters) stable growth for a crack that is already several inches long.

The resulting instability points for the J-R curves that we obtained in the laboratory are shown for a range of pressures in Tables 7 and 8.

Table 7. Predicted Crack Length (in inches) at Instability for Through-Wall Crack in Tension

	Temperature			Pressure (psi)			
Material	(°F)	50	100	150	200	250	300
A515-70	68	>96	33	15	8.4	5.4	3.7
A515-70	68	>96	38	17	9.6	6.2	4.3
A515-70	-40	>96	24	11	6.1	4.0	2.7
A515-70	-40	>96	31	14	7.8	5.0	3.5
A515-70	-40	>96	28	12	7.0	4.4	3.1
TC-128B AR	5	>96	58	26	14	9.2	6.4
TC-128B AR	11	>96	42	18	10	6.7	4.6

Table 8. Predicted Crack Length (in inches) at Instability for Thumbnail Crack in Tension and Bending

	Temperature			Pressure (psi)			
Specimen	(°F)	50	100	150	200	250	300
A515-70	68	>4	>4	>4	3.8	3.2	2.6
A515-70	68	>4	>4	>4	>4	3.9	3.3
A515-70	-40	>4	3.5	2.8	2.3	1.8	1.5
A515-70	-40	>4	>4	>4	3.4	2.8	2.3
A515-70	-40	>4	>4	3.5	2.8	2.3	1.9
TC-128B AR	5	>4	>4	>4	>4	>4	3.7
TC-128B AR	11	>4	>4	>4	>4	>4	>4

5.0 DISCUSSION

The local fracture model calibrated using round bar tests predicts the stress-strain and cleavage failure response of the simulated gouge test and the bend specimens reasonably well. The prediction is better for more acute features such as the 1/8-in. radius gouges than for blunt features such as the 1/4-inch radius gouges and the bend specimens, but errs on the conservative side, predicting that cleavage occurs at lower stresses and strains than actually occurs in tests (Figures 25 and 26). Thus, the model can be applied with confidence to a wide range of tank car damage situations.

The model for A515-70 weld heat-affected zone (HAZ) is essentially the same as for A515-70 base metal except that the results show slightly more scatter and somewhat higher strength for the HAZ [compare Figures 15(a) and 15(c)]. There appears to be little indication that the HAZ is particularly brittle, but it has a slightly lower ductility and more scatter in the failure stress and strain than the base metal. However, field experience has shown that welds can be significantly inferior to base metal, so we suggest that validating the Guidelines using these A515-70 weld results is not sufficient.

Fortunately, the Guidelines require validation only in two cases when damage involves welds. In all other cases, if damage involves a weld in any way, the tank must be unloaded. One case in which weld damage may be allowed is when there are cracks in welds used to attach reinforcement plates and brackets. The other is when scoring or gouging removes only the weld reinforcement. We will partially abandon the local fracture approach when validating these two guidelines, but will use conventional fracture mechanics below to show that these guidelines are valid nevertheless.

5.1 CRACK STABILITY

Under the assumption that the steels tested in this program are representative of all DOT112 tank cars, Tables 7 and 8 provide the pressure and crack size information needed to evaluate the safety of cars with cracks with and without dents. From Table 7 we conclude that, at 250 psi and in the absence of dents, cracks as short as 4.0 inches would be unstable, at least at -40°F (-40°C). However, again in the absence of dents, through-wall cracks longer than 8 ft (2.4 m) are stable below 50 psi tank pressure. (This observation disregards the rather obvious fact that such a crack would leak prodigiously!) Table 8 shows that thumbnail cracks at dent roots can be unstable at surface lengths as short as 3.5 in. (89 mm) at 100 psi and -40°F (-40°C).

Because practically any dent is longer than 3.5 in. (89 mm), our results further support the premise that cracks in dents should be considered unstable and can easily run the length of the dent and convert to through-wall cracks. If the dent is longer than the instability length given in Table 7 for cracks without dents, then the resulting through-wall crack would be unstable and the tank would fail catastrophically.

There appear to be two extremes of conservatism in reformulating the dent Guidelines based on the information in Tables 7 and 8. The first approach would be to assume that all dents are cracked, and that therefore the Guidelines should contain limits on dent length versus pressure. The limit lengths would be the crack lengths given in Table 7, possibly divided by a safety factor. This approach appears to be overly conservative given that dent cracking is very rare and appears to have occurred only in conjunction with other damage or welds and that dents are often longer than the lengths given in Table 7.

The second approach to reformulating the dent Guidelines would be to assume that dents are uncracked unless they occur in conjunction with other damage such as scores or gouges (or contain visible cracks) or in conjunction with welds. In this approach, dent length is disregarded, with the exception that any dent 8 ft (2.4 m) long or longer would necessarily involve a weld since tank car plates are maximum 8 ft (2.4 m) in extent. This second avenue is the same as for the current dent Guidelines except for the limits on radius of curvature, which we have shown to be of little value.

There are many possible approaches between the two extremes just described. One possibility would be to assume that dents are uncracked unless they occur in conjunction with other damage or in conjunction with welds, but to apply the Table 7 limits to any otherwise undamaged or dent that falls within a certain a certain distance of a weld but does not involve the weld directly. Another possibility would be to again assume dents are uncracked unless with other damage or welds, but to limit length to some length less than 8 ft (2.4 m) to allow a safety margin. We might also require that, regardless of length or pressure, all dents within a certain distance of a weld be considered to involve the weld even if the dent does not cross the weld. This again allows for a margin of safety.

Tables 7 and 8 and Figure 46 show that predicted instability crack lengths for as-rolled TC-128B steel at 10°F (-12°C) are longer than those for A515-70 (A212B) at room temperature. Thus, newer, TC-128B cars are predictably more flaw-tolerant than older A212B cars, and the safety of the overall car population will increase as A212B cars are withdrawn from the fleet.

We note that the fracture toughness of tank car shell plates is neither specified directly by DOT or AAR nor indirectly by AISI. Thus, the laboratory results in Table 7 probably do not represent the lowest toughness in the fleet. However, tank car welding procedures must be qualified by dropweight and tear tests. Although these tests do not guarantee that a steel or weld has a particular fracture toughness, the likelihood that a steel and weld could pass the dropweight and tear tests yet have low fracture toughness appears to be negligible.

5.2 EVALUATION AND VALIDATION OF THE GUIDELINES

Individual parts of the Guidelines and their validity are discussed as follows.

5.2.1 Guidelines for Cracks

The Guidelines for cracks require unloading if any cracks are visible, with the exception that cracks in welds used to attach brackets or reinforcement plates are not critical unless the crack extends into the base metal. The Guidelines for cracks read as follows:

- A *crack in the tank metal indicates serious damage. Cracks in welds, used to attach brackets or reinforcement plates, are not critical unless the crack extends into the base metal.*

- *Any crack found in the base metal of a tank, no matter how small, justifies unloading the tank as soon as possible. However, if in a yard, the car may be carefully moved to a designated remote location in the yard for transfer.*

- *When a crack is in conjunction with a dent, score, or gouge, the tank should be unloaded as soon as possible without moving it.*

Two parts of this guideline that require validating are the part regarding attachment weld cracks and the part that states that a car in a yard may be moved. Pellini reports at least one rupture originating from a crack in an attachment fillet weld (Austin, Manitoba) [Reference 3, page 2]. In that case, the rupture occurred during the accident when massive denting led to a stress concentration at the change in stiffness between the base metal and the attachment. When there is no denting, scoring, gouging, rail burn, or wheel burn associated with an attachment weld crack, the effect of the stress concentration is much less critical. Usually, attachments and reinforcements are lightly stressed. Furthermore, even if an attachment weld crack reaches base metal, it should not extend in an unstable fashion unless it is longer than the limits given in Table 7 or unless there is combined damage. As shown in Table 7, the crack stress intensity for a base metal crack without other damage is simply too low to drive the crack unless the crack is

several inches long. Attachment weld cracks are unlikely to be this long, although the Guidelines could be modified to say that attachment weld cracks are limited to, say, 3.5 in.

An attachment or reinforcement weld crack could be critical if it is highly stressed during re-railing. Fortunately, all the welds likely to be highly stressed are between attachments and doublers, not between attachments and the tank itself. At worst, a crack would extend through a doubler. For example, if a relatively large crack is located in the longitudinal weld along the upper edge of the stub sill and the car is dragged laterally by the stub sill, a long crack could result. This crack could readily extend into the doubler but not into the tank itself.

The part of the Guidelines stating that a cracked car may be moved if the crack is neither in a weld nor in conjunction with any other form of damage appears to be valid, *provided the length limits in Table 7 are not exceeded*. Such cracks appear not to be able to run, even under the lowest temperature conditions likely to be found in the field.

Explosion bulge tests on tank car plate [4] have confirmed that cracks are difficult to initiate in base metal. Given the difficulty of initiating a crack in base metal at field temperatures, the person performing damage assessment should be suspicious as to how a base metal crack got there. The inspector should try to determine whether there is a gross defect in the base metal.

5.2.2 Guidelines for Gouges

The Guidelines for scores imply that scores affecting the weld bead above the base metal are benign:

- *Scores or gouges crossing a weld and removing only the weld reinforcement are not critical.*

Even if a scored weld reinforcement results in an undetected crack completely through the weld bead, the situation is relatively safe as long as the crack is shorter than given in Table 7. Further support is provided by Pellini's rebuttal in Reference 3, p. 9, to the NTSB report [9] on the Waverly, Tennessee, accident. Pellini notes that, in experiments designed to replicate the Waverly weld crack just before catastrophic rupture, very low temperatures or dynamic loads had to be applied to cause fracture propagation. Thus, two pieces of evidence support the Guideline assumption that weld reinforcement damage indeed appears to be benign.

The Guidelines for base metal gouges require unloading when gouge depth versus tank pressure exceed limits given in tables in the Guidelines.

- *Tanks having scores or gouges should be unloaded in place when the internal pressure exceeds half of the allowable internal pressure listed in the tables below. Tables 1 and 2 show the allowable score depths and allowable pressures for 340W and 400W tanks, respectively.*

Validating the gouge guidelines therefore requires that we validate the tables. According to the results of SRI's simulated gouge coupon tests at -238°F (-150°C), shown in Figures 24 and 25, the weakest specimen failed at a nominal hoop stress of 53 ksi (372 MPa), which corresponds to a tank pressure of 499 psi (3.44 MPa). The corresponding tank pressure is computed assuming a 60-in. (1.52-m) radius and 9/16-in. (14.3-mm) thick shell. The results of the tests involving specimens with blunt gouges indicate that cleavage failure was preceded by considerable plastic flow, which began at about 54 ksi hoop stress, corresponding to 508 psi (3.50 MPa) tank pressure. To estimate the pressure for gouge root yielding at room temperature, we scale down by the ratio of the minimum allowable yield stress at room temperature (38 ksi or 262 MPa) to the yield stress at -238°F (-150°C) (113 ksi or 779 MPa). We obtain a corresponding hoop stress of tank pressure of 18 ksi (124 MPa), corresponding to a tank pressure of 171 psi (6.4-mm). These results pertain to the deepest gouges allowed in the tables, 1/4-in. deep.

The Guideline Tables 1 and 2 allow a pressure of 127 psi (876 kPa) for 1/4-in. (6.35-mm) deep gouges in 340W tanks. Therefore, the Guidelines for 1/4-in. (6.35-mm) gouges in 340W tanks appear to be valid, with a safety factor almost 4 for cleavage fracture and 1.3 for complete root yielding, based on the simulated gouge coupon tests. The flow stress increase due to work hardening would increase this latter safety factor to at least 1.7.

To validate the tables for 3/16-, 1/8-, and 1/16-in. (4.7-, 3.2-, and 1.6-mm) gouges, we apply the calibrated finite element model. We obtain hoop stress and tank pressures for 5% probability of failure as shown in Table 9. Table 9 also contains stresses and pressures corresponding to 1/4-in. (6/4-mm) deep gouges, obtained from the finite element model. Safety factors are based on the pressure for full plastic yielding of the gouge root, with the yield and ultimate stresses scaled down to the minimum allowed for A212-B Grade 70 steel, 38 ksi (262 MPa), and 70 ksi (483 MPa), respectively.

Table 9. Hoop Stresses and Tank Pressures for Cleavage and Plastic Yield Obtained from Finite Element Simulations

Gouge Depth (in.)	Hoop Stress for Cleavage (ksi)	Tank Pressure for Cleavage (psi)	Hoop Stress for Plastic Flow (ksi)	Tank Pressure for Plastic Flow (psi)	Table 1 Guidelines Allowable Pressure (psi)	Safety Factor
1/16	97	909	43	403	191	2.1
1/8	71	666	38	356	170	2.1
3/16	53	497	33	309	149	2.1
¼	36	338	26	245	127	1.9

5.2.3 Guidelines for Wheel Burn

Wheel burns are very similar to scores or gouges, except that wheel burns may exhibit metallurgical effects caused by frictional heating and rapid cooling. The Guidelines limit wheel burn depth to 1/8 in. (3.2 mm). Ignoring possible metallurgical changes, we can compare with the results of the finite element calculations for 1/8-in. (3.2-mm) gouges presented in Table 9. From Table 9, we estimate that a 1/8-inch (3.2-mm) deep wheel burn ought to sustain a tank pressure around 666 psi (4.59 MPa) before cleavage failure and 356 psi (2.45 MPa) before full plastic yielding at the root of the burn. The latter pressure exceeds relief valve pressure (255 psi) with a safety factor of 1.4. The stated pressures for cleavage are based on 5% probability.

The above analysis does not consider deleterious effects of frictional heating. In the Phase I literature search for this project, a reference [20] to metallographic cross sections of wheel burns showed that the heat-affected zones were of the order of 0.004 in. (102 µm) thick. The zones sometimes contained cracks, but these arrested without extending out of the zone. The Phase I report concluded that the metallurgical effects may not be significant, but that the insignificance should be established by analysis and experiments. Given our experience with the brittleness of flame-cut A515-70 plate edges and the lack of brittle edges in TC-128B plate, we suppose that TC-128B tanks are less susceptible to frictional heating damage. In any case, even if there is an undetected crack at the root of a wheel burn, the situation appears not to be critical, as was shown above in Figure 49 and Table 7 regarding cracks loaded in tension without bending. The crack driving force is simply too low for the crack to extend.

5.2.4 Guidelines for Dents

5.2.4.1 Long (Rail Burn) Dents

The Guidelines indicate that a long rail burn dent can reduce the rating of a tank by 50%.

- *Sharp dents in the shell of the tank (cylindrical section) which are parallel to the long axis are the most serious as these dents drop the rating of the tank by 50%.*

The validity of this statement is not clear, because long rail burn dents have resulted in tank rupture at pressures around 200 psi (i.e., a reduction in tank burst rating of perhaps 75%). The Newman and Raju [19] fracture mechanics analysis results in Figure 49 and Table 7 show why long dents parallel to the long axis of the tank can be hazardous. Let's assume that the dent root contains a 0.25-in-deep, 1.38-in-long thumbnail crack. With the crack plane oriented parallel to the long axis of the tank and for 5/8-in.-thick plate, 60-in.-radius, and 250-psi tank pressure, Newman and Raju [19] show that, when the crack is subject to hoop tension only, the peak J-integral is around 17 lbf-in./in.^{2} When a dent has been formed inward and then pushed outward by the tank pressure, a bending moment of 10,000 lbf-in./in. is combined with the tension and the resulting J-integral is 114 lbf-in./in.^{2} The bending moment due to the dent has increased the J-integral applied to the crack by a factor of 7.

Apparently, if there is a crack with applied bending moment, the crack will likely propagate. Without a dent there can be no moment. Thus, as Pellini repeatedly states, a crack can run the length of the dent. If the dent is long, the crack will be long and the tank contents will be released all at once. If the dent is short, the crack will be short, and the tank contents will be released more slowly (i.e., this will result in a leak-before-break situation).

The bending moment acting on a longitudinal dent is determined mainly by the plastic yield moment of the plate, rather than by the dent depth or angle. For this reason, the Guidelines need not consider dent depth or angle. This suggests that depth be considered in any modification of the Guidelines.

If there is a visible crack, the Guidelines appropriately suggest that rupture is possible. The question then becomes whether or not an undetected crack is likely to occur at the bottom or shoulders. The Guidelines and accident experience [3] suggest that, if the dent crosses a weld, a crack is likely, at least for A212 and TC-128B as-rolled tanks. The present Guidelines also suggest that 4-in.-radius dents in A212B tanks and 2-in.-radius dents in TC-128B tanks (or sharper dents) will likely contain macroscopic cracks. The validity of the present dent Guidelines

hinges on the validity of these radii limits. Our finite element analyses and dent/un-dent tests indicate that these radii limits are not justified and should be removed from the Guidelines.

When this research program was originally designed, we planned to perform simple three-point bend tests on tank car plate. We expected that plates bent in the lower shelf, cleavage regime, would fail somewhere near the bend radius limits in the Guidelines. If the failure radius was found to be any greater (less sharp bend), the dent guidelines should be considered invalid. When we performed those tests, however, we obtained the unexpected result that the plates failed at much larger radii, around 8 times the Guideline limits. These results suggest that dents found postaccident had to have been formed in the ductile regime and that it is the later behavior that is important. Thus, the dent situation is more complex than originally thought.

The Guidelines state that:

> "1. *For dents in the shell of tank cars built prior to 1967, the tank should be unloaded without moving it under the following conditions:*
>   -- *A minimum radius of curvature of 4 inches or less;*
>   -- *Have a crack anywhere;*
>   -- *Cross a weld; or*
>   -- *Include a score or gouge.*
>   *Dents with a radius of curvature more than 4 inches are not a problem by themselves.*
>
> 2. *For dents in the shell of tank cars built since 1967, the tank should be unloaded without moving it under the following conditions.*
>   -- *A minimum radius of curvature of 2 inches or less;*
>   -- *Have a crack anywhere;*
>   -- *Cross a weld;*
>   -- *Include a score or gouge; or*
>   -- *Show evidence of cold work.*
>   -- *Dents with a radius of curvature more than 2 inches are not a problem by themselves.*"

Obviously, if a crack is visible at the root of a dent, the situation is critical, and there is no need to worry about how the crack got there. If the dent involves a score or a gouge, the guideline implicitly suggests that there could be a crack, too. If the dent involves a weld, the Guidelines and field experience indicate the likelihood of a crack, at least in A212B and TC-128B as-rolled tanks. The Guidelines suggest that a crack in a dent in otherwise undamaged metal; i.e., away

from a score or weld, is unlikely unless the dent is creased sharper than 4-in. radius for A212B or 2-in. radius for TC-128B. Our results suggest that a crack in a dent in otherwise undamaged metal is unlikely regardless of the radius. In fact, the sharpest radii can exist only at the lowest, safest pressures. Otherwise, high pressures make dents flatten out to large radii of curvature.

For cleavage fracture to occur at a dent root, the steel would have to be on the lower shelf of the transition curve and the cleavage stress at that temperature would have to be exceeded. Our laboratory tests indicate this is unlikely to occur at field temperatures without impact loads. Tests in which welded A515-70 plates were bent to sharper than 1-in. (25.4-mm) radius at room temperature did not result in failure. Similarly, tests in which TC-128B as-rolled specimens were bent to 1-in. (25.4-mm) radii at -112°F (-80°C) also did not lead to failure. When either steel was cooled to -238°F (-150°C), cleavage failure did result, albeit at 30-in. (760-mm) radii. This result suggests that dent formation would always result in rupture during an accident if tank steel were on the lower shelf. Thus, cleavage failure in undamaged metal does not appear likely under field situations simply because lower shelf conditions cannot be reached.

In any event, the possibility of cleavage fracture occurring at the root of a dent could be ascertained by laboratory tests in which specimens are bent at room temperature, then bent back at -238°F (-150°C) to see whether the bending moment at the instant of cleavage could occur in a dent in a pressurized tank as determined by a finite element calculation. Because we recorded the loads during the -238°F (-150°C) bend tests, we already have an estimate of the bending moment for cleavage to initiate. These estimates do not take into account the prior plastic straining that would occur in the case in which a bend is first formed inward, but the literature suggests that this correction is relatively small and in fact improves the metal's resistance to cleavage [12].

The bending moment at failure is shown on the right-hand axis in Figure 27. Moments are typically 12-14 kip•in./in. (55-60 kN•m/m) at cleavage failure. The plastic moments at the bottom of a fully yielded and work hardened dent at room temperature and at -40°F (-40°C) are estimated to be 6.2 kip•in./in. (27.6 kN•m/m) and 10 kip•in./in. (35 kN•m/m), respectively. Thus, with increasing moment, yielding occurs well before cleavage, and cleavage failure therefore appears unlikely to occur at the root of a base metal dent that is otherwise uncracked or unscored. Yielding occurs at bending moments that are a factor of 1.6-2.0 less than bending moments required for cleavage.

5.2.4.2 Short or Broad Area Dents

The Guidelines imply that broad area dents in heads are benign unless combined with other damage or if bends are particularly sharp.

- *Massive dents in heads of the tank are generally not serious unless gouges or cracks are present with the dents.*

- *Small dents in heads not exceeding 12 inches in diameter in conjunction with cold work in the bottom of the dent are marginal if they show a radius of curvature less than 4" for tanks built prior to 1967 or less than 2" for tanks built since 1967. If at all possible, such tanks should be unloaded in place. In any case, the tank should be moved as little as possible and promptly unloaded.*

Considerations similar to those for rail burn dents apply here. These Guidelines need to be modified to remove reference to radius of curvature. The reference to cold work needs to be removed as well, since all dents involve cold work. Possibly, pressure versus length limits similar to those in Table 7 could be introduced to the Guidelines. However, in comparison to rail burn dents, the situation is mitigated by the three facts. First, the bending moment and tensile stresses are likely to be lower because head stresses are generally lower than shell hoop stresses. Second, the distance a crack could likely run is shorter. Third, head metal is often thicker than shell metal because of the way the head is formed.

5.2.4.3 Effect of Dent "Snap-Through" Instability

One failure mode seen in aerospace shells such as rocket fuel tanks is "snap-through" instability leading to dynamic fracture [21]. If a pressurized shell is dented inward by a blunt load, a diamond-shaped buckle pattern can result that has sharp creases at the corners. This pattern can be demonstrated using an empty aluminum beverage can. With a slight increase in internal pressure, this buckle pattern can become unstable and snap through to the original shape. The inertia of the shell material and contents carry the shell past the equilibrium shape, and high membrane tensions sufficient to rupture the shell can result. The propensity for snap-through depends on the relative resistance that the shell material provides to bending. Thick shells, ductile shells, and shell materials with strong work hardening tend to enhance stability. At present, we do not know the propensity for tank car for snap-through instability. We do not know of any cases of delayed fracture caused by such an event.

5.3 RERAILING METHODS FOR UNDAMAGED CARS

The above tank car simulations provide the information needed to determine lifting loads and the relative severity of the service pressure. The static stresses produced by the lading are small relative to the stresses induced by pressure. Because the lifting operations in salvage of derailed tank cars are performed statically and the tank car is typically lifted by the bolster or stub sill, we would expect the stresses in lifting operations to be very similar to those computed above. As a result, the pressure in the tank car is the most significant factor in determining the stresses that could result in a cleavage rupture.

The above results indicate that neglecting the lifting loads will not significantly reduce the factors of safety in evaluating a damaged tank car. The possible exception is if the most critical damage in the tank car is located adjacent to the stub sill or bolster. Because of the stress concentrations in this area of the tank with service loads, damage in these locations would be most significantly influenced by the salvage operations.

5.4 LIMITATIONS OF THE RESULTS

The results obtained in the present program are limited mainly because we cannot anticipate every damage situation or anticipate every defect in materials or construction techniques. There is always some probability, very small but nevertheless borne out by field experience [3], that defective steel or welds could slip past inspection.

The crack stability analyses presented above depend on measured fracture toughness properties of tank car steel. Unfortunately, there is (or was) no specification for the fracture toughness of A212B or TC-128B. Thus, the stability analyses are limited to the extent that the fracture properties measured in our tests reflect the properties of the steel in the fleet. Fortunately, TC-128B base metal and welds must pass Charpy impact tests, and welders and welding procedures are inspected repeatedly during tank car fabrication. The probability that a tank car plate or weld could pass the Charpy and weld inspections yet end up having low fracture toughness is low but may not negligible. One remedy would be to add fracture toughness specifications to the tank car steel and welding specifications. However, the added specification is no guarantee that a region of low toughness would not exist somewhere on some tank car.

The Guidelines themselves are limited because the Guidelines depend on the inspector being able to see damage. Insulation, jackets, the ground, or other obstructions may prevent damage from being seen. Reference 3 mentions at least two cases in which long rail burn dents were buried in insulation. These dents later ruptured catastrophically. There may be other buried dents in the fleet.

There are other limitations. For example, neither the Guidelines nor the present results address fire damage. The present results pertain mainly to DOT 112A340W cars, and no attempt has been made to extrapolate to other pressure cars or nonpressure cars.

Despite these limitations, the results are useful because we have been careful to err on the conservative side in our validation. We have verified our findings using the local fracture approach, the engineering approach, reports of field experience, and the overall rarity of serious accidents. We feel that none of the Guidelines found to be valid in the present effort could later be found invalid.

6.0 CONCLUSIONS

Existing AAR Accident Damage Assessment Guidelines lack validation. To validate the Guidelines, SRI International performed a research program combining laboratory tests and computer simulations. The approach was to focus on DOT 112A340W tanks and use laboratory tests on A515 Grade 70 plate and welds and TC-128B as-rolled plate to calibrate a finite element failure model. SRI also performed laboratory tests to directly simulate damage in the form of gouges and dents.

The research program provided the following results pertaining to DOT 112A340W tanks:

- The Guidelines involving cracks are valid, for the most part because the Guidelines require tank unloading for almost any crack. For the exception when a crack is in an attachment weld, the Guidelines are valid because, unless the crack is in concert with other damage, such cracks may result in leaks, but are unlikely to extend catastrophically.

- The Guidelines for base-metal scores and gouges are valid, with safety factors ranging from 1.3 to 2.1. The Guidelines for scores or gouges removing only weld bead reinforcement are valid because of the extra strength of the weld filler metal and because, even if the weld contains an undetected crack, the crack is unlikely to extend catastrophically in the absence of other damage; e.g., a dent.

- The Guidelines for wheel burn are valid with a safety factor of roughly 1.4.

- The Guidelines for otherwise undamaged dents need to be modified to remove dependence on dent radius of curvature, because radius of curvature has little bearing on propensity for failure. At pressures above approximately 100 psi, dents are forced back out to yield large radii of curvature and can almost disappear at relief valve discharge pressures.

- Dents without other damage such as cracks, scores, or gouges and dents that do not involve welds appear unlikely to crack no matter what the radius of curvature. However, dents with cracks are dangerous, because cracks at dent roots can easily extend, driven by the pressure-induced bending moment. Thus, it appears that the dent Guidelines should be reformulated to be based on an assessment of the likelihood that a dent contains a hidden crack. Two extremes to this assessment are either to assume that all dents contain cracks or to assume that dents without obvious cracks, scores, or gouges and that do not involve welds never contain cracks. The best approach is probably somewhere in between.

- Salvage operations on undamaged tank cars are unlikely to generate stresses of any significant magnitude compared to allowable pressure stresses in the tank.

- We have developed a computational tool that allows extension of the Guidelines to other tank cars, damage scenarios, and salvage operations.

The reliable 15-year history of the Guidelines is, in itself, partial validation. The history implies a reasonable level of conservatism since, fortunately, only very few catastrophic delayed ruptures have occurred, and those ruptures occurred in cases where the tank damage would not have passed the Guidelines' rules.

7.0 RECOMMENDATIONS

The Phase I literature search and the validation effort described above have uncovered several issues important to damage assessment that could be addressed to improve the Guidelines validation. To address these issues, we offer several recommendations in the following paragraphs.

We investigated the effect of rerailing loads on undamaged tank cars and found that rerailing stresses are small compared to pressure stresses for pressures of about 100 psi and above. We approximated the effect of rerailing loads on damaged cars by applying the loads computed for undamaged cars to small sections of damaged plates using finite element models. This approximation assumes that damage is localized and does not alter grossly the global geometry of the tank. Thus, this approximation may be inaccurate in cases of large or deep dents. To verify the limits of the approximation and to understand the need for the Guidelines to address rerailing methods, we recommend the following.

- Perform finite element simulations in which damage is simulated by impacting a car as described above and then applying simulated rerailing loads. A variety of dent orientations

and locations should be explored. The resulting stresses can be compared with failure stresses determined previously to assess the likelihood of rupture.

The above analysis could also include loads experienced by cars in regular train service, which would give some indication of the risk of undetected damage, e.g., rail burns hidden under insulation.

The local fracture approach to validating the Guidelines has resulted in a computational tool that allows extension of the Guidelines to other tank cars, damage scenarios, and salvage operations. We recommend that this tool be applied to address the effects of different lifting scenarios on tank cars with damage. We also recommend that the local fracture approach be extended to the case of a reversed cycle of plastic deformation as occurs at the root of a dent that undergoes in/out bending.

In addition to the above, several recommendations contained in the Phase I final report [1] remain to be addressed. Namely, to improve the reliability and usefulness of the Guidelines, we recommend that the following research be initiated.

- Refine the safety factors for wheel burns and gouges by investigating the effects of frictional-heat-induced metallurgical changes at the root of the burn, the effects of root roughness on gouges, and the effects of work hardening on both. Although the effects appear to be minimal, they should be confirmed by small-scale laboratory tests.

- Assess the possibility of creep and environmentally assisted crack growth leading to delayed rupture. The J-integral tests described above could be extended to include creep crack growth measurements and environmentally assisted crack growth measurements.

- Evaluate the applicability of current NDE equipment and recommend use of suitable NDE techniques in the Guidelines. NDE is an established tool for assessing cracked pressure vessels and may be suitable for use on damaged tank cars in cases where cracks are hidden. In addition, there may be unconventional NDE techniques that could indicate the presence of dents, scores, gouges, or wheel burns hidden against the ground or beneath jacketing.

- Monitor and participate in the activities of the committee on Post-Construction Standards of the Pressure Vessel and Piping Division of the American Society of Mechanical Engineers.

95

8.0 ABBREVIATIONS AND GLOSSARY

AAR	Association of American Railroads
AAR/TTCI	Association of American Railroads, Transportation Technology Center, Inc. Pueblo, Colorado
CMOD	Crack-mouth opening displacement
DOT	United States Department of Transportation
DYNA3D	An explicit dynamic finite element code for analyzing materials and structures
EPFM	Elastic-plastic fracture mechanics, for the analysis of cracks in situations where a yielded region that is large relative to specimen dimensions emanates from the crack.
FRA	Federal Railroad Administration, within the DOT
HAZ	The heat-affected zone is an area in the undisturbed tank metal next to the zone actual weld material. This zone is less ductile than either the weld or the plate due to the effect of the heat on the welding process.
LEFM	Linear elastic fracture mechanics, for analysis of macroscopic cracks
NDE	Nondestructive evaluation
NDT	Nil ductility temperature. The temperature below which a specially prepared welded plate specimen impacted by a falling weight fractures in a brittle manner, absorbing little energy.
SGFAS	Slide-graph fracture analysis system. Developed by Pellini for the rapid determination of fracture resistance of steel structures, based on shifts of the NDT.
cold work	Cold work is deformation of steel when it is bent at ambient temperatures without benefit of heat treatment or suffers an impact or static load (i.e., a tank sliding over a solid object with a rounded point).
crack	A crack is a narrow split or break in the tank metal that may penetrate through the tank metal.
dent	A dent is a deformation that changes the tank contour from that of original manufacture as a result of impact with a relatively blunk object (coupler or end of an adjacent car).
gouge	A gouge is removal of the tank or weld metal along the line of contact with another object. This causes a reduction in tank metal thickness.
internal pressure	Internal pressure is the force against the internal surfaces of the tank caused by the vapor pressure of the contents.
jacket	The jacket is the first thin steel outer shell that holds the insulation or thermal protection in place and protects the tank from the elements. The jacket is not designed to hold the leaking contents of the car.

radius of curvature	Radius of curvature is used to describe the sharpness of a curve (dent). A small radius of curvature indicates a small circle and a sharp bend, whereas a larger radius of curvature indicates a larger circle and a more gentle band.
rail burn	A rail burn is a long dent, usually parallel to the length of the tank which crosses a weld and causes cold work. It may be caused by the tank passing over a section of rail.
score	A score is a relocation of tank or weld metal so that the metal is pushed aside along the line of contact with another object. This causes a reduction in tank metal thickness.
tank	"Tank" in this document refers to the actual tank car tank.
transition temperature	Transition temperature is the point where the properties of steel change from ductile to brittle.
wheel burn	A wheel burn is similar to a gouge but is caused by prolonged wheel contact with the tank.

References

1. Giovanola, J. H., and D. A. Shockey, "Literature Search and Evaluation Pertaining to Damage Assessment of Tank Cars Involved in Accidents," Phase I Final Report prepared for the Association of American Railroads Transportation Technology Center, Subcontract No. 940986 under Federal Railroad Administration Contract No. DTFR53-93-C-00001, Task Order 115, SRI International (Project 7483), Menlo Park, CA (October 1995).

2. Davis, J. C., AAR private communication (1997).

3. Pellini, W. S., "Analysis of Tank Car Failures Related to Rail Burn Dents," Association of American Railroads, Report No. R-551, Chicago, Illinois (June 1983).

4. Pellini, W. S., "Feasibility Analysis for Tank Car Applications of New Microalloyed and Controlled Rolled Steels—Description of Fracture Properties and Comparisons with Steels in Present Use," Association of American Railroads, Report No. R-543, Chicago, Illinois (April 1983).

5. Phillips, E. A., and W. S. Pellini, "Phase 03 Report on Behavior of Pressure Tank Car Steels in Accidents," Association of American Railroads, Report No. RA-03-6-48 (AAR R-553), Chicago, Illinois (June 20, 1983).

6. Pellini, W. S., "Slide Graph Fracture Analysis System," Association of American Railroads, Report No. R-552, Chicago, Illinois (June 1983).

7. Pellini, W. S., "Guidelines for Fracture-Safe Design of Steel Structures," Association of American Railroads, Report No. R-455, Chicago, Illinois (November 1980).

8. Pellini, W. S., "Guidelines for Fatigue-Reliable Design of Steel Structures," Association of American Railroads, Report No. R-490, Chicago, Illinois (September 1981).

9. National Transportation Safety Board, "Derailment of Louisville and Nashville Railroad Company's Train No. 584 and Subsequent Rupture of Tank Car Containing Liquefied Petroleum Gas Waverly, Tennessee" Railroad Accident Report No. NTSB-RAR-79-1, Notation 2313B, Washington, DC (February 22, 1978).

10. *Metals Handbook, 7th Edition* (Metals Park, Ohio, American Society for Metals, 1965), p. 65.

11. *Metals Handbook, Volume 1, 8th Edition* (Metals Park, Ohio, ASM International, 1978), p. 195.

12. Beremin, F. M., "1983, "A Local Criterion for Cleavage Fracture of a Nuclear Pressure Vessel Steel," Metallurgical Transactions A, Vol. 14A (November, 1983), pp. 2277-2287.

13. Whirley, R. G., and B. E. Engelman, "DYNA3D—A Nonlinear, Explicit, Three-Dimensional Finite Element Code for Solid and Structural Mechanics—User Manual," Report UCRL-MA-107254 Rev. 1, Lawrence Livermore National Laboratory (November 1993).

14. Owen, D.R.J., and E. Hinton, *Finite Elements in Plasticity: Theory and Practice* (Swansen, United Kingdom, Pineridge Press, 1980).

15. "Standard Test Method for J_{IC}, A Measure of Fracture Toughness," ASTM E 813-87 (ASTM, Philadelphia, 1987).

16. "Standard Test Method for Determining J-R Curves," ASTM E 1152-87 (ASTM, Philadelphia, 1987).

17. Reuter, W. G., J. D. Mudlin, R. L. Harris, F. M. Haggag, W. L. Server, and J. S. Epstein, "Evaluation of Damaged Tank Car Structural Integrity," Department of Transportation, Federal Railroad Administration, Office of Research and Development Report DOT/ FRA/ORD-88/02 (January 1988).

18. Tada, H., P. Paris, and G. Irwin, "The Stress Analysis of Cracks Handbook," Del Research Corporation, St. Louis (1973).

19. Newman, J. C., and I. S. Raju, "An Empirical Stress Intensity Factor Equation for the Surface Crack," *Engr. Fracture Mechanics* **15**, 185-192 (1981).

20. Rocheleau, D., "Tank Car Wheel Gouge, PROX 80665, Bonfield Derailment," Report #LP 41/95, File #580-3 R95H0003, Transportation Safety Board of Canada, Gloucester, Ontario (February 1995).

21. Bushnell, D., *Computerized Buckling Analysis of Shells* (Dordrecht, The Netherlands, Martinus Nijhoff, 1985).
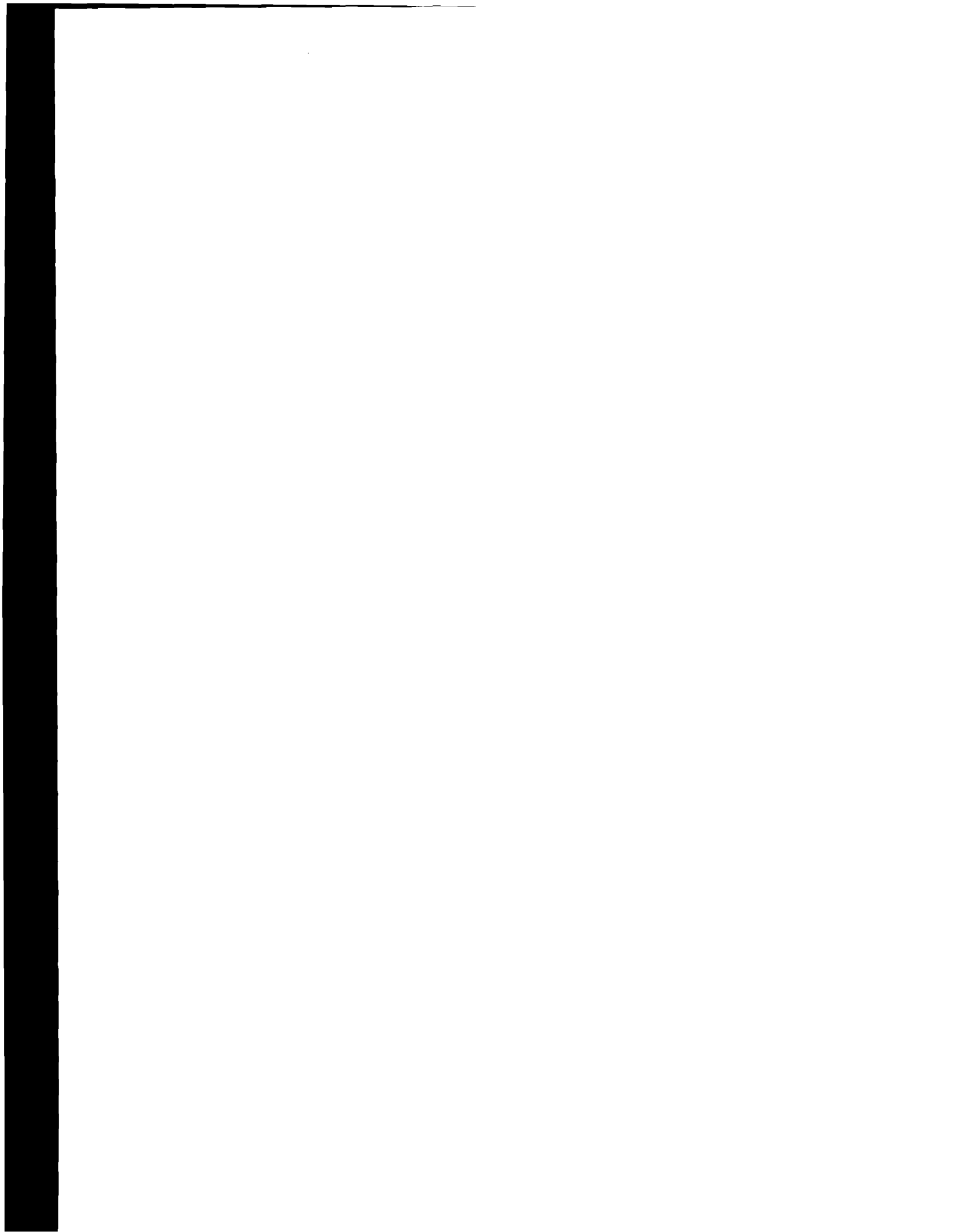
APPENDIX A:

A515-70 PLATES USING WELD PROCEDURE I.T.1.2

WELDING PROCEDURE SPECIFICATION

WPS#: 1.T.1.2

Qualified by PQR#: 1.T.1.2, 1.T.1.3, 1.T.3.2

Material Specification: AAR TC128 GRB TO SAME or P1 TO P1

Welding Process: SUBMERGED ARC WELDING (TANDEM)

Manual or Machine: MACHINE

Position of Welding: FLAT (1G)

Filler Metal Specification: SFA 5.17

Filler Metal Classification: EM12K (LINCOLN L-61)

F No.: 6   A No.: 1

Flux: LINCOLN 780

*Weld Metal Grade:

Type of Backing: FLUX (LINCOLN 780)

Shielding Gas: N/A   Flow Rate (CFH): N/A

Single or Multiple Pass: MULTIPLE

Single or Multiple Arc: MULTIPLE

Welding Current: LEAD ELECTRODE (DC) TRAIL ELECTRODE (AC)

Polarity: LEAD ELECTRODE (REVERSE) TRAIL ELECTRODE (N/A)

Electrical Stickout: 1-1/4" +/- 1/8"

Welding Progression: N/A

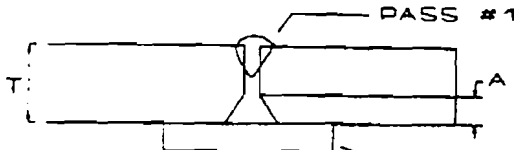Root Treatment: REMOVE SLAG WITH SCALING HAMMER

Preheat: 50°F   Interpass Temperature: 500°F

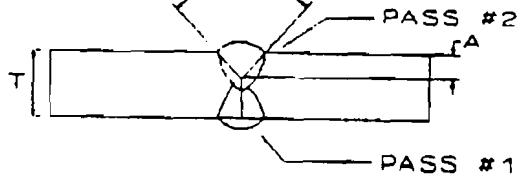Postweld Heat Treatment: 1200°F / 1 HOUR

DETAIL 1A

T = 0 - 1/16"

— PASS #1

T

A

FOR THICKNESS <= 1/2", "A"=5/32" FLUX
FOR THICKNESS > 1/2", "A"=7/32" BACKUP

DETAIL 1B

90 degrees

— PASS #2

T

A

— PASS #1

LINCOLN L-61 ELECTRODE / 780 FLUX

DETAIL	THICK-NESS	PASS NO.	POS.	DIA.	AMPS	VOLTS	TRAVEL SPEED	REMARKS
1A	7/16"	1	1G	5/32"	600-650	30	34-36	DC
1A	7/16"	1	1G	5/32"	600	37	34-36	AC
1B	7/16"	2	1G	5/32"	850	32-33	34-36	DC
1B	7/16"	2	1G	5/32"	600	37	34-36	AC
1A	5/8"	1	1G	5/32"	625-675	31	32	DC
1A	5/8"	1	1G	5/32"	600	37	32	AC
1B	5/8"	2	1G	5/32"	900	34	32	DC
1B	5/8"	2	1G	5/32"	600	37	32	AC
1A	9/16"	1	1G	5/32"	625-675	31	34-36	DC
1A	9/16"	1	1G	5/32"	600	37	34-36	AC
1B	9/16"	2	1G	5/32"	900	34	36	DC
1B	9/16"	2	1G	5/32"	600	37	36	AC

80 degrees
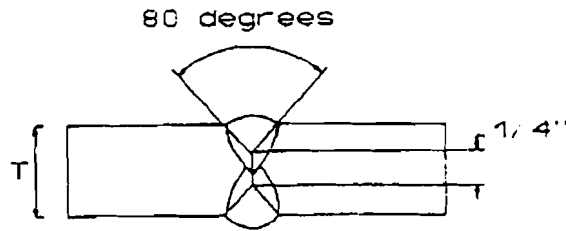
DETAIL 2

LINCOLN L-61 ELECTRODE / 780 FLUX

DETAIL	THICK-NESS	PASS NO.	POS.	DIA.	AMPS	VOLTS	TRAVEL SPEED	REMARKS
2	11/16"	1	1G	5/32"	700-750	33	32	DCRP-LEAD
2	11/16"	1	1G	5/32"	750	39-40	32	AC
2	11/16"	2	1G	5/32"	900	35	32	DCRP-LEAD
2	11/16"	2	1G	5/32"	750	39-40	32	AC
2	13/16"	1	1G	5/32"	750	33	32	DCRP-LEAD
2	13/16"	1	1G	5/32"	700-750	39	32	AC
2	13/16"	2	1G	5/32"	900-950	35	32	DCRP-LEAD
2	13/16"	2	1G	5/32"	700-750	39	32	AC
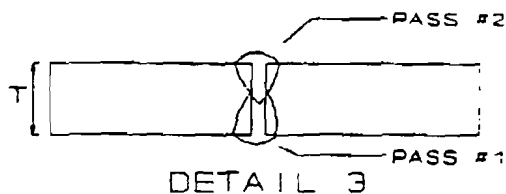
PASS #2

T

DETAIL 3

PASS #1

LINCOLN L-61 ELECTRODE / 780 FLUX

DETAIL	THICK-NESS	PASS NO.	POS.	DIA.	AMPS	VOLTS	TRAVEL SPEED	REMARKS
3	7/16"	1	1G	5/32"	600-650	30	34-36	DC
3	7/16"	1	1G	5/32"	600	37	34-36	AC
3	7/16"	2	1G	5/32"	850	32-33	34-36	DC
3	7/16"	2	1G	5/32"	600	37	34-36	AC
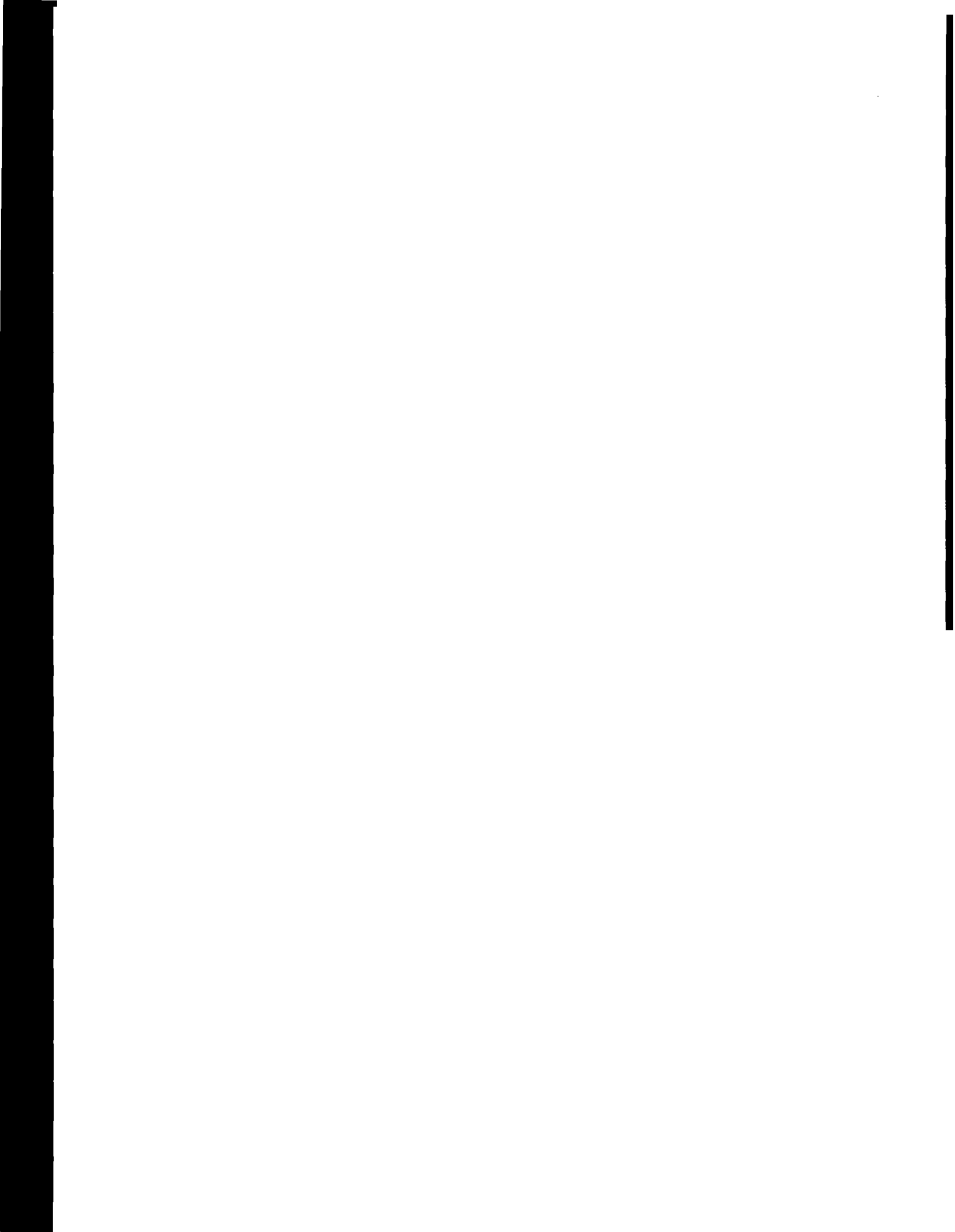
APPENDIX B:

FAILURE ANALYSIS OF TANK CAR ACFX 80417

B1.0 INTRODUCTION

On May 25, 1995 tank car ACFX 80417, a 112T340W car, was impacted on the A-end by a locomotive at Flomaton, AL. The ambient temperature was 90F. The impact resulted in a large dent in the head and a transverse buckle 33-inches inboard of the body bolster as shown in Figure B-1. The stub sill and body bolster were sheared away upon impact. The vinyl chloride lading began to escape from a crack at the end dent which was plugged before an attempt was made to right the car. As the car was being righted a second leak began from a 35-inch long crack that was within the transverse buckle. As transverse dents with large radii of curvature which do not cross welds are not considered critical by the current guidelines, a metallurgical examination was carried out to determined the origin and nature of this crack.
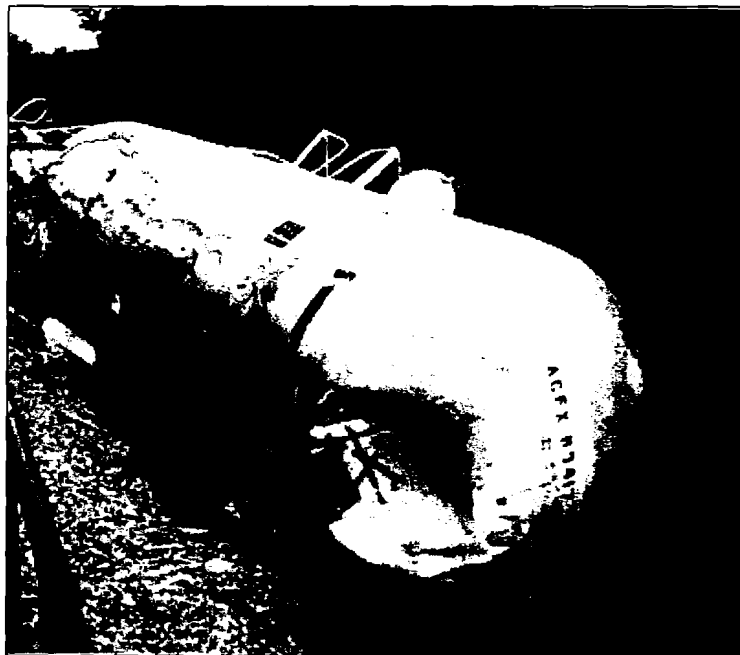

Figure B-1. View of ACFX 80417 After Impact

B2.0 VISUAL EXAMINATION

Figure B-2 shows the transverse crack within the buckled area of ACFX 80417. One half of the fracture is shown in Figure B-3, and the chevron patterns on the fracture face indicate that the crack initiated from the toe of the weld securing the lower bracket of the placard holder. This weld appears to have been a manual arc weld. There appears to be a 1/32 to 1/16-in.-long heat-affected-zone tear at the origin of the 36-in.-long crack, Figure B-4. There is no visible evidence of fatigue cracking at the origin. Further, the entire 36-in.-long crack was brittle. No evidence of plastic fracture was evident by visual inspection and there was no measurable lateral expansion or contraction along the thickness of the plate.

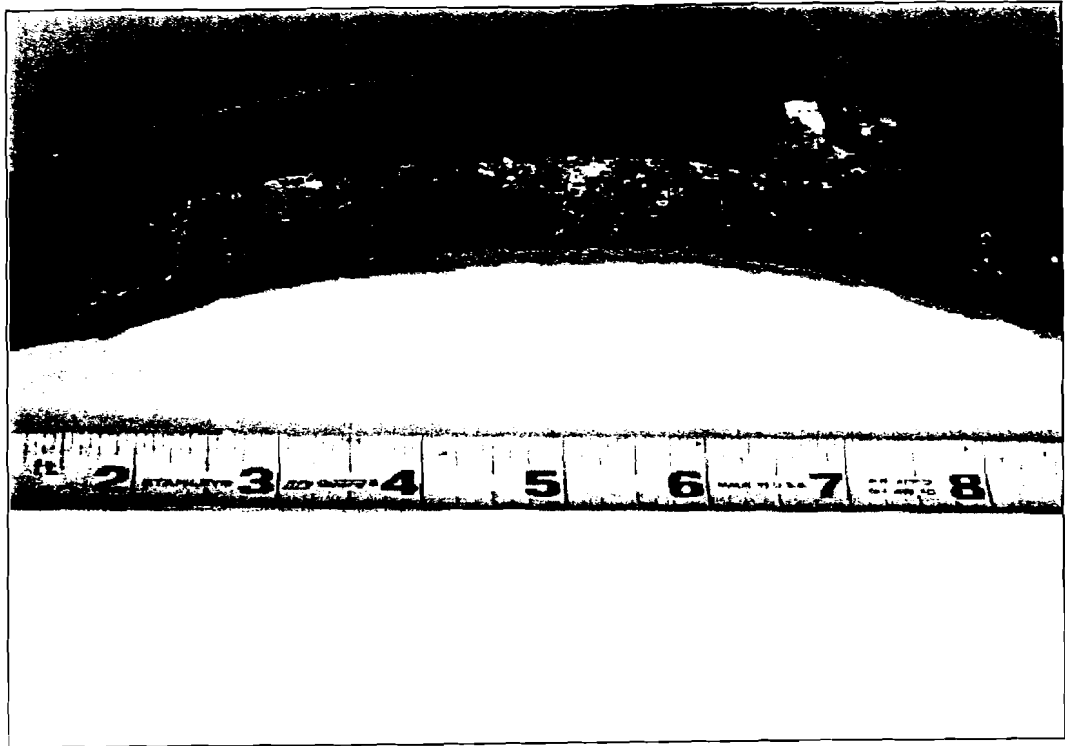**Figure B-2. Buckle and Crack in ACFX 80417**

Figure B-3. Fracture Surface with Chevron Marks Indicating
Origin of Crack at the Toe of Placard Weld

Figure B-4. Origin of Crack at Toe of Placard Weld

B3.0 CHEMICAL ANALYSIS

The results of the chemical analysis of a sample remove from the plate are given in Table B-1. The chemical composition of the plate is within the specification for TC-128-B steel.

Table B-1. Chemical Composition of Plate Containing Circumferential Crack in ACFX 80417

Element	TC128B Specified Check Analysis Requirements, Weight Percent	Results of Check Analysis, Weight Percent
Carbon	<0.29	0.20
Manganese	0.92-1.46	1.12
Phosphorus	<0.035	0.006
Sulfur	<0.040	0.018
Silicon	0.13-0.45	0.21
Vanadium	<0.08	0.036
Copper	<0.35	0.26
Nickel	<0.25	0.08
Chromium	<0.25	<0.01
Molybdenum	<0.08	0.04

B4.0 IMPACT TESTING

One set of longitudinal and one set of transverse Charpy v-notch specimens were cut from the base material of the plate and fractured at temperatures between 0 and 100°F. The results of the charpy test was shown in Table B-2. While Charpy values are not specified for TC-128-B they can be compared to values from other plates given in reference 1. As can be seen from the plot of the fracture energy versus temperature in Figure B-5 the values for the specimens from ACFX 80417 lie along the lower bound of the range of expected properties for TC128B.

**Table B-2. Charpy V-Notch Impact Properties of Plate Containing
Circumferential Crack in ACFX 80417**

Temperature, F	Energy, ft.-lbs.	Lateral Expansion, mils	Shear, %
Transverse Specimens			
-20	10	8.5	0
0	16	12	1
20	17	22	2
45	18	22	10
80	29	29.5	40
100	25	29.5	60
Longitudinal Specimens			
-20	11	12.5	1
0	17	15	2
20	27	25	3
45	36	36	35
80	47	45	55
100	43	46	65

Given the relatively low Charpy test values, dynamic tear tests were conducted on a set of specimens from the plate and a set from the weld heat-affected-zone. The dynamic tear test is similar to a Charpy test except that a larger specimen, using the through thickness of the plate is used. Because the actual thickness is tested plane strain conditions are more likely to be preserved, and a true measure of the ductile to brittle transition is obtained. The tests were conducted in accordance with ASTM Specification E-604. The values of fracture energy versus temperature for the base metal are shown in Figure B-6, and the values of fracture energy versus temperature for the heat-affected-zone are shown in Figure B-7. The ductile to brittle transition for the base metal and for the heat-affected-zone appears to occur at approximately 100°F.
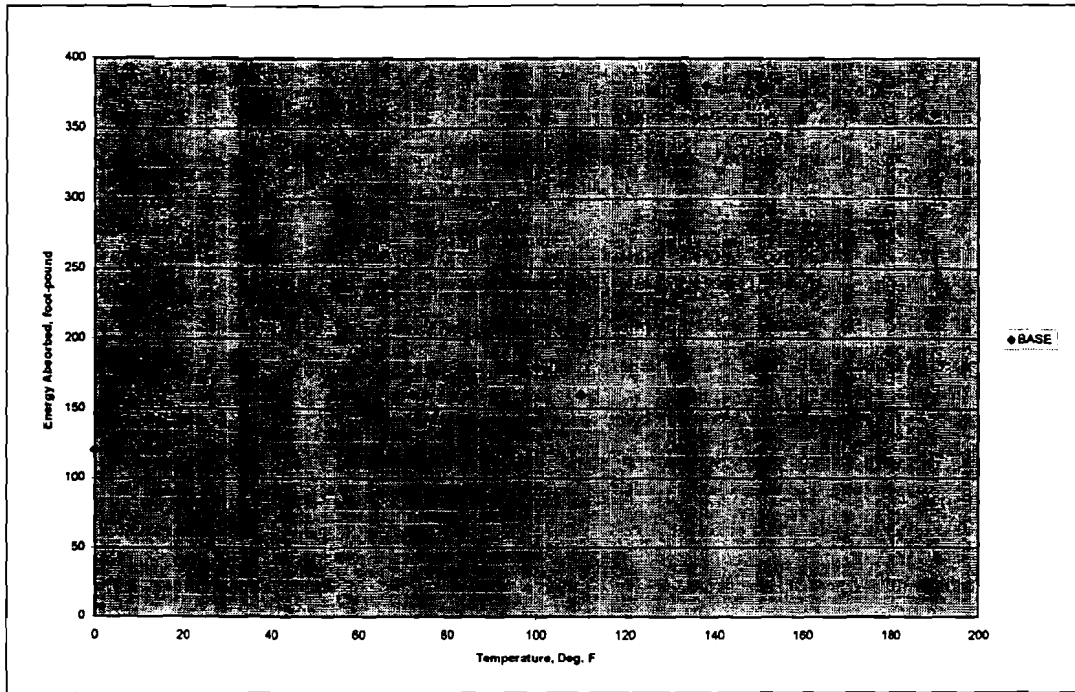
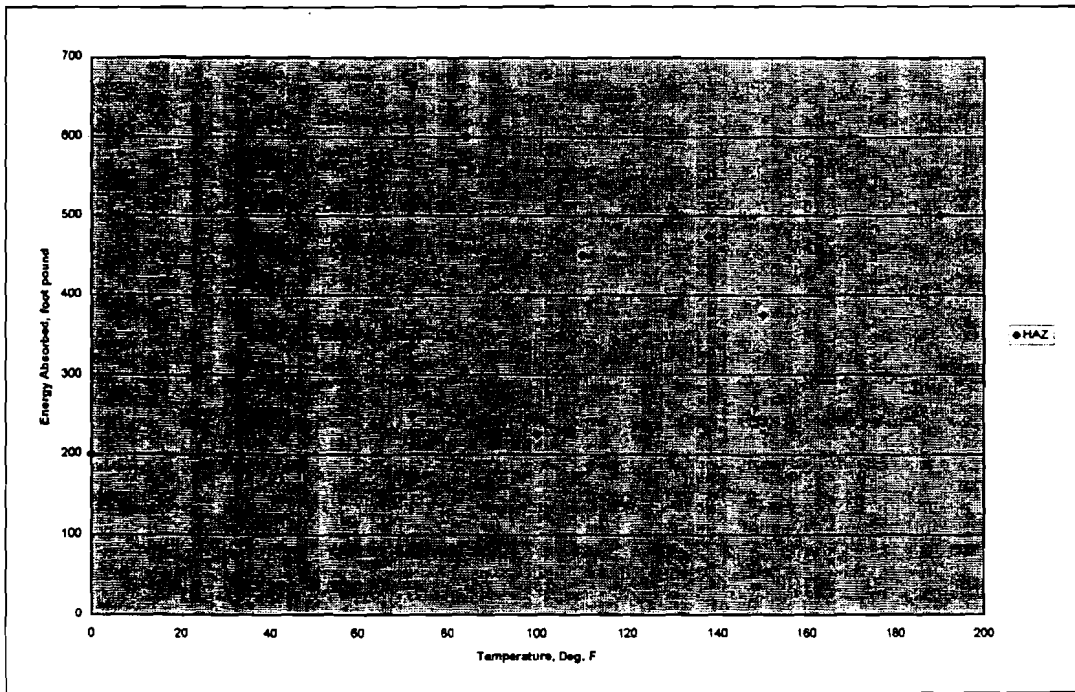Figure B-5. Base Metal Dynamic Tear Test Results

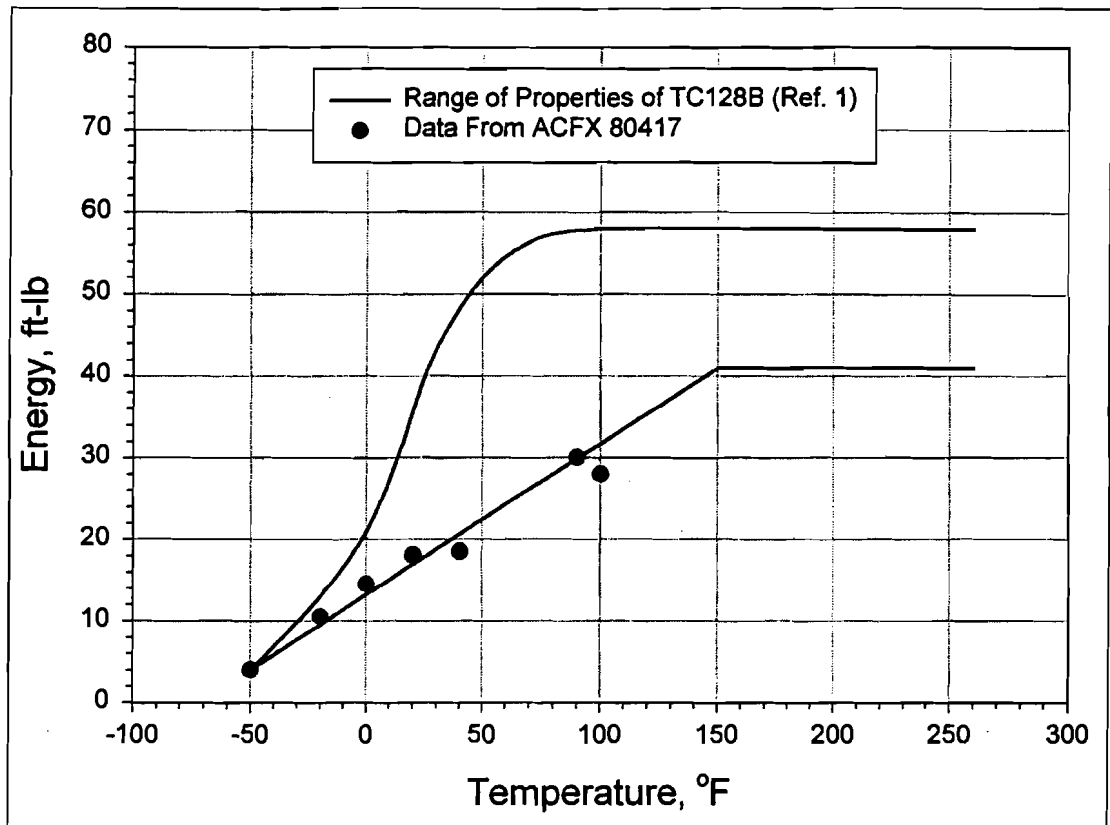Figure B-6. HAZ Dynamic Tear Test Results

B-7

Figure B-7. Charpy V-Notch Properties in Vicinity of Crack

B5.0 FRACTURE TOUGHNESS TESTING

The fracture toughness of the base metal was determined by J-integral test according to ASTM Standard E 813. Two specimens were tested at SRI. One specimen, tested at 5°F failed in a completely ductile manner while the second specimen, tested at 11°F, failed in a brittle manner indicating an apparent fracture toughness, K_Q, of 88.3 ksi√in.

The microstructure of the heat-affected zone, Figure B-8, shows a mixture of Widmanstätten ferrite side and intergranular plates with no evidence of martensite indicating proper cooling. Further, a microhardness survey across the weld, heat-affected-zone, and base metal shows a relatively uniform hardness profile, Table B-3.

Figure B-8. Microstructure of Base Material, Etched in 2% Nital, X100

Table B-3. Knoop Microhardness Values of Placard Weld Area

Location	Knoop Hardness	Brinell Hardness*
Weld	210	195
Weld	194	176
Weld	202	185
Weld	172	156
Weld	222	205
HAZ	224	210
HAZ	243	230
HAZ	231	216
Base Metal	174	159
Base Metal	201	185
Base Metal	212	195

*Converted from Knoop Hardness Value.

B6.0 METALLOGRAPHIC EXAMINATION

Metallographic specimens were cut from both the base metal and weld area of the plate. The steel in the unetched condition shows the inclusions to be a mixture of ASTM E45 Type A2 Heavy sulfides and Type D2 Light (globular oxides). Micro cleanliness rating of 15 plates of TC128B reported in reference 1 give a minimum and maximum worst field inclusion areas of 0.60 and 2.30% respectively. The ASTM E-45 rating may be converted to area percent using a conversion table given in reference 2. The inclusion area in the specimen from ACFS 80417 would be equivalent to 0.85% area. The structure of the base material, when etched with a 2% nital solution, shows the expected mixture of ferrite and pearlite with some minor banding, Figure B-9. The grain size is ASTM 9, which is in agreement with other data for non-normalized TC128B.
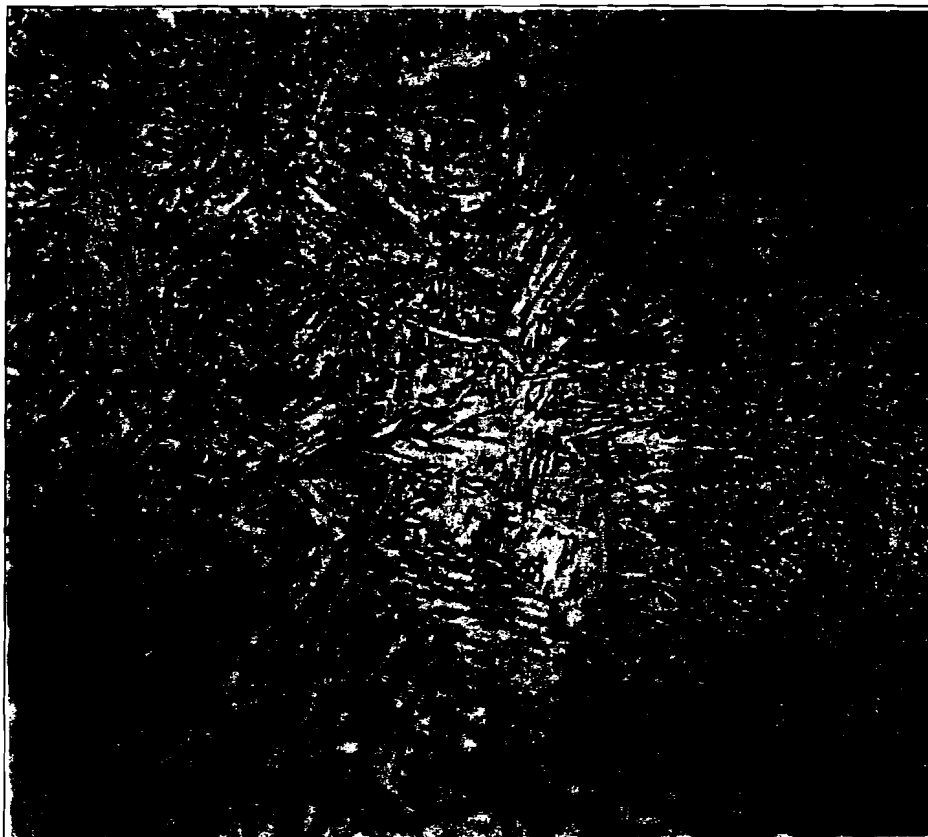

Figure B-9. Microstructure of Heat-Affected Zone, Etched with 2% Nital, X400

B7.0 DISCUSSION

Given the small size (<1/16") of the crack that initiated the 35-inch long brittle fracture, the stress to cause the break must have been near the yield stress. Given the comparatively low vapor pressure of the vinyl chloride lading (49.9 psi at 68°F) two other stress conditions must have been present. First, as the buckle surrounding the crack was formed, the inside of the plate was yielded in tension and the outside of the plate was subject to yield in compression. This yielding has the effect of imparting a residual tensile stress in the outside of the plate and a residual compressive stress in the inside of the plate. The longitudinal stress of approximately 2,300 psi due to the lading pressure would by additive to the residual stresses. Finally, it is surmised that when the car was being righted the stresses caused by lifting or rolling introduced an additional stress, which in combination with the residual and internal pressure stresses, produced sufficient stress to trigger the brittle fracture. Additionally, the fact that the Charpy v-notch impact values were at the lower limit of the measured values for other heats of TC128B contributed to the occurrence of the fracture.

B8.0 CONCLUSIONS

- The Plate of ACFX 80417 which contained a circumferential fracture with a buckle was within the specified composition for TC128B steel.

- The grain size, microstructure, cleanliness, and hardness are within the range of measured values for other heats of TC128B.

- The Charpy v-notch impact values were at the lower limit of the measured values for other heats of TC128B. The relatively low fracture energy properties of the steel contributed to the possibility of fracture.

- The dynamic tear test indicates that the brittle fracture could occur at temperatures less than 100°F.

- The 35-inch long circumferential crack originated from a 1/16-inch crack that formed at the toe of the weld securing the placard bracket holder. This weld appears to have been made manually.

- The 35-inch crack ran in both directions away from the origin and was entirely a brittle fracture over its entire length.

  - The major driving force of the crack was the residual stress imparted by the over yield buckling of the plate.

References

1. R. J. Eiber and L. L. Olson, "Material Study on Steels Used in Current and Former Tank Car Construction and from Cars Involved in Accidents," Association of American Railroad Report R-193, August, 1975.

2. R. A. Rege et al., "Microcleanliness in Steel-A New Quantitative TV Rating Method," *Applications of Modern Metallographic Techniques*, ASTM STP-480 (Philadelphia, 1970), p. 264.